Integrating analogue and numerical modelling techniques for improved simulation of coupled regional tectonic processes and depositional systems

Alexander Thomas Hughes-Wharton

A thesis submitted to Royal Holloway University of London for the degree of Doctor of Philosophy

Department of Earth Sciences

Royal Holloway, University of London

Surrey, TW20 0EX

Declaration of Authorship

I, Alexander Thomas Hughes-Wharton, hereby declare that this thesis and the work presented in it is entirely my own. Where I have consulted the work of others, this is always clearly stated.

Signed: _____

Date: _____

Acknowledgements

It's been a long journey, nearly five years from arriving for my PhD induction to typing these acknowledgements, with many ups, downs and an interruption in-between. Although the thesis has one name on the front, it wouldn't have been possible without a network of support.

Firstly, my supervisors. Jürgen, your enthusiasm and depth-of-knowledge spanning the several facets of geoscience my project involved has been enormously helpful. In what were often long periods of solitude in the analogue modelling laboratory, or even just with the project in general, your excitement (commonly akin to a child on Christmas morning) of the experiments I was running provided huge motivational boosts. I hope you get to take that sabbatical soon; you deserve it.

Pete, never afraid to be devastatingly critical. Your methods are less 'constructive criticism', but more 'tear it apart and leave the correct building blocks to try again'. Challenging me at every turn, I've been had no choice but to adapt and will be a better researcher for it.

Financially, the project was supported by funding from the COMPASS consortium.

The majority of the experimental setups were made possible with the help of Jerry Morris, whose ability to bring conceptual ideas/drawings to life as lab apparatus has been invaluable. Supporting me in recording of the experiments (amongst a plethora of other lab-based matters) was Kevin D'Souza, who probably assisted and distracted in equal measure over the span of the project.

Friends, there's too many to mention, but thank you to everyone across the department and externally who's kept me sane over the years. Particularly my row in 202B, you know who you are.

Rebecca, thank you for putting up with me. The support you've given me over the years has been amazing and I've been so fortunate to have you by my side through

all of this. There's been countless times where I've been sounding out ideas to you, and many more where I've probably been venting, yet you've always sought to help however you can (you'll probably spell-/grammar-check this very paragraph). I'm looking forward to moving on (and out) with you, I know you think it's about time I got a job.

To Mum and Dad, I'm a doctor. It isn't the 'pristine white coat with a stethoscope around my neck' variety you perhaps dreamed about for me when I was young (I've got the white coat, it's just extremely grubby and the pockets are filled with mica flakes), but it's something I've had to fight and work for and am extremely proud of. Thank you for the opportunities you gave me, that you never had, I wouldn't be here without you. Mum, I know you'd be proud.

Abstract

Sedimentary basins in tectonically active settings, such as rift basins, are characterised by complex, dynamic depositional environments, with the interplay between sedimentation and tectonic processes controlling basin architecture and resource distribution. Scaled 3D analogue sandbox experiments with high-resolution digital 3D deformation monitoring, constrained by geological and geophysical data, can realistically simulate upper-crustal brittle deformation on crustal to basin-scale and allow kinematic and mechanical analysis of complex 3D fault systems. First-order syn-kinematic sedimentation can be conceptually applied to the surface of evolving experiments, permitting investigation of its effect on fault localisation, linkage and displacement and resulting tectonic basin subsidence. However, to date, this process has been done manually; by depositing incremental, homogeneous sand layers on top of the evolving experiment surface to simulate tectonic loading. Consequently, current syn-kinematic sedimentation methods are not capable of simulating complex stratal architectures or incorporating depositional controls like eustasy and climate variations. Conversely, numerical stratigraphic-forward modellers are able to produce these more complex stratal geometries, including their controlling parameters; however, they currently lack the ability to simulate the complex tectonic subsidence of basins realistically, or in sufficient spatial resolution.

This thesis develops a new integrated experimental method by applying cellular numerical stratigraphic forward modelling to dynamically scaled analogue sandbox experiments, permitting realistic incremental deposition of syn-tectonic sediments. Surface topography and displacement components (e.g. subsidence) of the analogue experiment are derived by 3D-Stereo Digital Image Correlation (DIC) and yield inputs for the cellular carbonate stratigraphic forward modelling software (SFM - CarboCAT). Incremental, scaled sediment input is then calculated using this data combined with suitable production parameters (production rate, surface light intensity, extinction coefficient etc.). This enables a realistic calculation of spatial

distribution and volumes of sediment facies to be incrementally deposited onto the surface of the evolving sandbox experiment.

Initially, a cellular sieving device was developed and tested to permit deposition of calculated incremental sediment volumes onto the experiment surface; a cellular array of tubes allows deposition of heterogeneous material volumes onto the corresponding surface location. This apparatus is capable of repeatedly depositing heterogeneous sandpacks with locally controlled volumes and homogeneous mechanical properties.

The integrated analogue-numerical workflow was then systematically tested in a series of static (depositional ramp) and dynamic (asymmetric half-graben) analogue experiments with varying initial parameters for both the analogue and numerical models. Model evolution is purely deterministic, producing diverse final architectures solely as a result of initial parameters and ongoing feedback between the analogue tectonic subsidence history and the SFM-derived sediment loading.

Deposition of SFM calculated sediment volumes onto the analogue model produce more realistic syn-tectonic depositional patterns and facies distributions than current methods can achieve. This method could be upscaled in the future by a computer-controlled, semi-automatic sieving device with higher cell numbers. These larger-scale experiments would be capable of simulating more complex, tectonically-controlled settings like segmented rift basins or passive margin sedimentary basins affected by gravity-driven deformation, as well as investigating the role of climatic impacts on basin evolution. Findings have potential to improve understanding of basin evolution and subsequent facies distribution, with implications for resource exploration.

Table of Contents

List of Figures & Tables

1 Introduction

1.1 Rationale

Sedimentary basin development within syn-rift settings on continental margins is highly complex, due to the interplay between tectonic and sedimentary processes. Two methods which attempt to recreate the development of sedimentary basins in these settings are computer-based numerical modelling and lab-based physical analogue modelling. Extensional sandbox models have been shown to be representative of upper crustal deformation and kinematic behaviour if sufficient similarity in the scaling of parameters such as geometry, density and time are met (Brun et al. 1999). However, syn-kinematic sedimentation applied to analogue experiments is currently somewhat basic, commonly being flat topped and filling available accommodation, not adequately simulating the complex sedimentary evolution of tectonically controlled sedimentary basins, e.g. across half-grabens (Ravnås and Steel 1998; Gawthorpe and Leeder 2000) (Figure 1.1) or carbonate structures such as atolls, which can achieve up to 50° dip angle at their margins (Betzler et al. 2016).

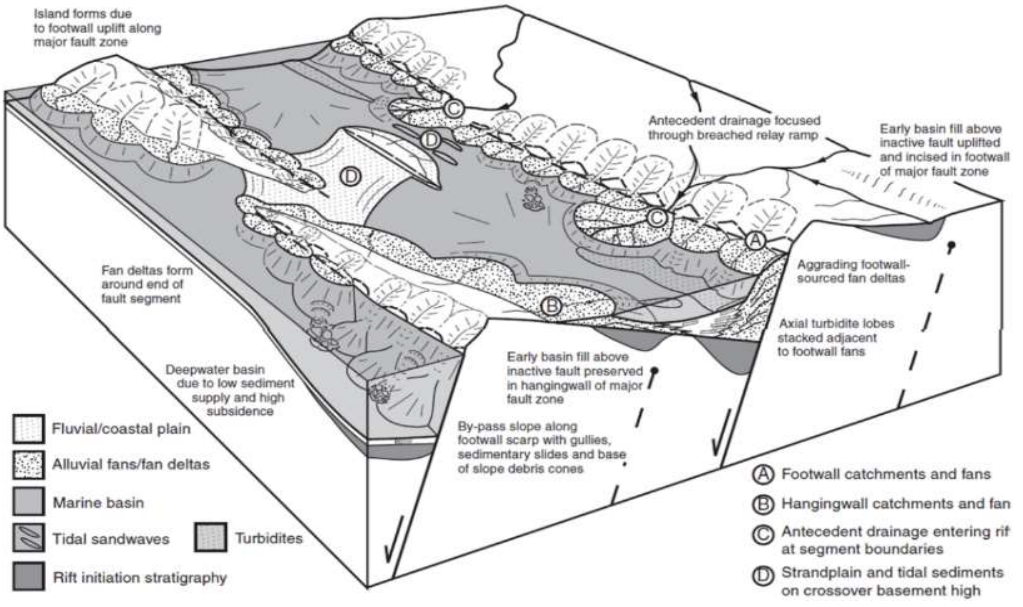

Figure 1.1: Diagram highlighting the variety of deposystems active simultaneously within extensional half-graben settings at syn-rift stage (Gawthorpe and Leeder 2000).

More in-depth attempts to recreate syn-kinematic sedimentation have been made, e.g. Adam et al. 2012, which models sequence development such as aggradation, however there is potentially still a further improvement that can be realised by modelling facies development in greater detail.

The alternative field of stratigraphic forward models have been argued to replicate natural stratigraphic patterns (Bosence and Waltham 1990; Williams et al. 2011); though typically models have extremely simple subsidence patterns, which are also not being dynamically affected by ongoing sedimentation.

In an original approach, this work integrates numerical stratigraphic forward models (SFM) with basin-scale 3D analogue models (AM). This workflow permits both realistic tectonic evolution as well as subsequent basin fill distribution. Of particular note, is that for the first time, these two features occur within a single integrated model. Given that sedimentation has been shown to have a demonstrable effect upon tectonic evolution (Bialas and Buck 2009), governing future accommodation, insights to feedback mechanisms between the two may be obtained using the workflow, a previously impossible investigation.

Development of this novel workflow has trialled multiple approaches, demanding significant time investment. The project required conceptualisation of the base idea, development and testing of various setups (both constructing physical analogue apparatus and producing numerical scripts) and has eventually been brought to conclusion; successfully achieving the desired goal of integrating the two modelling procedures.

The final integrated methodology may be used in future to simulate more complex, tectonically-controlled settings like segmented rift basins or passive margin sedimentary basins affected by gravity-driven deformation, as well as investigating the role of climatic impacts on basin evolution. This work will improve understanding of dynamic basin evolution and the resulting architectures; including tectonic controls on sediment transport, subsequent facies distribution and the impact of sedimentary loading on fault pattern and kinematics. Findings will be of particular importance for companies involved in E&P activity on continental

margins, enabling a more accurate prediction of the subsurface by verifying seismic interpretation, reducing exploration risk.

This project forms part of the COMPASS (Continental Margin Process Analysis, Structures & Stratigraphy) group research, an integrated and multi-disciplinary approach to the analysis of the geodynamic, lithospheric, tectonic and sedimentary processes that control basin formation and the genesis of petroleum systems on rifted continental margins. The current group objective is the design and development of effective interlocking multi-scale models and workflows capable of integrating numerical and analogue experiment techniques for the simulation and tectono-stratigraphic analysis of rift basins and conjugate passive margins (Figure 1.2).

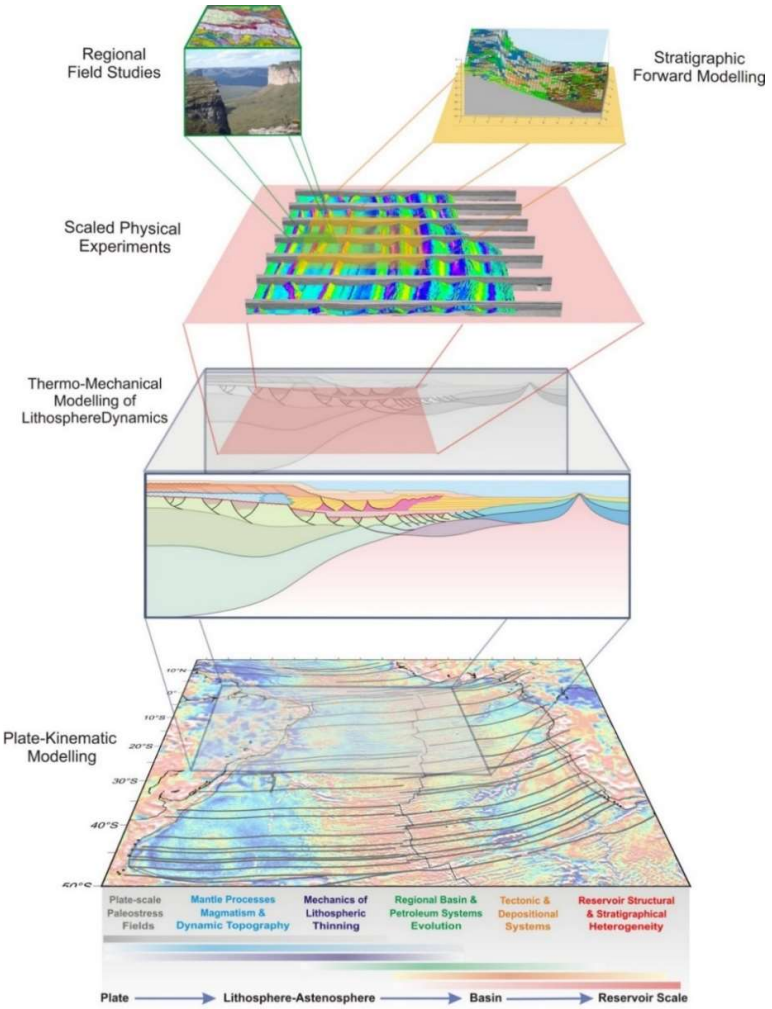

Figure 1.2: COMPASS summary highlighting the variety of experimental methods used for multi-scale analysis and simulation of rifted continental margin processes

1.2 Outline of Approaches

1.2.1 Analogue Modelling (AM)

Scaled 3D analogue sandbox experiments (example in Figure 1.3), constrained by geological data and high-resolution digital 3D deformation monitoring, are able to simulate fault localisation, linkage, displacement and resulting tectonic basin subsidence, including syn-kinematic sedimentation (aggradation, progradation, base level), with high spatial and temporal resolution (Adam et al. 2012).

Syn-kinematic sedimentation, when applied to extensional analogue sandbox experiments, typically infills all the available accommodation developed by ongoing tectonic subsidence, excess can be removed using a scraper on a guide-and-rail system. This typically produces mostly homogeneous, flat-topped syn-kinematic sedimentation intervals, as shown in the figure below. As such, analogue experiments cannot adequately simulate more complex depositional architectures or processes (e.g. fan and clinoform systems) and their non-tectonic controls under variable paleo-depositional settings, which are additionally controlled by climate, sea level change, sediment supply and facies distribution.

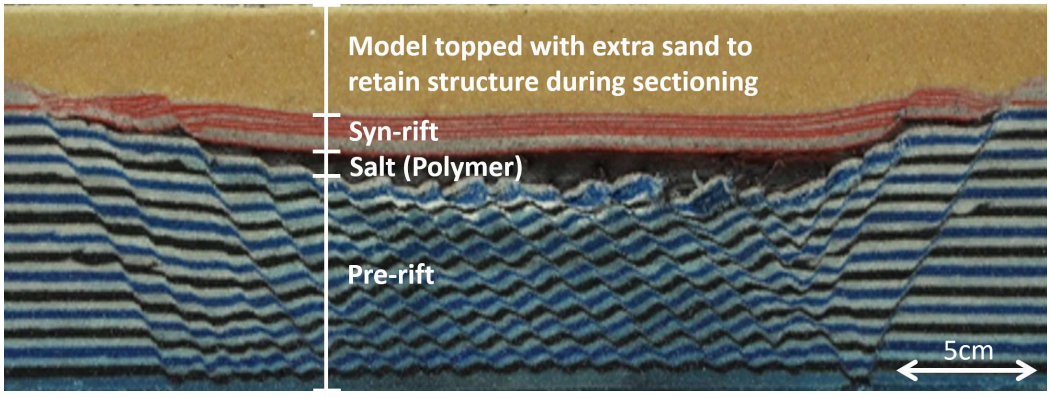

Figure 1.3: Example analogue experiment cross-section of a symmetrical rift basin including post-rift salt and syn-rift sedimentation. Pre-rift topography (shown in repeating blue-white-black-white) initially deposited as horizontal layers, undergoes extension. During this, silicon polymer is deposited to mimic the physical characteristics of a salt body, with a final syn-rift succession above that (shown in repeating red & white)

1.2.2 Digital Image Correlation (DIC)

During analogue model evolution 3D surface deformation is monitored by high-resolution digital cameras with a stereoscopic setup, recording time-series digital stereo images. Surface evolution, subsidence and fault kinematics of the experiments are analysed with 3D displacement data and computed strain obtained from 3D Digital Image correlation (DIC) (examples in Figure 1.4). DIC is a high-resolution optical 3D deformation monitoring technique adapted for analogue deformation experiments that allows full quantification of small and large-scale model deformation (Adam et al. 2005).

For the purpose of this study it is employed to record ongoing evolution of surface topography (DEM) yielded as elevation/bathymetry values (z) in sub-millimetre x, y increments. This data provides the incremental high-resolution input surface for the numerical modeller to generate sedimentation patterns onto. The evolution of the sandbox topography through time is also used to calculate subsidence based on the elevation difference between the initial and final surfaces for a given increment.

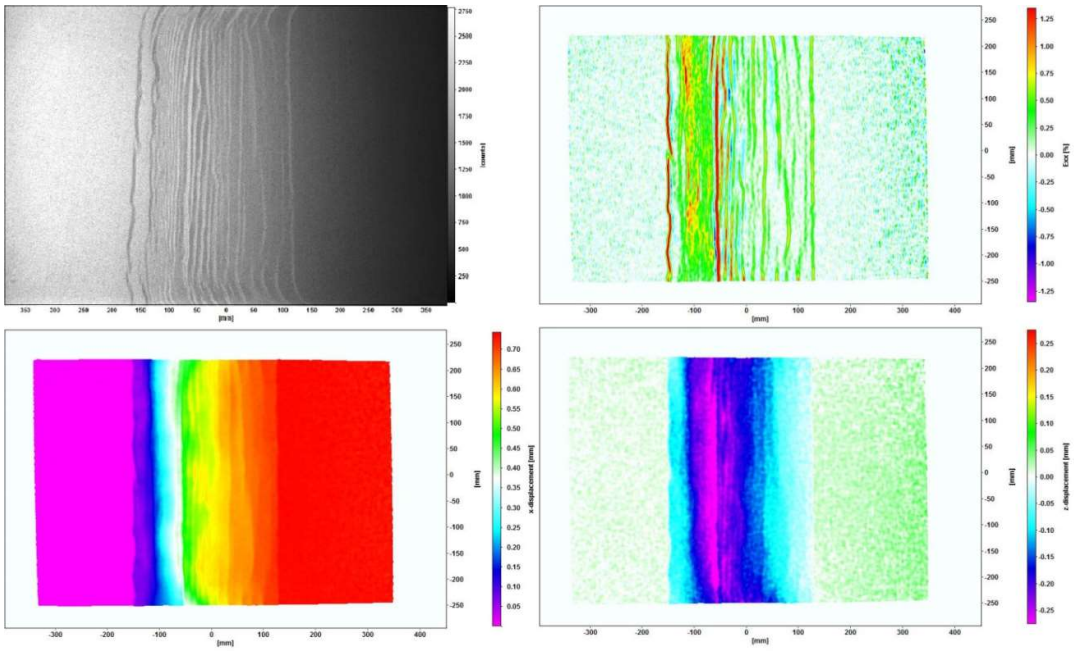

Figure 1.4: Example DIC data taken during extension of a 3D rift experiment. Top Left: Oblique light raw image. Top Right: Horizontal strain. Bottom Left: Horizontal displacement. Bottom Right: Vertical displacement (i.e. subsidence). *NB images are the surface of the pre-kinematic sandpack shown in figure 1.3 at the final stage of extension before the rift is topped with silicon polymer

1.2.3 Stratigraphic Forward Modelling (SFM)

Stratigraphic forward modelling is a tool permitting geologists to forward project the deposition and evolution of sedimentary facies within a stratigraphic framework with given prior boundary conditions (e.g. Bosence and Waltham 1990; Aurell et al. 1995; Williams et al. 2011). For work included within this thesis the SFM software used is CarboCAT (Burgess 2013) (Figure 1.5), an entirely deterministic forward model that uses a cellular automaton to calculate lithofacies spatial distributions and hence determines the accumulation of heterogeneous carbonate strata in three dimensions. Written in MATLAB 7.6.0 as a series of M-files (scripts containing MATLAB commands to be executed in a logical order), it has a GUI (Graphical User Interface) that allows the user to specify parameter files to utilise with customisable inputs (e.g. lithological information, timesteps, initial topography) and initialize/run the model. CarboCAT encompasses various geological processes, including tectonic subsidence (derived from DIC data of the sandbox surface), eustatic sea-level oscillations, water depth-dependent carbonate production rates in multiple carbonate factories, lateral migration of carbonate lithofacies bodies, and a simple representation of sediment transport.

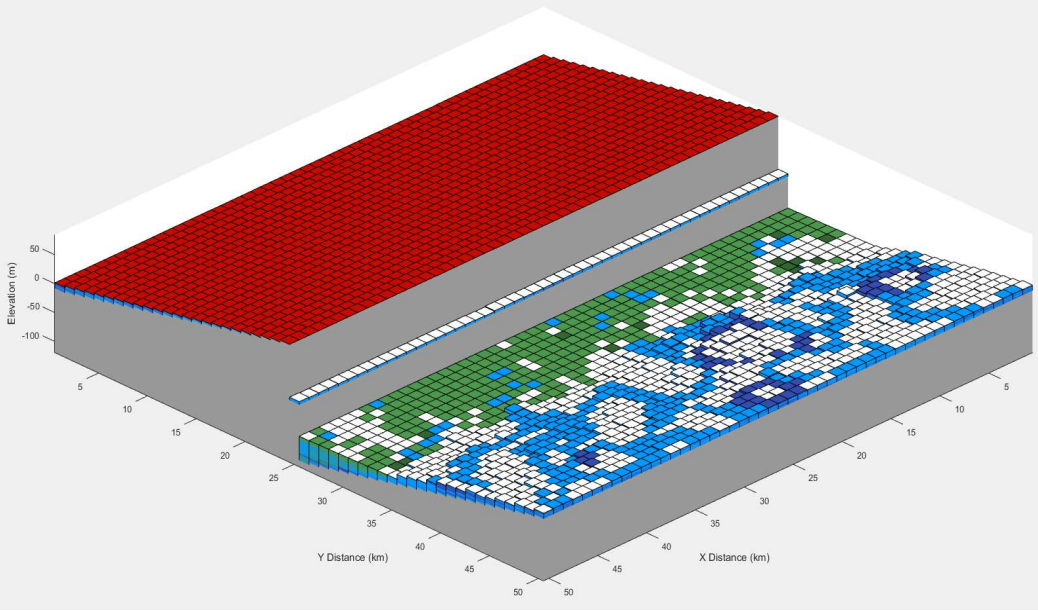

Figure 1.5: Example CarboCAT output displaying carbonate generation across a half-graben. Each cell is in a discrete state; red (subaerially exposed), blue (actively producing carbonate lithofacies), green (transported carbonate material), white (unoccupied). Transported material is a fraction of produced volumes, there is no erosion occurring of either subaerially exposed or submarine cells.

CarboCAT models enable reproduction of genuine carbonate architectures, displaying intricate stratal patterns such as interfingering (Burgess 2013). Whilst work has demonstrated the software can handle complex basin subsidence and the response of carbonate deposystems (Kozlowski 2017), sedimentation infilling the created accommodation does not dynamically impact tectonic evolution within the computer simulation.

1.3 Integrated Analogue-Numerical Workflow

The approaches outlined in 1.2 are integrated together to produce the complete workflow. The order of the process is outlined below (Figure 1.6). Detailed information about the specific method and application of each step is outlined later in the thesis.

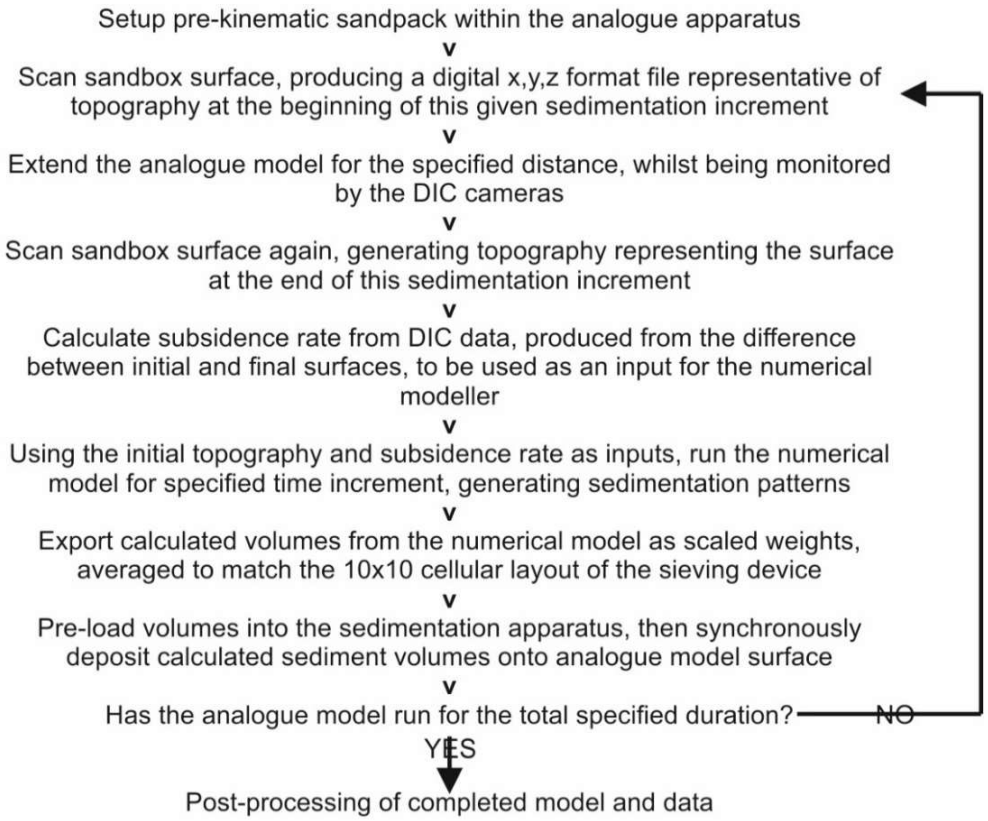

Figure 1.6: Flow chart illustrating the integrated workflow procedure between analogue and numerical models

1.4 Thesis Outline

Initially a geological background is provided, giving an overview of tectonics within extensional settings with focus on sedimentary fill at syn-extension stage **(Chapter 2)**. A background of the relevant analogue and numerical modelling techniques is then given **(Chapter 3)**.

To integrate the two modelling approaches, the cellular output of the SFM needs to be replicated onto the analogue surface. Therefore, an apparatus is designed which can be pre-loaded with the calculated volumes of sediment, before depositing it into the correct locations on the analogue surface. To achieve valid results with experiments incorporating the sedimentation device, the sandpack deposited is required to have coherent mechanical properties (density and internal friction profile) to the underlying pre-kinematic layers which are to be deposited by hand. To determine the correct specification for the device, a range of properties are tested, enabling production of a prototype (**Chapter 4**).

Following on from the production of a prototype, proof-of-concept is demonstrated by application of the SFM software to an evolving sandbox experiment. Imaging of the experiment surface with DIC cameras produces digital topographic data, which can be input to the SFM and populated with realistic sedimentation patterns. These volumes are then re-deposited onto the sandbox surface at their relevant positions using the apparatus produced in Chapter 4. Results demonstrate that the workflow achieves replication of calculated sedimentation patterns onto the analogue surface with capacity to develop into complex 3D structures with repeated layering, whilst also depositing a sandpack with the desired mechanical properties **(Chapter 5)**.

The next step was to apply the integrated analogue-numerical process to a kinematic sandbox experiment with subsidence being dynamically derived from the ongoing tectonic deformation of the surface. Discrete subsidence rates are calculated from the topographic change for individual sedimentation increments.

Dependent upon the extension rate, calculated sediment volumes and subsequent tectonic loading applied to the model varies considerably. Deposited over several sedimentation increments, final architectures vary significantly, solely due to feedback between the analogue and numerical modelling techniques **(Chapter 6)**.

A short summary of the main results is then provided, followed by a discussion and evaluation of approaches taken and limitations imposed by the modelling procedures. A number of suggestions are also made for future work and improvement **(Chapter 7)**. Finally, a list of conclusions is given **(Chapter 8)**.

2 Geological Background

This Chapter provides an overview of the processes which lead to continental extension and ultimately rifting in the form of brittle failure of the upper crust, as well as the style of surface deformation and subsequent infilling of this created accommodation. Focus is given to carbonate sedimentation as it is being calculated by the stratigraphic forward modelling software used in the project.

2.1 Process of extension and rift style

Continental rifts are characterised as linear zones where the Earth's lithosphere is undergoing stretching and thinning accommodated by normal faulting, potentially leading to continental breakup and ocean floor spreading, typically perpendicular, to the developing coastlines if successful. Being present within passive margin stratigraphies, rift basins are key areas of interest for ongoing research. The high preservation potential of sediments and fossils not only yields insights to early continental breakup, but also means many major petroleum provinces are located within syn-rift sedimentary fills, necessitating improved understanding to yield better exploration and production results. Exploration activity has enabled detailed mapping of subsurface rift basins through seismic acquisition. Onshore analogues of exposed basins have provided insights as to the timing and style of deformation, with fault system evolution being observed in the stratigraphic record (Gibson et al. 1989) and subsequent sedimentation being primarily controlled by normal fault slip. Erratt et al. (2010) demonstrate examples of the complex interplay between sedimentation and tectonics in these settings, with sedimentation and erosion (surface processes) being shown to have an impact on syn- and post-rift tectonic evolution (Burov and Cloetingh 1997; Burov and Poliakov 2001; Olive et al. 2014). Scaled experimental models have also provided valuable information (review provided by Koyi 1997), such as insights to syn-rift salt tectonic processes (Costa

and Vendeville 2002). Both individually and jointly, seismic, field and experimental methods have improved understanding of the evolution and subsequent deformation observed within rift basins.

Rifted continental margins form because of the extension and stretching of the lithosphere prior to continental breakup and ocean floor spreading, producing a surface expression of extensional faulting of the brittle upper crust. Typically, the location of rifting is determined by reactivation of pre-existing lithospheric weaknesses, demonstrated both in nature (Korme et al. 1997; Ring 1994; Versfelt and Rosendahl 1989) and models (Corti 2012). The mechanism driving initiation of extension is split into two classes, active and passive. Passive rifting implies direct application of opposing forces to create extension. These are contributed from the effects of slab pull and slab push acting at the plate boundaries. Active rifting is caused by thermal erosion of the lower lithosphere due to upwelling mantle material, driven by general mantle convection or plumes. Upwards movement coupled with the heat flow causes erosion of the lithosphere, causing the material to collapse under gravitational force and spread, resulting in rifting. Active rifting typically produces wider, more prevalent ocean basins.

To explain the extensional process there are two main models, pure shear (McKenzie 1978) and simple shear (Wernicke 1981). Hybrid theories have also been put forward which encompass aspects of both pure and simple shear; flexural cantilever model (Kusznir et al. 1991) and delamination model (Lister et al., 1991)

The Mckenzie model (1978) states that the lithosphere is evenly stretched over a given area, occurring instantaneously. For most basins this yields plausible results, provided the true stretching was shorter than 20My (Jarvis and Mckenzie 1980). This stretching of the lithosphere produces the initial subsidence in the basin and results in the development of typically symmetrical half-graben topography. Following on from the initial stretching, thermal re-equilibration takes over and maintains isostatic equilibrium with the cooling of the asthenosphere, producing thermally derived subsidence. This phase is over a much longer timescale, typically 60-100Ma (Jarvis and Mckenzie 1980), which is longer than the duration of most

stretching periods (McKenzie 1978). Rifting occurs by continual thinning of the lithosphere accommodated by the stretching of the central graben region.

The Wernicke model (1981) states that the basin undergoes a simple shear regime, characterised by asymmetrical stretching. This is accommodated by a large detachment fault which runs from the surface to lower lithosphere/asthenosphere. The main zone of the crust undergoing extension is located deep within the lithosphere, away from the surface expression. Consequently, the zone of thermal upwelling is also not proximal the extensional domain, which implies lower overall subsidence as the asthenosphere cools. Simple shear drives strongly asymmetric rift styles.

As stretching occurs, the rift style begins to develop. The dominant style of faulting in continental rifts depends upon 'α' (acute angle between rift trend and relative displacement direction between opposite sides of the rift). If $\alpha<30°$, conjugate sets of strike-slip faults develop. If α is approximately 30° a diverse range of faulting can develop, including strike-slip, normal faults or a combination of the two. If $\alpha>30°$, normal faulting dominates (Withjack and Jamison 1986).

Rift style is primarily controlled by four main factors (Withjack et al. 2002):

- Tectonic activity prior to rift onset
- Angle of rifting ('α')
- Ongoing sedimentation and subsequent deformation of pre- and syn-rift strata (the targeted improvement to analogue modelling by this work)
- Tectonic activity after rifting ceases

Based upon these factors, a 'standard' rift basin was characterised by Withjack et al. (which most natural rift basins have attributes from), along with four end-member variations, of which attributes from multiple types can combine (Figure 2.1):

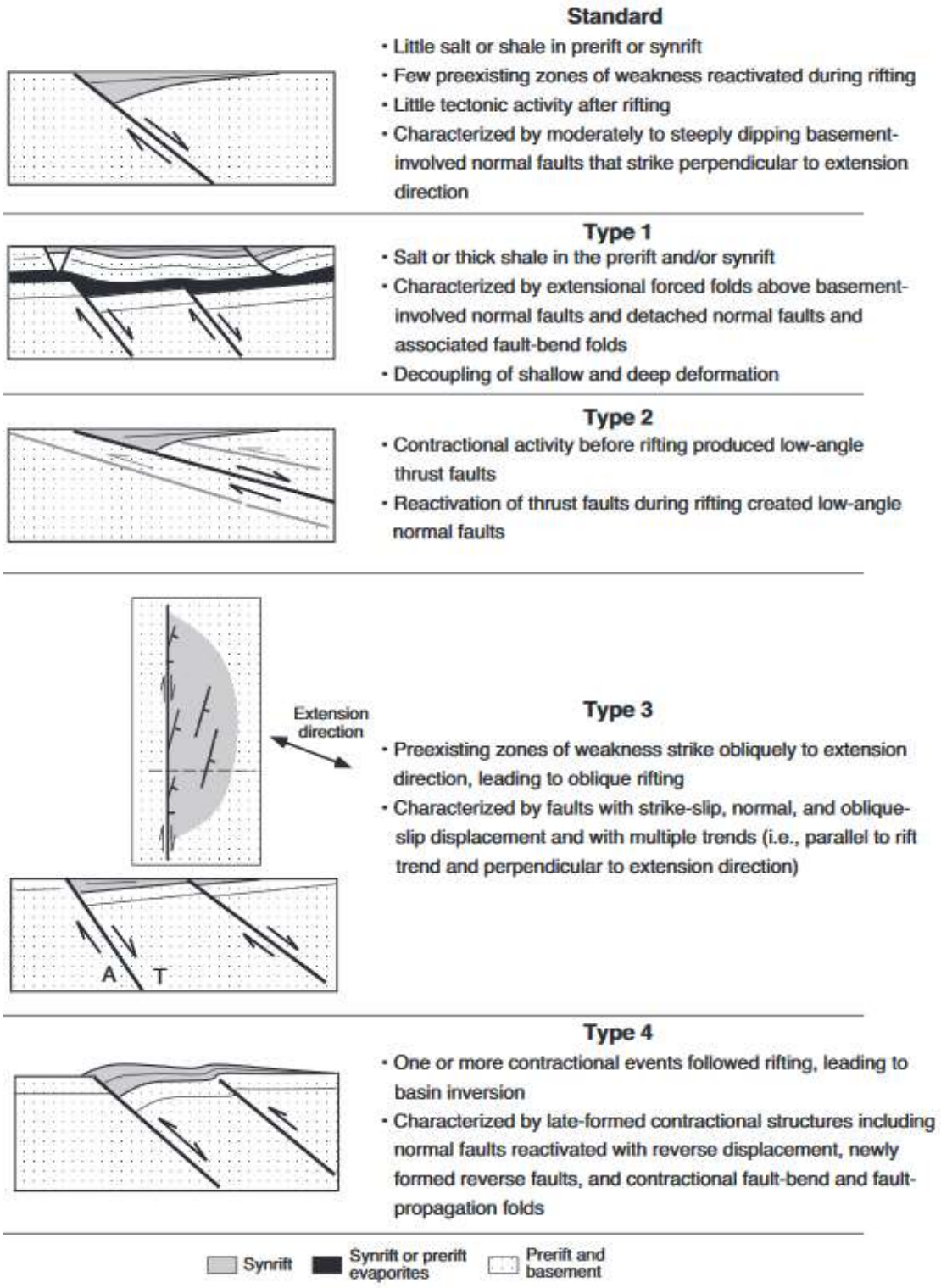

Figure 2.1: Standard rift basin morphology, including four potential end-member scenarios. (T=Movement Towards, A=Movement Away) (Withjack et al. 2002)

As subsequent extension occurs, the lithosphere stretches and density of faulting at the boundaries increases, developing fault swarms. These events produce only limited vertical movement and affect the magmatic segments of the rift floor. In these zones the thinned lithosphere is weakened by the ongoing magmatic activity which both drives the extensional faulting and is deposited in the subsequent space. This process is self-reinforcing, with the feedback between strain localisation, magma injection and lithospheric weakening facilitating the splitting of continental lithosphere (Corti et al. 2003). The magmatic segments then begin to act as spreading ridges which mature within transitional lithosphere. Over time the activity in transitional zones diminishes and they become passive margins.

2.2 Fault profiles and interaction

At a regional scale, initial structure is controlled by the development and subsequent slip of limited boundary faults to accommodate basin subsidence. The structure of these is commonly asymmetric and is a product of the lithospheric weakness orientation, relative to active extension direction. The two dominant types of rifting are orthogonal and oblique, with the method of formation previously studied using analogue models (McClay and White 1995; Zwaan et al. 2020) and numerical plate reconstruction models (Brune et al. 2018).

Orthogonal or pure rifting yields long (35-60km surface expression, Jackson and White 1989) boundary faults, with large associated slip, commonly in the region of several hundred metres. This has also been investigated with scaled 3D analogue models, which showed that orthogonal rifts typically yield simple, symmetric to asymmetric graben systems that demonstrate high uniformity along strike (McClay et al. 2004). Rift boundaries are denoted by lengthy border faults which form by linkage of shorter segments via breaching of relay ramps. Faulting within the basin is also typically at a high angle to the direction of rifting (i.e. also orthogonal).

Oblique rifting however, produces typically en-echelon fault arrangements and lower overall subsidence, generating lower accommodation and thus thinner sedimentary fills. Relative to the rift orientation, perpendicular extension and parallel shear act in tandem to produce rifting (Withjack and Jamison 1986). The final width of the rift is also subject to the lithospheric composition. This has been investigated using both numerical (Buck 1991) and analogue modelling (Brun et al. 1999). Two end-member modes of rifting are possible, either narrow rifting, resulting from strong, cold crust and/or mantle lithosphere. Alternatively, weaker/hotter lithosphere, defined by the absence of a strong upper mantle, encourages wider rifting (Gueydan et al. 2008). Narrow rifting is defined as having a width lower than lithospheric thickness, usually in the range of 50-100km, such as found in the East African Rift System. Wide rifting is characterised as being largely accommodated by the formation of half-graben arrangements, with rift widths being several hundred km, such as Basin and Range, W. USA.

Owing to the non-continuous nature of the weaknesses, the initial rift segments which form are distributed typically in either loose or en-echelon arrangements (Corti 2008) and, to create a continuous rift system, these need to be linked together (Figure 2.2). The factors controlling the mode of rift interaction (Allken et al. 2011; Allken et al. 2012) determing whether this occurs either by transfer zones, involving a discrete fault system which connects two segments together (hard linkage) or by accommodation zones, where the faults do not connect, and deformation is distributed (soft linkage) (Rosendahl 1987; Morley 1990; Morley 1999; Morley 2002). The evolution and pattern of rift interaction zones has been shown to have an impact on facies distribution and subsequent hydrocarbon migration/trapping (Paul and Mitra 2013), potentially leading to the development of successful petroleum systems.

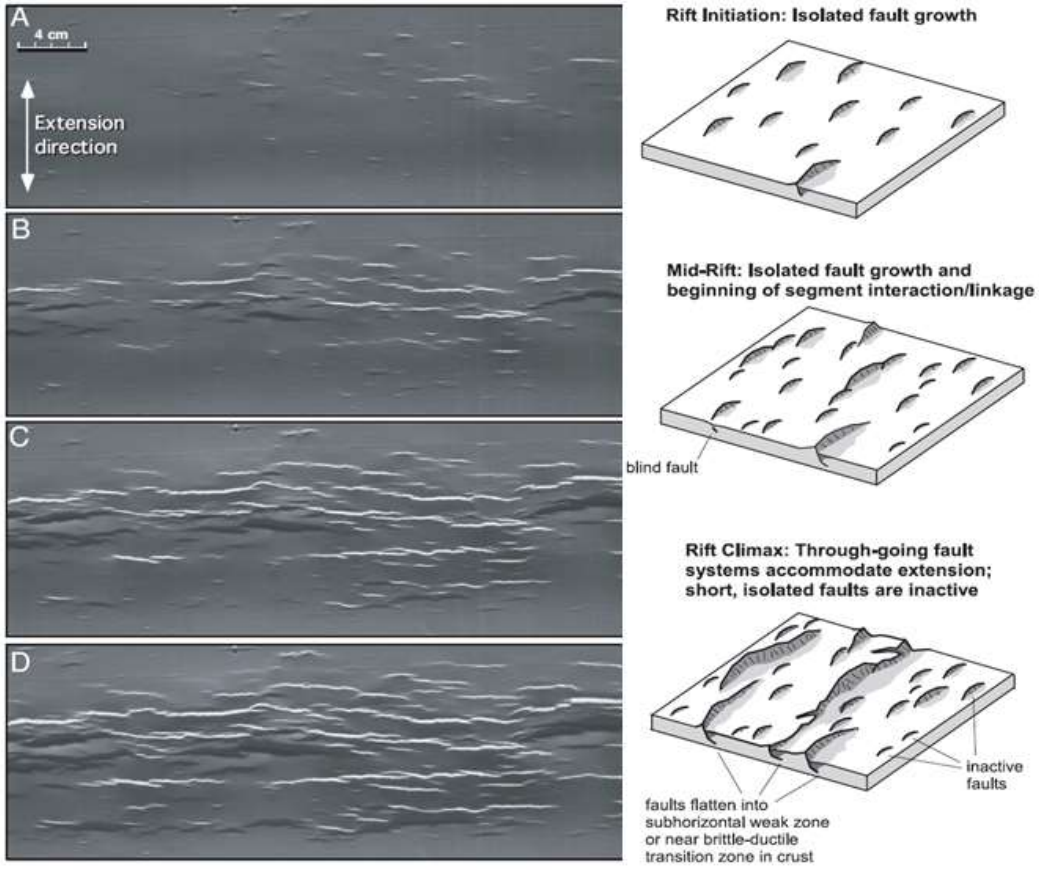

Figure 2.2: LEFT: Map view of an analogue experiment showing the development of normal faulting in extensional settings over time. Most faults begin initially as isolated features and link over time. The observed geometries and development are largely akin to those observed in nature (Withjack et al. 2002). RIGHT: Diagram showing typical fault initiation, propagation and linkage in extensional settings (Dorobek 2008).

Oblique extension has been shown to drive rift segment linkage (Zwaan and Schreurs 2017), with extension direction acting as a key influence (Figure 2.3). Right-stepping rift segments are more likely to connect via dextral oblique extension, due to the growth direction being together. This is opposed to sinistral extension which results in propagation either in parallel or apart, so linkage is uncommon, however it can lead to linkage by a strike-slip-dominated transfer zone if there exists sufficient lateral distance between segments. The inverse is true for mirrored systems.

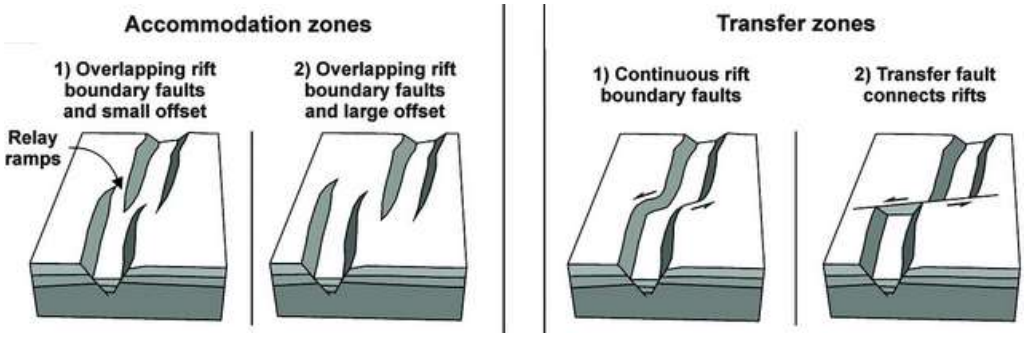

Figure 2.3: Schematic diagram of accommodation and transfer zones displaying different methods of fault linkage (Modified from Zwaan and Schreurs 2017)

Rift linkage is also potentially influenced by structural inheritance; however, this is only of note when extension direction is suitable for reactivation, otherwise rifts commonly align perpendicular to extension. If reactivation of structural inheritances does occur, then the produced transfer zone typically follows its orientation, which can lead to oblique extension when they attempt to move perpendicular to extension (Zwaan and Schreurs 2017).

The interplay between these tectonic factors is what initially drives the extension and largely dictates the path that future evolution will follow. Subsequent extension is provided by further brittle failure of the crust in the form of extensional faulting. This is what drives the evolution of the topography and determines the colonisation and further influence of syn-rift sedimentation, by influencing factors such as drainage, relief and accommodation. This gives rise to a variety of surface geomorphologic expressions between rifts, typically having either

a clearly-defined central axis which locates the highest extensional strain, as commonly observed in symmetric rifts. Alternatively, the strain can be broadly distributed, and no clear axis observed (Dorobek, 2008). Overall, the controlling factors on rift symmetry are still poorly understood (Allen and Beaumount 2016).

Characteristic of the extensional morphology produced are tilted fault blocks, with rift basins being composed from numerous half grabens (Gawthorpe and Leeder 2000; Schlische 1991). Syn-rift rotation involves upper crust extension accommodated by faulting and stretching of lower crust and lithospheric mantle by plastic deformation, with tilting of the surface sections occurring because of slip down listric faults due to relative footwall uplift and adjacent hanging-wall collapse (Leeder and Jackson 1993). The style of faulting also has an impression upon the surface expression of imbricate fault blocks. Uniform tilting of beds is driven by planar faulting, whereas differential tilt implies listric fault geometry (Wernicke and Burchfiel 1982). The tilt direction also has limited functionality when investigating transport directions, as the tilt direction can be either away or in the same direction as transport (Wernicke and Burchfiel 1982).

2.3 Depositional systems in extensional settings

Basin fill in extensional settings commonly denotes a range of depositional environments, which occur as a direct result of the ongoing tectonic activity. Sedimentary fill within rifts is of importance due to extensive, long lasting subsidence which enhances preservation potential (Gawthorpe and Leeder 2000). Pre-existing topography and drainage patterns exhibit a strong control upon sedimentation by dictating the provenance/lithology of sedimentary fill, as well as the location of initial depocenters. Non-tectonic effects such as eustatic sea-level fluctuations and climate also determine whether the area is subaerially exposed/marine (Gawthorpe and Leeder 2000). Through time and space these factors will evolve and follow an approximate pattern in most rift basins (Ravnås and Steel 1998). If the mechanics governing the formation of these tectonically active basins are understood, it enables prediction of subsidence and stratigraphic fill (Bosence 1998).

The primary factor determining basin fill is the accommodation to sediment supply ratio (A/S) (Hinsken et al. 2007). Accommodation is defined as the available space which can potentially be filled by the sediment supply (Jervey 1988). Accommodation evolution is a combined product of local basin-floor rotation and differential subsidence because of fault slip, basinwide background subsidence and eustatic changes. Sediment supply is what determines how much of the available accommodation is filled, and in what manner. This is determined by drainage patterns from hinterland areas, in-situ production of sediments, as well as the size and yield of the local fault-block area.

Classification of half grabens is based upon this relationship between accommodation and sediment supply (Bohacs et al. 2000) (Figure 2.4). 'Sediment overfilled' is characteristic of basins which have been entirely filled by the sediment supply, resulting in a 'spilling-over' of sediment into adjacent sub-basins. 'Sediment-balanced' implies that the sediment supply was approximately equal with the ongoing subsidence, typified by basins which have been fully filled. 'Sediment-

underfilled or -starved' basins are characterized by subsidence outpacing the available sediment supply, resulting in the accommodation present being left mostly unfilled.

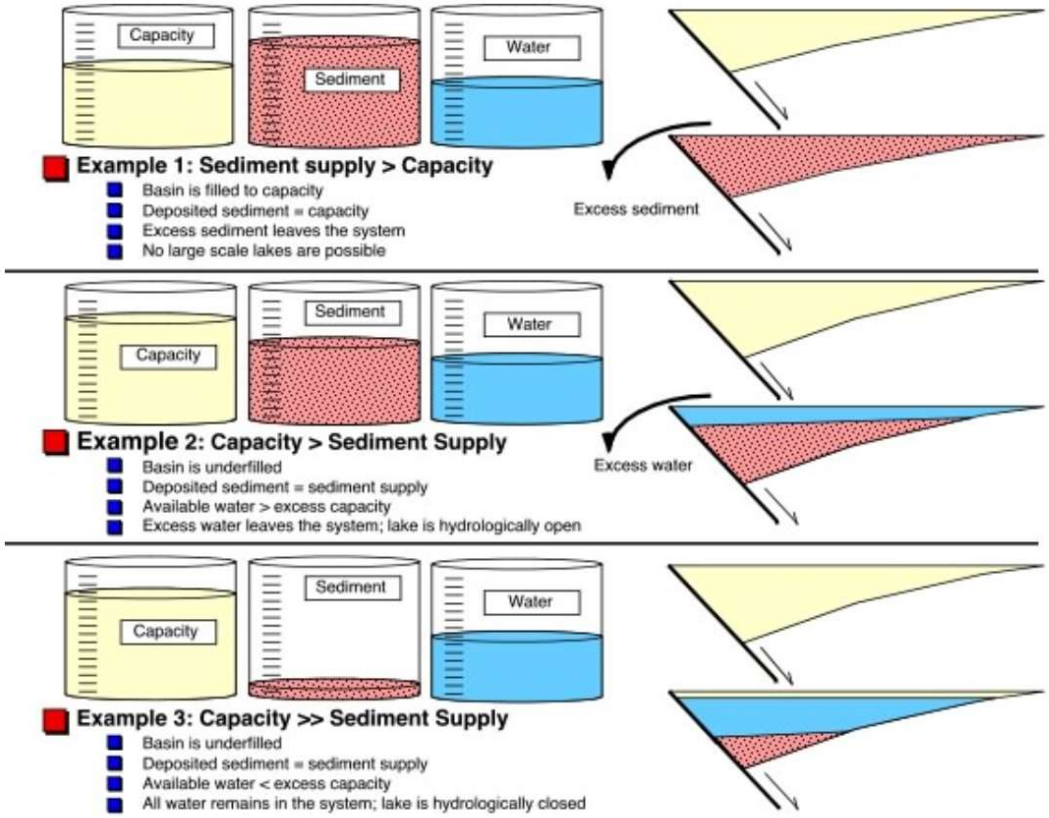

Figure 2.4: Relationships between Accommodation and Sediment supply (Modified from Withjack et al. 2002)

The relationship between accommodation and sediment supply will also strongly influence parasequence development. If accommodation generation outpaces the sediment supply, retrogradational stacking patterns occur. If the two are approximately equal, aggradational stacking dominates. When sediment supply is greater than accommodation generation, it leads to progradational stacking.

Rift basins can host a range of environments, dependent upon the water level, being either marine, non-marine or mixed, consisting of transitional environments (Figure 2.5). This is determined by the ongoing relationship between accommodation and sediment supply, with subsidence driving typically early-rift terrestrial environments entirely into the marine realm towards the late stage, due

to accommodation creation typically outpacing sediment supply. This influences the sediments deposited, normally resulting in a decrease in energy at the same point over time.

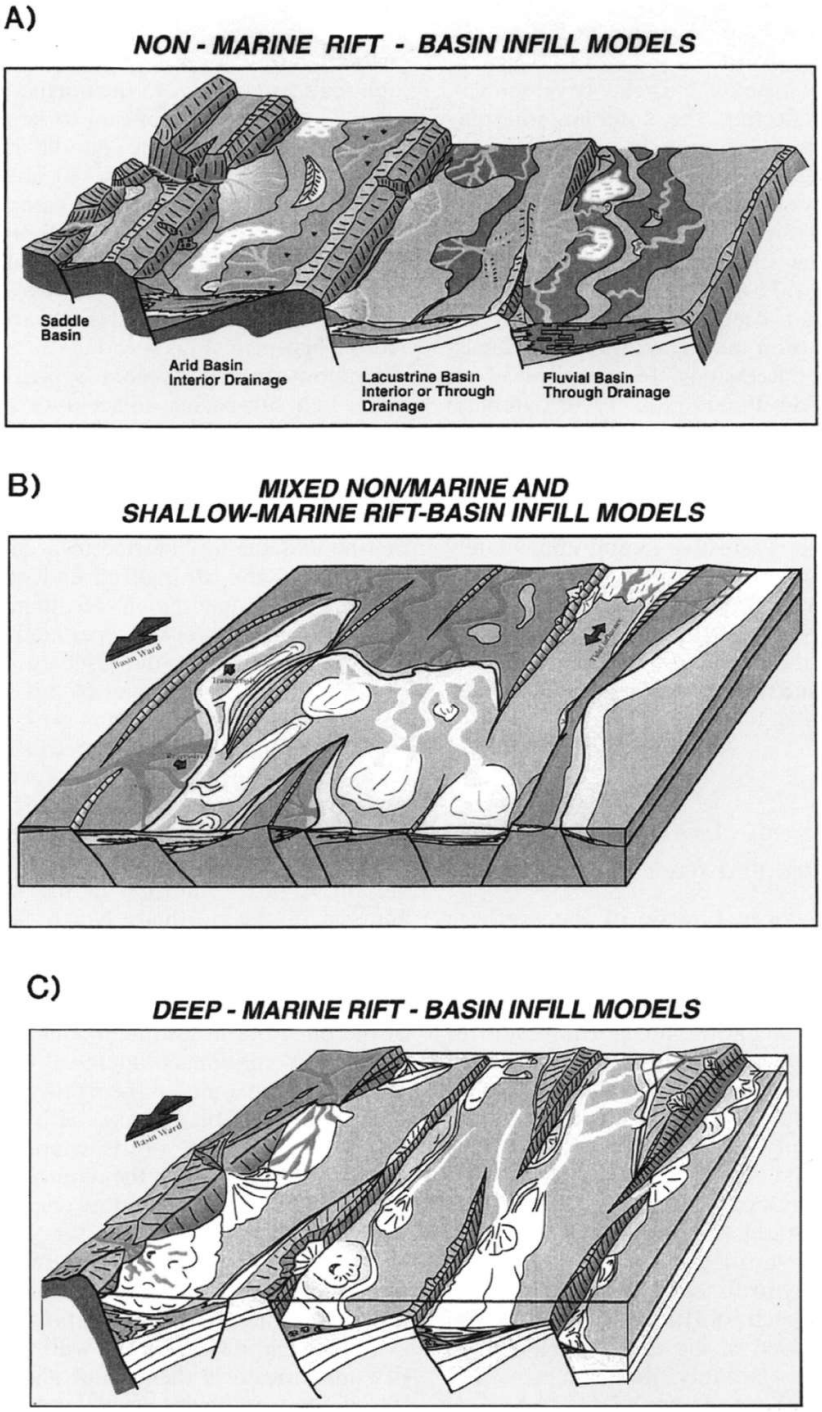

Figure 2.5: Evolution of rift basin settings through time. Transition from non-marine (A), to mixed non-marine/shallow marine (B), to finally deep-marine (C) (Ravnås et al. 2000).

Rift sedimentation stages are subdivided into syn-rift (early stage, climax stage, late stage) and post-rift, being separated by the post-rift/break-up unconformity.

Early stage sedimentation in rift basins is driven by the increasing rates of fault-related subsidence as the crust undergoes brittle failure, resulting in widening of the basin and establishment of relief due to extensional faulting. Tectonic subsidence typically outpaces sediment supply, with largely fluvial sedimentation eroding down into the newly established topography, establishing drainage patterns, both interior and axial, thus developing the location of major sediment depocenters (Jackson et al. 2006). Sedimentation at this stage is primarily clastic and produced by alluvial systems. At this stage, there is only minor tilt occurring of the establishing fault blocks, as a result (when observed perpendicular to the border faults) troughs form, which deepen towards the boundary faults. Dependent upon the style of rift basin being established, there can be either one set in asymmetric rifts, or two in symmetric.

This is the beginning of the wedge-shaped geometry typically observed which is driven by progressive fault-related subsidence, rotation and subsequent infilling. Rotation is due to slip down listric faults, dips increase with further slip, which is particularly evident in seismic. Examples of the wedge-shaped geometries produced by slip along normal faults were investigated by Schlische (1991). Produced stratal geometries are dependent upon both the style of faulting that produced the depocenter (Figure 2.6), as well as the relationship between accommodation and sediment supply.

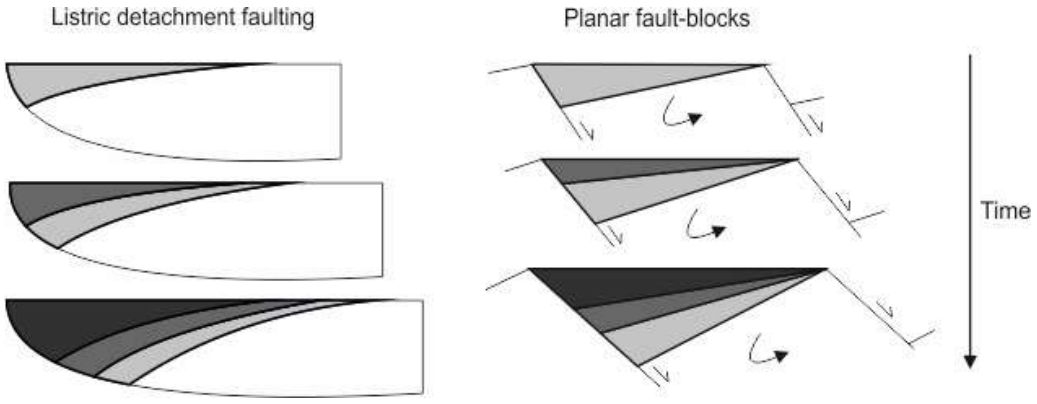

Figure 2.6: Observed differences in sediment infill geometries between listric detachment and planar fault-blocks. The original fault angle in fault-block settings increases due to the rotation of the planar faults (Modified from Schlische 1991).

At this stage drainage is still closed and any carbonate generation is in competition with ongoing fluvial sedimentation. Lacustrine settings begin to persist at the shallowest level of the basin, against the footwall. As subsidence continues, marine conditions become more pervasive and migration of the shoreline is controlled by the rotation and subsidence occurring within the half-graben producing accommodation, also coupled with the hinterland providing sediment supply. Steep gradients (stratal dip), typically around 2-3 degrees are common, however more extreme dips are attainable, with up to 10 degrees being observed in Late Jurassic sub-basins of the northern North Sea (Færseth et al. 1995). The rotation is a rapid process, driven by simultaneous subsidence of down-dip areas and uplift of up-dip.

Over time, basin linkage occurs through either burial (due to sedimentation) or breaching (due to subsidence / eustatic rises) of relay ramps which drives the rift from being hydrologically closed to open. The evolution of relay ramps (Ellis and McClay, 1988) has been shown to be highly influential on sediment pathways, governing the evolution of both marine and continental systems (Athmer and Luthi 2011). Though channel incision is also a possible mechanism for breaching of closed drainage systems, possibly prevailing over the tectonic effects of foot-wall uplift (Hemelsdaël and Ford 2014). However, if the incision rate of the channel is outpaced by the foot-wall uplift, then sediment flow may be redirected away from the fault, resulting in drainage reversal.

Syn-rift successions can have vastly different stratigraphic architectures dependent upon the sediment supply to accommodation ratio. The two logs (Figure 2.7) demonstrate idealised stratigraphic successions for sediment-underfilled/starved and sediment-balanced/overfilled. The general trends exhibited are an overall fining-upward signature for underfilled/starved basins, whereas with balanced/overfilled settings there is an initial period of fining upwards during rifting, which develops into a coarsening upwards succession in the late stage.

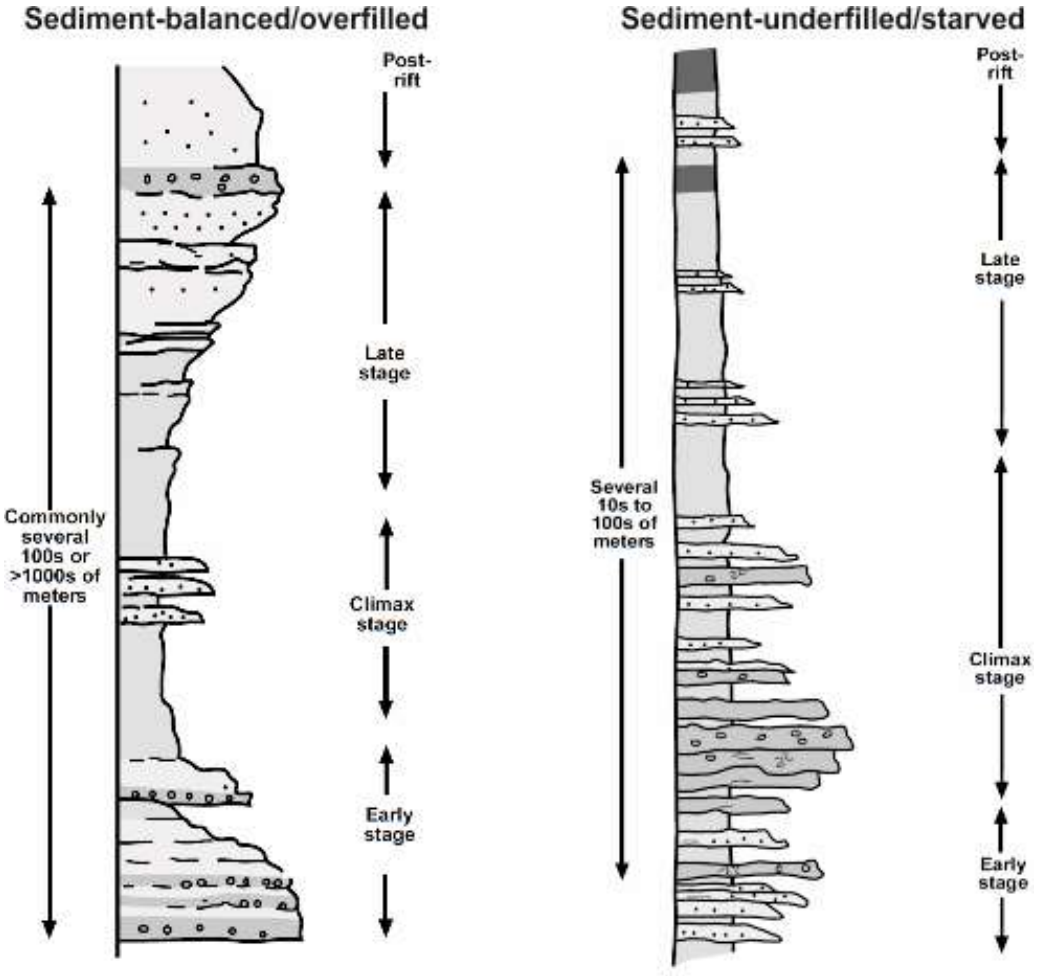

Figure 2.7: Schematic logs for two basinal syn-rift successions showing differences in deposited successions depending on the relationship between accommodation creation and sediment supply (Modified from Ravnås and Steel 1998).

In the early stage, both rifts are subject to increasing rates of subsidence as a result of faulting, which is occurring as the basin is widening. Sediment-balanced/overfilled commonly exhibit a fining upwards sequence at this stage, with aggradation. Sediment-underfilled/starved can have periodic coarsening upwards packages due to re-sedimentation of weathered material, even though subsidence outpaces supply.

At the rift climax stage high rates of tectonic subsidence outpace sediment supply in both examples. Within sediment underfilled/starved settings there is a fining upwards of the succession which continues through to post-rift settings because the sediment supply can no longer keep up with subsidence, especially with drowning of most clastic source areas. Within balanced/overfilled settings, aggradational/backstepping successions are deposited as the sediment supply starts to lag behind tectonic subsidence.

The differences between sediment balanced/overfilled and sediment starved successions are stark, owing to the established relationship between accommodation and sediment supply. In sediment balanced/overfilled settings, the sediment supply either outpaces or keeps up with the tectonic subsidence, producing a coarsening upwards succession into shallower settings. This consists of progradational sequences, marking a transition into shallower settings. Within the underfilled/starved settings, pervasive open marine conditions result in low energy, deep marine deposits. There is also potential for source rock development in these settings. Turbitite packages marking particularly high energy events can also occur.

2.4 Carbonate Sedimentation

Within depositional settings the water level dictates the exclusive production of carbonate in marine and lacustrine realms. A complication, relative to siliciclastic sedimentation, is carbonates are not only eroded and transported into basins but are also produced in-situ by organisms (Schlager 2005). Within active rift settings, isolated carbonate platforms are the most prevalent type of platform, forming on isolated highs driven by extensional faulting (Dorobek 2008). Though if the block is not fully submerged, the surface available for colonisation is reduced. The relationship between subsidence, fault movement and carbonate production are constantly in a delicate balance, with the active carbonate platform needing to exist within a production window, otherwise it will either be subject to erosion, if sub-aerially exposed, or drowned if subsidence exceeds production for a sufficient length of time (Schlager 2005). In between those two end-member scenarios, the accumulation versus accommodation will exert a strong control on the developed architecture, determining progradational, aggradational or retrogradational stacking patterns.

All large accumulations of carbonate are determined by mixtures of three distinct precipitation modes (Schlager 2005) (Figure 2.8):

- Abiotic, which dominates when there is an absence of biotic effects.
- Biotically induced, implies that the organism begins the activity of precipitation, however organic influence has a negligible effect. Products of this method are commonly indistinguishable from abiotic.
- Biotically controlled, the organism determines the location and length of process, as well as commonly the composition/crystalline structure of the mineral. Skeletal material can further be subdivided into: photo-autotrophic (e.g. cyanobacteria/algae) and heterotrophic (e.g. foraminifera/molluscs) organisms.

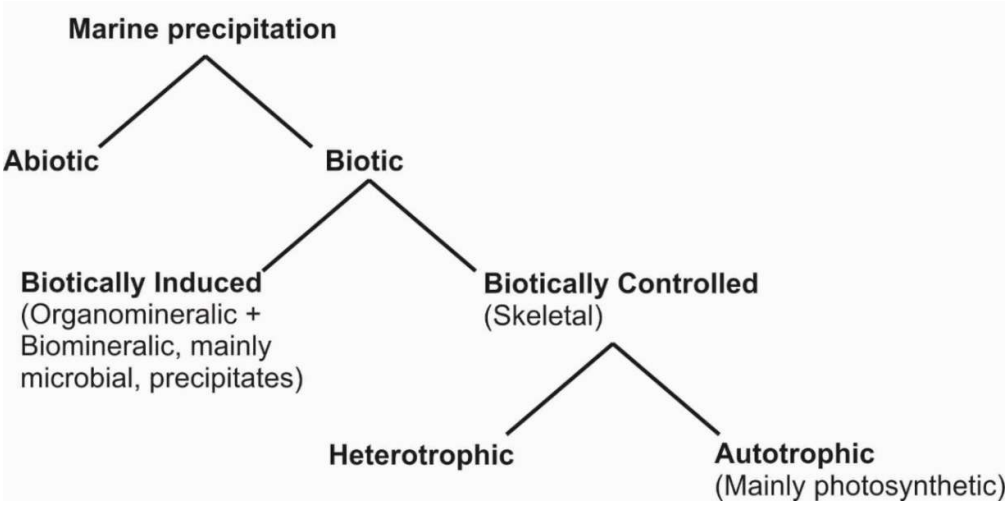

Figure 2.8: Different modes of carbonate precipitation and their relevant factories (Redrafted from Schlager 2005).

The mixtures formed by the three precipitation modes can then be grouped into three 'factories' which differ based upon the dominant precipitation mode, Mud-mound (M), Cool-water (C) and Tropical (T) (Figure 2.9). Carbonate factories are defined as benthic associations located within the photic zone, which generate carbonate material either from crystallisation of skeletal remains or precipitation from seawater (Schlager 2005).

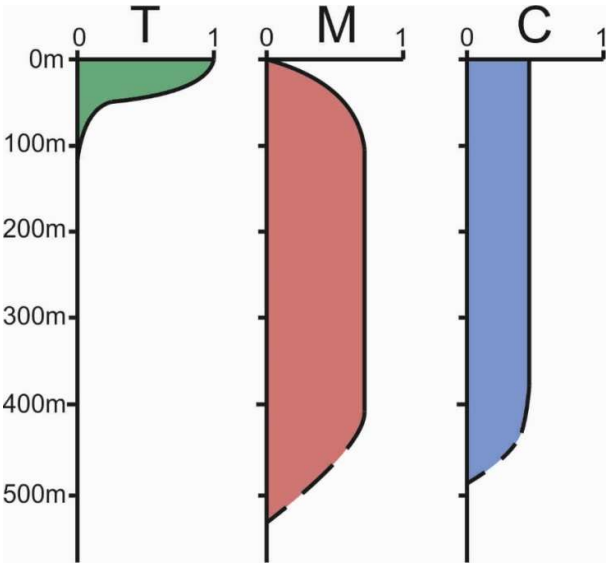

Figure 2.9: Production rates varying with water depth for each of the three carbonate factories (Redrafted from Schlager 2005). Dashed lines indicate poorly constrained data, so the profile is an approximation at that point.

The tropical factory is primarily biotically controlled precipitates, particularly photo-autotrophic, resulting in the factory dominating at shallow depths (typically at maximum 100m). Abiotic precipitates such as cements are present. T-factory carbonates produce wave-resistant structures by framebuilding or rapid cementation, independent of shoreline position. Ramps over time evolve into rimmed platforms on the marine highs. It dominates shallow, warm waters due to needing high oxygen competition meaning low available nutrient, typically being present in lower latitudes. Drowning of this carbonate factory type however is a substantial risk due to its narrow production window.

The cool-water factory is almost entirely composed of biotically-controlled heterotrophic precipitates. Sedimentation is typically a skeletal mixture of sand-granule size, which rarely undergoes lithification. This is due to a low availability of soluble aragonite in cooler settings and results in the factory having extremely limited reef-building potential. The profile shown in figure 2.9 is driven by the factory not being in competition with the T-factory due to temperature and sufficiently high energy to not allow burial by clastics. Due to being both photic and aphotic, the production window is wide.

The mud-mound factory is developed by the interplay between mud-mounds, micrite and microbes which produce a characteristic fine-grained carbonate hardground in-situ. Typical setting is low light and high nutrients, usually environments low in oxygen, but not fully anoxic. Lithification is rapid and can potentially extend over thousands of cubic metres. The factory has potential to build platforms and develops rims at shelf edge. Production is also possible around methane seeps in deep sea settings.

The precipitation of carbonates by the three factories typically dominates on positive areas of blocks, though these can also be affected by siliciclastic input, commonly this occurs due to upwards filling of the accommodation. The lows can also be subject to carbonate deposition, providing that production is able to keep-up with subsidence rate and they are not being buried under excess siliciclastic material. As is common with marine syn-rift systems, initial deposition is in the form

of a transgressive succession, typically of siliciclastic to mixed facies, unconformably above faulted pre-rift basement.

Figure 2.10 displays a typical distribution of syn-rift carbonate platforms. At this stage, land-attached platforms are rare. Commonly, highs of tilted fault blocks provide a more readily available substrate for factories to dominate on. The specific geometry of the block can result in different platform characteristics developing (Dorobek 2008). Combined with the effect of wind, this can produce asymmetrical facies distributions due to energy differences. Localised, fault-controlled differential subsidence is pervasive, which combined with fault growth, linkage and interaction exerts a controlling effect upon sedimentary distribution (Dorobek 2008).

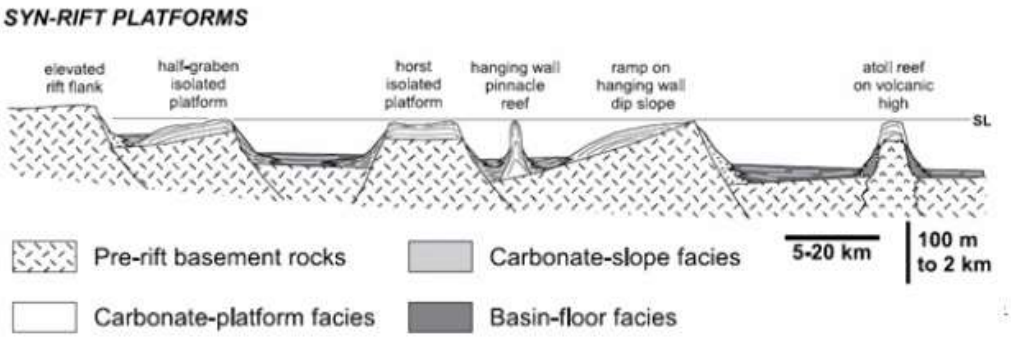

Figure 2.10: Schematic diagram displaying typical carbonate architectures developed within syn-rift settings (Dorobek 2008).

As extension continues, active carbonate platforms can also be cut by faulting. This then leads to two potential end-member outcomes (Fabbi and Santantonio 2012). Either sedimentation is rapid enough to keep pace with the fault slip, resulting in the carbonate platform continuing to be laterally continuous across the fault blocks. Alternatively, the subsidence will outpace sedimentation, drowning the hanging wall, with carbonate production continuing on the foot wall.

Within transfer and accommodation zone settings, platform geometry will largely be dependent upon structural configuration. Transform faults yield aggradational margins (Cross and Bosence 2008), however, relay ramps, because of limited subsidence, exhibit progradational stacking patterns. Commonly these progress from low relief ramps into escarpment margins (Wilson et al. 2000). The impact of

relay ramps upon carbonate platform evolution is currently poorly understood, with a systematic study yet to be conducted.

As rifting continues into the late syn-rift to early post-rift phase (Figure 2.11), land-attached platforms may begin to develop due to ongoing subsidence or erosion of riff-flank uplift. Within land-attached platforms, clastics can also be present, producing mixed sequences (Cross and Bosence 2008). The previously isolated platforms which dominated during early-mid syn-rift stages may also begin to coalesce into larger, composite platforms (Schlager 2005). Drowning of outboard platforms of reefs can also occur due to rapid subsidence.

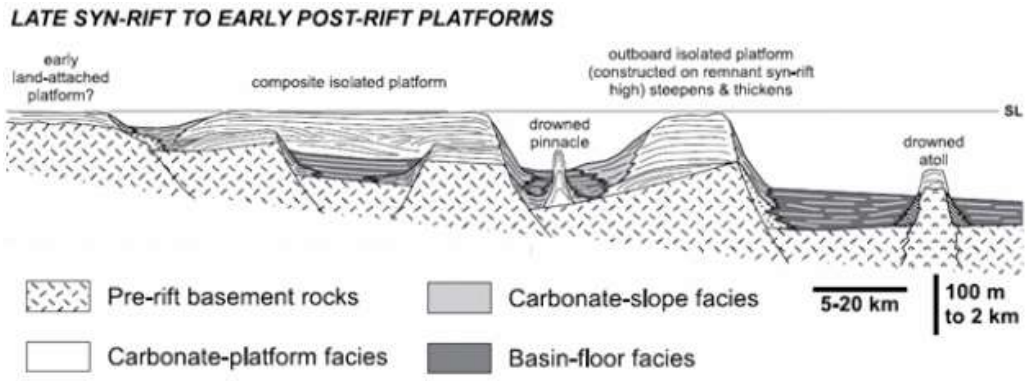

Figure 2.11: Schematic diagram displaying typical carbonate architectures developed within late syn-rift to early post-rift settings (Dorobek 2008).

3 Modelling Background

3.1 Analogue Modelling

3.1.1 Overview

This section provides a background to the analogue modelling materials and techniques employed in the process of this project. Specific details pertaining to experiments run will be included within subsequent Chapters.

Ever since the first documented analogue experiments over two centuries ago by Sir James Hall (1815), the technique has developed from an abstract representation to a fully quantitative technique for simulating a suite of geological processes, with a summary of major developmental changes provided by Koyi, 1997. The relative simplicity of this physical modelling approach and the insights it yields have driven interest, leading to its well-known application. Laboratory-scaled experiments enable observation and quantification of both spatial and temporal evolution of tectonic deformation. As a result of this, deformation processes and the governing parameters can be systematically investigated, with the findings directly applicable to ongoing economic exploration.

Analogue experiments are typically driven using electrical or mechanical forces and are split into two main categories: natural-gravity models (using the Earth's gravitational field) (Figure 3.1) and centrifugal (using rotational forces to produce enhanced gravitational forces). Centrifugal models typically have a limited size which can impact upon resolution, as well as having only very limited monitoring during deformation, detailed photos or laser scans can only be undertaken once the model is removed from the centrifuge after each model run (Corti et al. 2004). Given that syn-kinematic sedimentation and model scanning is a cornerstone of this project, centrifuge models, if available, would be unsuitable, therefore all work contained within this document utilises natural-gravity modelling.

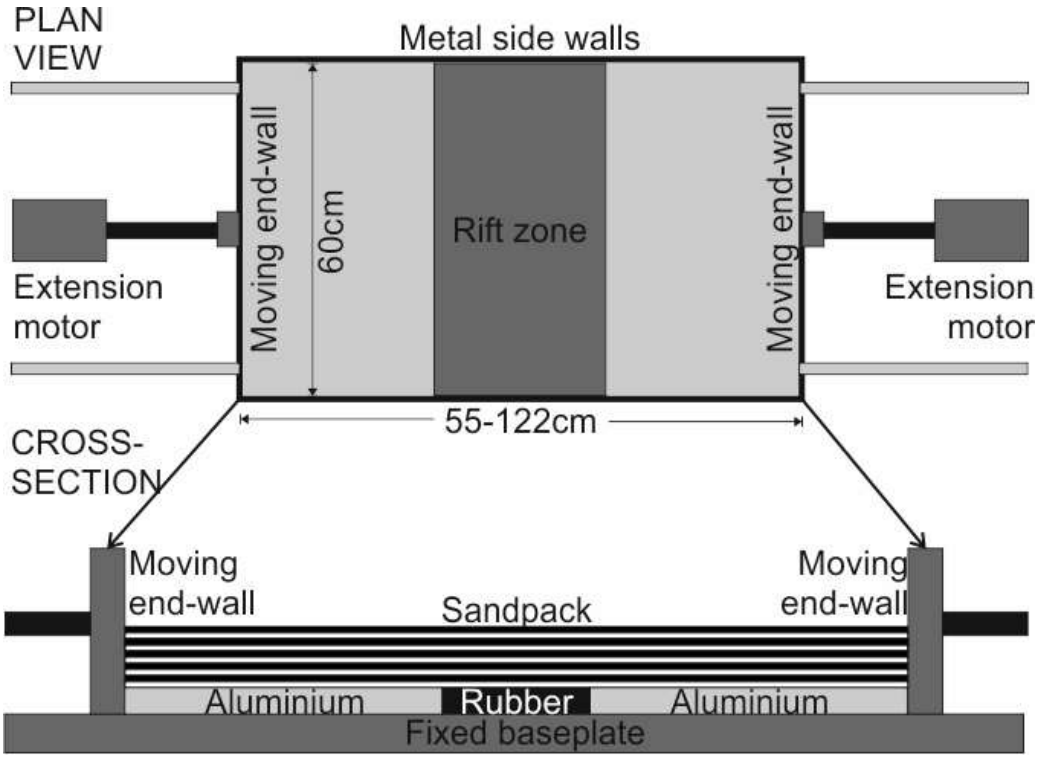

Figure 3.1: Schematic of an example 3D rift setup for analogue modelling experiments. Two motors attached to mobile end-walls enable either symmetrical or asymmetrical extension of the sandpack depending upon whether one or both are active. The extension is accommodated by a rubber sheet which can be stretched laterally (Based on McClay et al. 2004).

The first sandbox modelling experiments were conducted by Cadell (1889) investigating the formation of fold and thrust belts in the Scottish Highlands. Over time, the continued efforts in this area of research have successfully simulated geodynamic processes, providing insights to the complex tectonic patterns and evolution of rift systems.

Within the context of this thesis, efforts seek to apply the developed methodology to kinematic analogue models, specifically extensional. An example extensional apparatus is pictured below in Figure 3.2. Models typically produced within the labs at Royal Holloway (e.g. McClay and Ellis 1987; McClay 1990; McClay et al. 2004) have an initial, 'pre-kinematic', mechanical stratigraphy deposited, which is then extended at a suitably scaled rate (an overview of alternate analogue model setups, which are beyond the scope of this study, are provided by Zwaan et al. 2019). Whilst extension is ongoing there is the option to input further granular material to the produced accommodation, representing syn-tectonic sedimentation and imparting a tectonic loading. Commonly the kinematic motion is driven by motors,

with stretching accommodated either by a plastic/acrylic sheet detachment above a footwall block or a rubber sheet connecting two metal plates. Depending on the geometry of the rubber sheet, the rift can be controlled to be symmetrical/orthogonal/oblique. 2D glass-sided deformation rigs can also be employed to permit detailed monitoring of internal evolution, despite the zones adjacent to the glass being affected by friction, they are argued to be valid as the same structures are commonly observed along strike, deeper within the model, even if slightly laterally offset (Zwaan et al. 2016).

An alternate analogue modelling apparatus (Figure 3.2) is used for work within this thesis. Originally used to conduct analogue modelling of inverted domino-style basement fault systems by Jagger and McClay (2018), the setup consists of four angled metal plates which simulate rigid domino-style basement fault blocks. Extension, and later compression, is accommodated by a motor-driven worm screw which is attached to an underlying trellis attached to the fault blocks. This setup permits progressive rotation and development of syn-extensional growth strata which are being deposited.

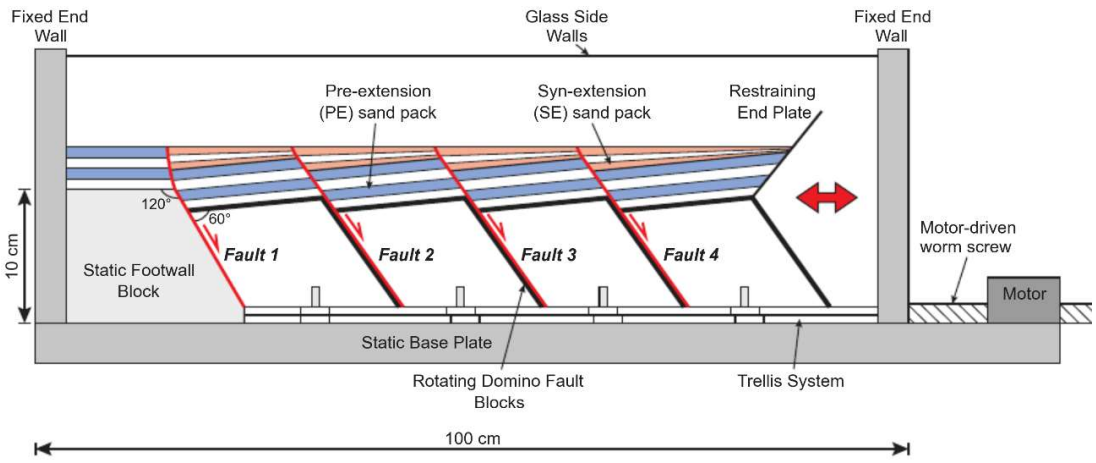

Figure 3.2: Schematic of the 2D deformation rig capable of modelling extension and inversion of domino-style basement fault systems. Blue–white layers overlying the rigid basement blocks indicate the pre-kinematic sandpack. Red–white layers indicate the syn-kinematic sandpack (Jagger and McClay 2018).

For work within this thesis the apparatus is simply used to model extension, however Jagger and McClay (2018) modelled inversion, producing characteristic hangingwall 'harpoon' stratal geometries and asymmetric contractional fault-propagation folds which have been observed in natural examples (e.g. West Nantuna Basin, Indonesia (Burton and Wood 2010) and Southern North Sea (Jackson et al. 2013).

Other recent analogue modelling experiments have investigated a wide range of different factors: how rift style affects subsequent deformation (Corti 2008), what influence lithosphere rheology structure has on rift architecture (Brun 1999), factors determining the style of extension (Michon and Merle 2003), development of strain bands yielding insights to extension related faulting (Adam et al. 2005), how extensional deformation is affected by magma injection (Corti et al. 2003), how the geometry of normal faults is related to the presence of décollement levels (Vasquez et al. 2018), how syn- and post-extension sedimentary patterns have a major influence on the evolution of diapirism and configuration of basins (Moragas et al. 2017).

3.1.2 Scaling

Extensional sandbox models are, in essence, simplified laboratory replicas of natural rift systems and have been shown to be representative of natural processes if sufficient similarity in the scaling of parameters such as geometry, density, time is met (Brun et al. 1999), as they are effectively undergoing the same evolution as in nature, just at a smaller scale and over a shorter duration. The scaling ratio for a parameter between the model and natural prototype is given by the model quantity divided by equivalent natural quantity (Hubbert 1937). Analogue experiments are split into three types of similarity, all of which need to be achieved for a model to be appropriately scaled: geometric, kinematic and dynamic (Hubbert 1937).

Geometrical similarity is defined as when all equivalent lengths are proportional, and angles are equal between the model and natural example. Within this thesis, the derived geometric scaling of silica sand is 1cm within the model is equivalent to 1km in nature (Schellart 2002).

Kinematic similarity is achieved when a geometrically scaled analogue model undergoes changes of shape and/or position over a proportional timescale to that of its natural counterpart. Time scaling (t) enables accurate sedimentation rates required to simulate first order characteristics (Adam and Krezsek 2012). Dependent upon what materials or conditions (sub-aerial / sub-marine) are employed for a particular model the time scale will differ. Sub-marine conditions are subject to the water column stabilising the slope, significantly reducing the amount of gravity-driven deformation versus sub-aerially exposed basins (Gemmer et al. 2005).

Dynamic similarity is defined as when two bodies are both geometrically and kinematically similar, resulting in a similar distribution of driving and resistive forces. Dynamic scaling of experiments is of utmost importance as it enables quantitative comparison of model geometry, kinematics and stresses to the natural example (Costa and Vendeville 2002). As the degree of dynamic scaling increases,

as does the validity of the model and any drawn conclusions (Ge et al. 1997). Hubbert (1937) produced the concept of dynamic scaling, producing ratios for principal mechanical quantities (area, acceleration, velocity, density, viscosity and stress), since then dynamic scaling has been adapted to a suite of geological processes; e.g. Reynolds number is the ratio of inertial and viscous forces (Fi/Fv).

Granular materials and silicone polymer, both common analogue modelling materials, have been demonstrated to possess suitable rheological properties to be scaled to natural conditions, for example, upper crustal values for scaled cohesion and coefficient of internal friction (Byerlee 1978). However, issues arise when both polymer and sand are present within an experiment. Since frictional strength is reliant on density, both the sand and polymer need to be individually scaled, as well as the ratio between them. Despite this, recently Brun and Fort (2011) have maintained that density scaling within analogue sandbox modelling is adequate, permitting them to be defined as dynamically similar.

3.1.3 Granular materials

Dry, granular materials are a well-established tool within analogue modelling to simulate upper crustal mechanical behaviours (McClay and Ellis 1987; Lohrmann et al. 2003). The reason for using granular materials is that, when sheared, their flow systems exhibit comparable deformation processes to those observed in the upper crust (Marone 1998), characterised by a complex, non-linear deformation processes, consisting of pre-failure distributed deformation and spontaneous shear localization (Adam et al., 2005). This enables granular sandbox models to be used in the study of tectonic deformation and its related kinematics.

Analysis of granular materials can be conducted using a ring-shear tester (example data in Figure 3.3), this is to demonstrate comparable behaviour to that exhibited by experimentally deformed rocks, representing brittle deformation of upper crustal processes being modelled. Testing is conducted by filling a cell with the desired material, which is then subjected to confining pressure as a set normal stress. Increasing shear stress is then applied to the cell and recorded by software. The early period is characterised by an initial elastic strain, superseded by plastic strain-hardening prior to failure known as 'peak friction/strength', at which the material begins to flow. The material then achieves equilibrium in a state known as 'dynamic friction' or 'residual strength' at the minimal force required to keep the body flowing (Panien et al. 2006). The shearing force is then stopped, and the sand body returns to rest, at which point the shear forces are reapplied in order to test the 'static strength'.

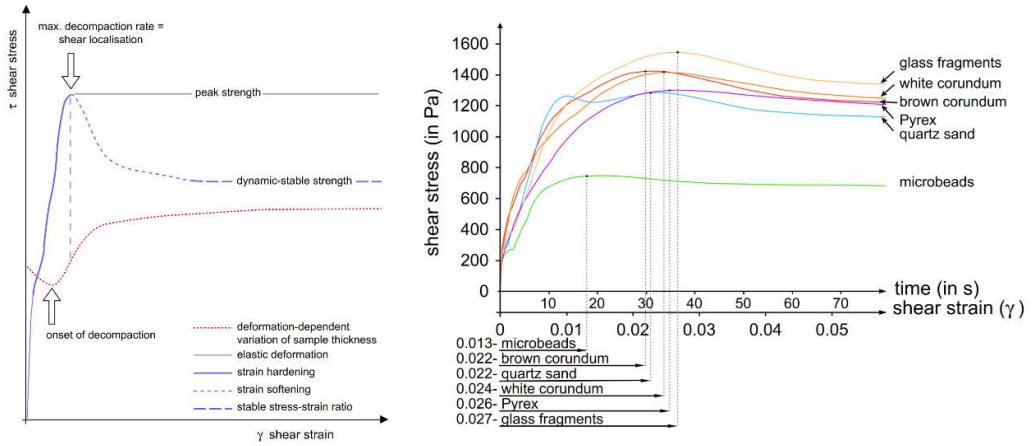

Figure 3.3: Left: A typical material testing plot shown by granular materials. Right: Different profiles shown by a range of granular materials commonly utilised in analogue modelling (Panien et al. 2006).

As the increasing shear strain is applied to the granular body, shear bands develop (as opposed to uniform deformation), this strain localisation process occurs around peak strength (Desrues and Viggiani 2004), or the point of failure where flow of the sand body begins (Krantz 1991). The shear bands represent dilatant zones where the regular arrangement of grains has been disturbed, yielding a localised area of deformation. During in plane strain experiments several bands can initiate simultaneously, however only one of these will fully mature during the strain softening which occurs after peak strength (Desrues and Viggiani 2004), representing fault development. Strain softening is dependent upon both the granular material and normal load applied, this continues until a state of equilibrium/stable value is reached, dynamic-stable strength (Panien et al. 2006) which represents continued motion of the fault. Stopping and resuming shear forces represents the force necessary to achieve fault reactivation (Krantz 1991).

Owing to their innate ability to flow, granular materials are unable to be simply classified as either a solid or fluid (Lohrmann et al. 2003). The volume of the initial diffuse deformation prior to peak friction is dependent upon properties such as grain shape, sorting and deposition technique. Higher sphericity/better sorted materials are subject to smaller amounts of diffuse deformation, which is largely why microspheres have become popular as they enable narrower fault zones to

develop, providing more structural detail and better scaling (Schreurs et al. 2006). A summary of common granular materials is provided in Figure 3.4.

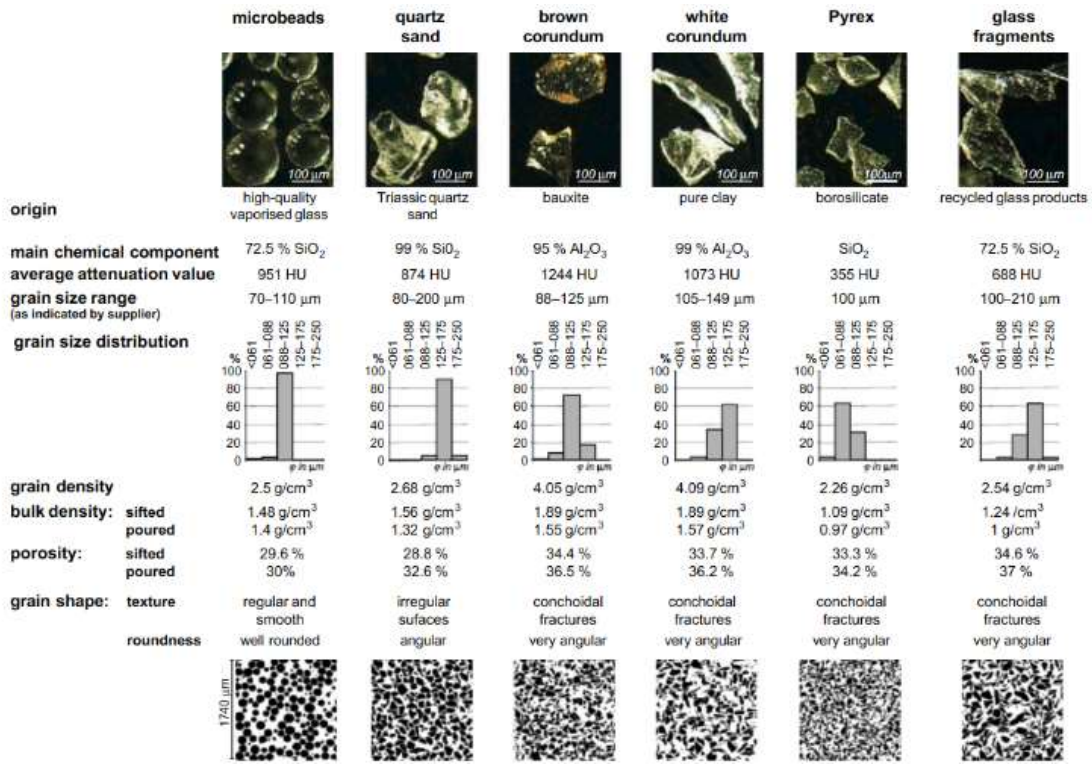

Figure 3.4: Physical characteristics of several granular materials to demonstrate the availability of variable properties (Modified from Panien et al. 2006).

Pure quartz sand is a widely used granular material and under normal gravity conditions portrays the upper crust as a brittle, homogeneous material. This approximation has been validated for first-order analysis of tectonic processes (McClay and Ellis 1987), however, recently it was shown that granular materials deform in a more complex manner. Lohrmann et al. (2003) demonstrated that pure quartz sand is characterised by pre-failure strain hardening and post-failure strain softening which continues until a stable value is reached, with the failure properties of granular materials being characterised by the coefficient of internal friction (how particles slide against one another) and cohesion (amount of shear stress the material can withstand when not confined by a normal stress). Whilst this was

demonstrated to affect the kinematics of upper crustal deformation in sandbox experiments (Lohrmann et al. 2003), the behaviour is still sufficiently like that exhibited by upper crustal rocks that previously drawn conclusions were still valid.

Natural sedimentary successions, however, are not homogeneous and have mechanical variations within the layers. These have been replicated in sandbox experiments by adding intermittent layers of vermiculite (McClay 1990) in order to yield a mechanical anisotropy within the sandpack. However, this can introduce issues with rheological scaling of the interfaces between these layers and the main sandpack which is problematic when analysing individual structures (Rossi and Storti 2003).

Artificial granular materials have also been developed such as glass microspheres (Krantz 1991) or siliceous microspheres (Rossi and Storti 2003). Microspheres have high sphericity, low density and negligible cohesion. As a result they can also be used to impart anisotropy or alternatively simulate other processes such as decollément layers. This is due to their high sphericity driving reduced cohesion and producing a lower coefficient and angle of internal friction than pure sand (Schreurs et al. 2006). Another characteristic of the artificial granular materials is potential for extremely fine particle size coupled with a high sphericity, which can be used to produce repeatable, thin layers. When combined with narrow fault zones, this yields more structural detail and better scaling than coarser counterparts (Scheurs et al. 2006).

Alternative granular materials that can be used are brown/white corundum and Pyrex which are primarily used in order to signpost layering when analysing models with X-ray CT scanners. This is because they have nearly identical mechanical properties, but markedly different attenuation values (Panien et al. 2006) (the reduction of the imaging beam's intensity by the material through which it passes).

3.1.4 Impact of preparation techniques

When depositing granular materials, there are two main methodologies in use, pouring and sifting (also referred to as sprinkling). Multiple works have demonstrated that dependent upon the method of deposition the coefficient of internal friction will vary by approximately 10-20% (Krantz 1991; Schellart 2000; Lohrmann et al. 2003). This has been observed in both sandbox experiments and ring-shear tests. This differentiation occurs as a result of dissimilar packing and manifests itself by different fault localisation or dip angle. Specifically, sifted grains have lower porosities, manifesting with a tighter packing arrangement, producing higher densities than materials which are poured. Due to this tighter packing in sifted materials, the grains have less ability to be rearranged by shearing forces, manifesting as a higher internal friction coefficient. The shape of the grains has been shown to affect cohesion; however, the actual grain size and sorting have been concluded to have a negligible effect (Schellart 2000).

Granular materials within analogue experiments are also often subject to additional manipulation after they have been sifted/poured onto the analogue stage, typically by scraping the surface using a height-adjustable guide and rail system. This yields sandpacks with near perfect planarity, however uniformity and reproducibility of local density are unknown due to the manipulation (Maillot 2013). To address this, wholly mechanical approaches to material deposition have been explored, as even when extreme care is used whilst depositing by hand, there will still be differences in mechanical properties that arise because of human error. For example, Maillot (2013) produced a device capable of depositing mechanically uniform, reproducible sandpacks, which is also argued to be more time efficient than traditional methods (Figure 3.5).

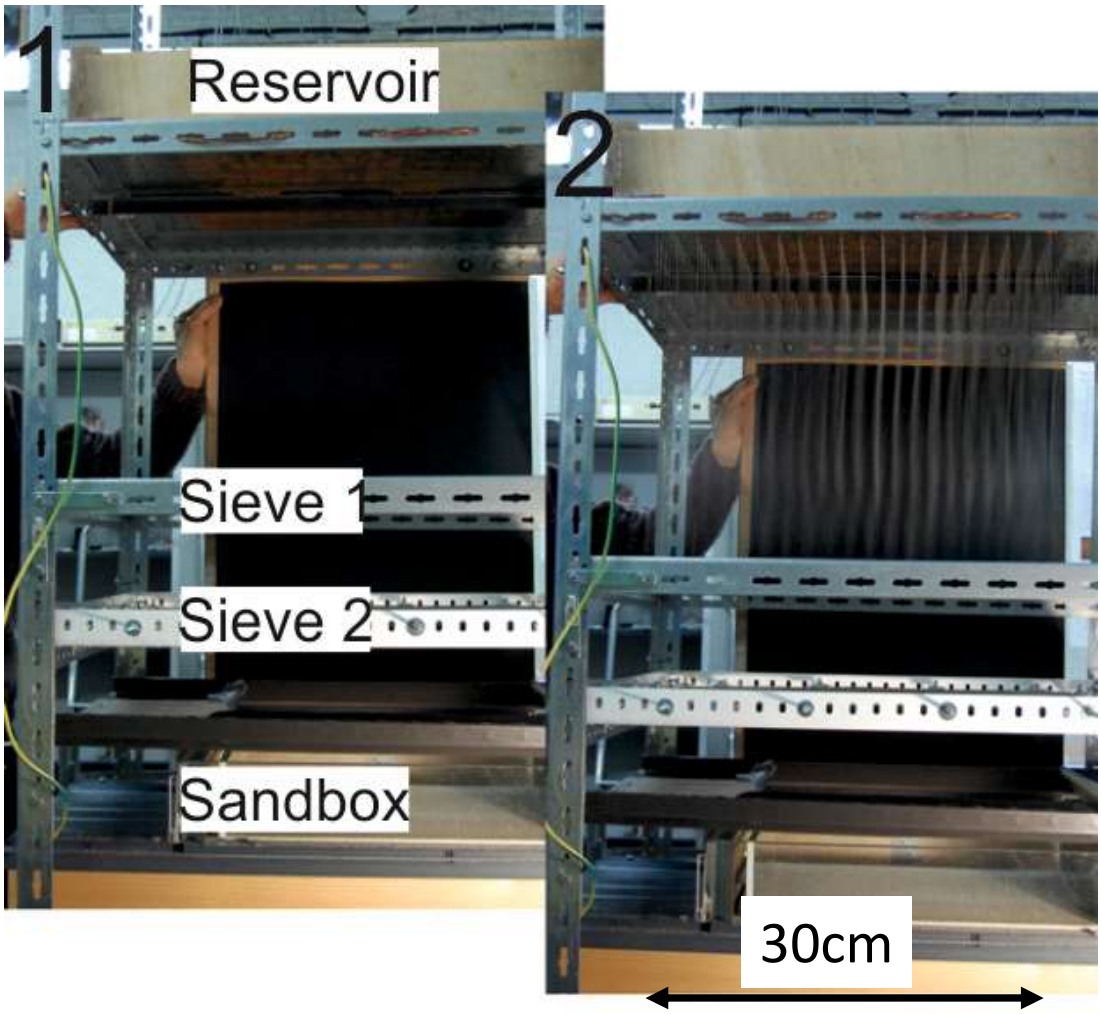

Figure 3.5: Mechanical sieving device produced by Maillot (2013). Granular materials are loaded into the reservoir and positioned over the experimental surface. Flow is then initiated by aligning holes in the reservoir base and passes through multiple sieves to produce a uniform falling pattern of sand onto the model surface below.

3.1.5 Experimental analysis

Non-destructive methods for data extraction from ongoing analogue experiments has been a rapidly evolving field, due largely to the fact that each analogue experiment run is effectively unique. The exact construction cannot be replicated; therefore, it has become vital to extract sufficient data without interfering with model evolution. The overall evolution of analogue models is of importance; however, the deformation also needs to be quantified (strain field/particle kinematics), and since inhomogeneous deformation in the form of strain localisation means that individual point measurements have only nominal importance, full-field measurements are necessary (Hall et al. 2012). Spatial and temporal evolution of strain distribution yields insights to the brittle deformation kinematics of the complex 3D structures forming. When fully quantified, this data can act as a proxy for tectonic fracture formations and be used in reservoir modelling (Adam et al. 2013).

Though not used within this work, non-destructive internal visualisation of the sandpack and related kinematic evolution is enabled by use of XRCT (X-ray computer tomography) which relies on different attenuation values within the sandpack to visualise internal structures at a high enough resolution to distinguish individual grains (Zwaan et al. 2016; Zwaan and Schreurs 2017). This enables 3D analysis of porosity, grain contact geometries and distributions. However, to understand the kinematics and deformation occurring 4D analysis needs to be introduced. The primary issue with XRCT monitoring is that the use of different granular materials to enable internal visualisation can impart unwanted anisotropy on the sandpack.

PIV (Particle Imaging Velocimetry) is a technique which enables calculation of velocity or flow patterns acting in fluids and gases, monitoring discrete grains and subsequent translation (Adam et al. 2005). 'Seeder' particles are purposefully mixed in with the flow pattern and can be tracked by optical cameras in either 2D or 3D. The captured images are correlated together, producing displacement data from the translation and distortion of successive images at a grain-scale resolution.

PIV has since been adapted to be used within analogue experiments, enabling investigation into structural evolution, strain localisation and surface processes in a new workflow known as DIC which enables quantitative results to be directly correlated with numerical examples.

Optical DIC (Digital image correlation) is a tool used for investigating the spatial transformation of surfaces in a series of recorded images (Figure 3.6). Its application enables sub-millimetre measurement and full quantification of incremental 2D/3D displacement fields and resultant strain affecting surface sand grains at a high spatial and temporal resolution at all appropriate scales (Adam et al. 2005; Adam et al. 2012) (Figure 3.7). Strain analysis can then be conducted which yields horizontal displacement, vertical displacement (subsidence/uplift) and horizontal strain, enabling quantification of structural evolution in both time and space. DIC has become the preferred monitoring tool and is to be used for the experiment runs conducted within this study, specifically 3D stereo DIC capturing time-series stereoscopic images of the model surface.

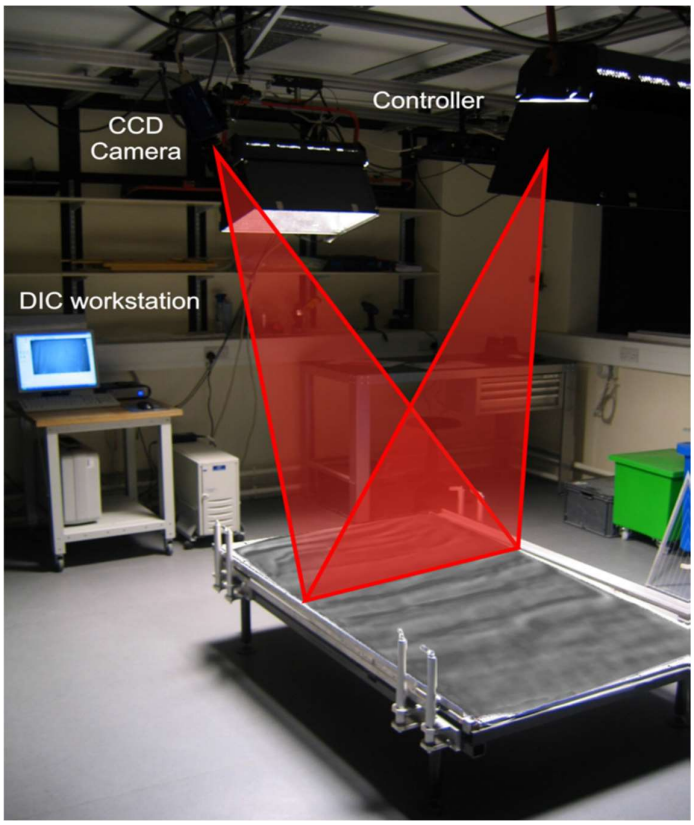

Figure 3.6: DIC monitoring apparatus in stereoscopic setup. (Adam et al. 2012)

DIC functions by full-field rigid body translations. Local evaluations of cubic subsets covering the model surface are calculated. Since digital images consist of discrete values, some interpolation is required in order to achieve sub-voxel accuracy when evaluating the transformation. 'Standard' or 'Continuum' DIC assumes a continuous displacement field. Therefore, when strain is being derived from displacement affecting separate subsets, continuity is implicit. Subsets are evenly spread across the area being examined. Alternatively, a 'Discrete' or 'Grain ID-tracking' DIC approach may be used, which recognises granular characteristics of both the captured images and the mechanical response. In this approach, the subsets are no longer regularly spaced, and are affixed to individual grains, following their profile. The subsets are assumed rigid, therefore subsequent 3D motion implies three component translation vector and rotation.

The digital cameras employed by the DIC technique yield a far higher resolution than standard XRCT images, more accurately analysing grain-scale deformation patterns. Additionally, DIC has the capability of high frame rate capturing, this is because the computational analysis occurs after the experiment is complete, so the only limiting factor is the capture rate. Recently, DIC and XRCT methods have been integrated (Adam et al. 2013; Zwaan et al. 2018), this has produced a tool capable of examining 3D structure and kinematic evolution within scaled analogue experiments, as well as being able to fully quantify strain in both time and space.

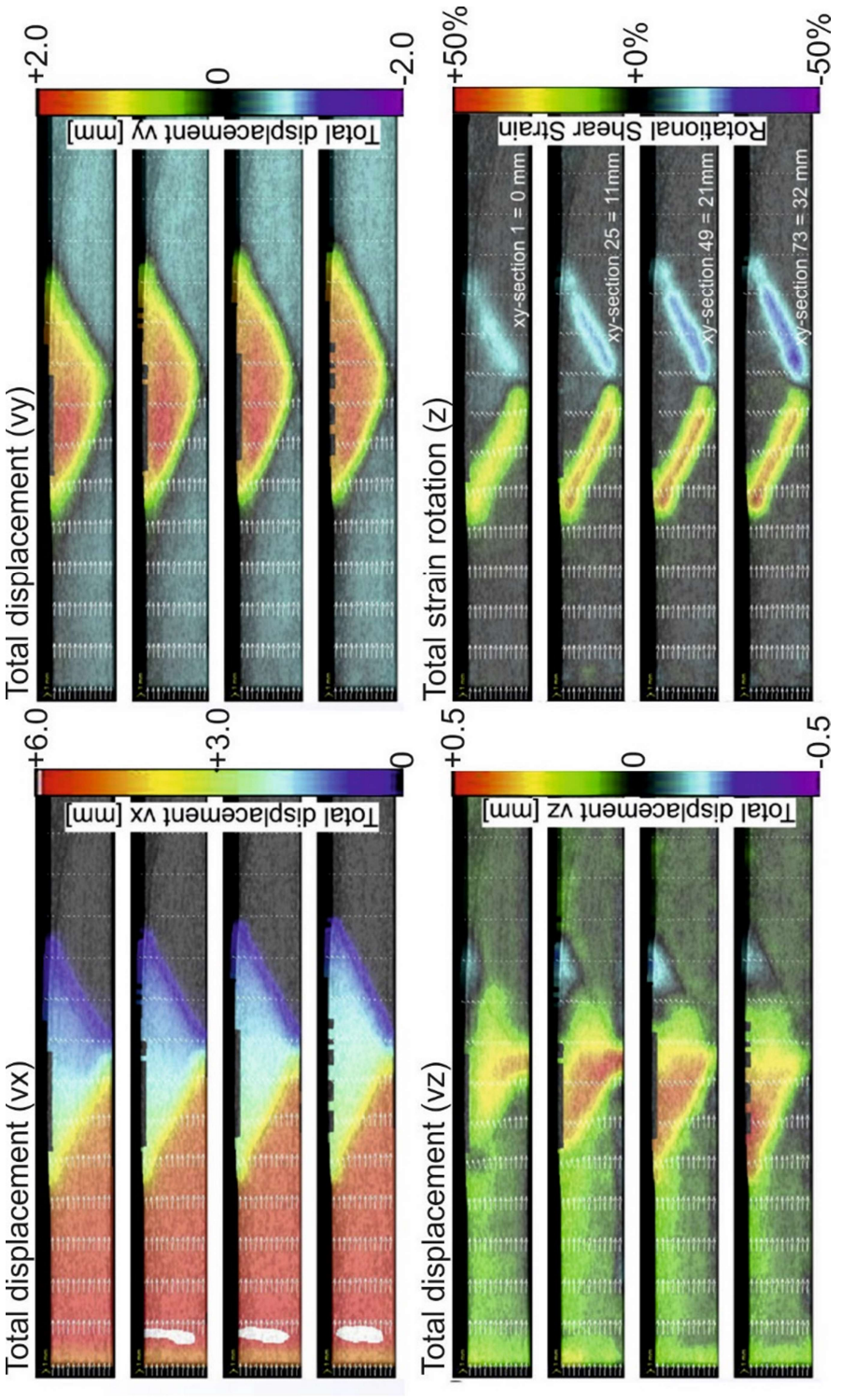

Figure 3.7: Example displacement and strain quantification data provided by monitoring apparatus. Images show stacked XRCT voxel space data from a shortening experiment displaying the 3D displacement and strain localisation which is developing shear zones. Data is cross-sectional, with the direction of shortening from left to right. vx (horizontal displacement parallel to shortening), vy (vertical displacement), vz (horizontal displacement normal to shortening) (Adam et al. 2013).

Once model evolution is complete, models are commonly sectioned to permit cross-sectional analysis (Figure 3.8). This is a destructive process, whereby the model is preserved by saturation with a gelling agent and sliced in thin intervals (typically around 0.3-1cm) and photographed as progressive sectioning occurs.

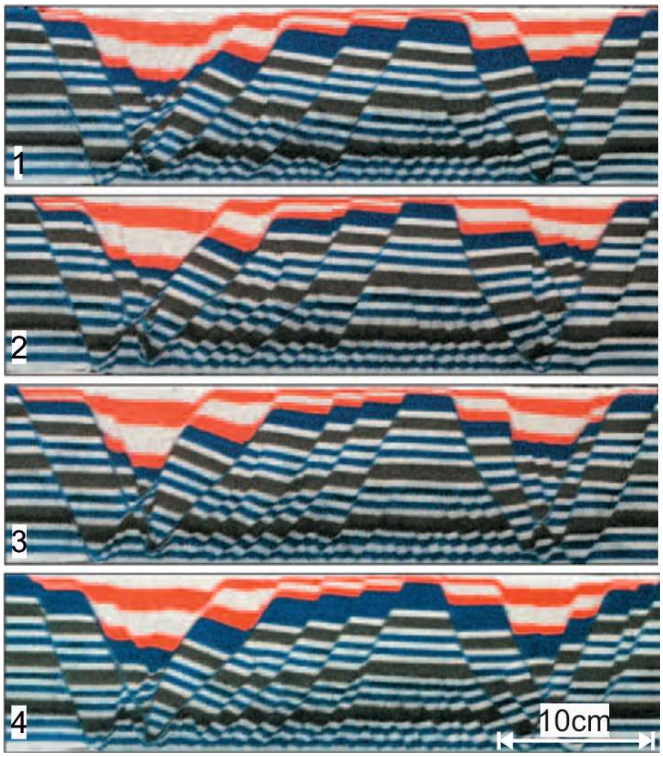

Figure 3.8: Example serial sections taken through an orthogonal rift experiment. 3cm gaps between each image (McClay et al. 2004).

Sectioning of analogue models enables an investigation into the internal structure. Whilst structural evolution can also be imaged through X-ray tomography, with use of materials with different attenuation values, the observed resolution is comparatively poor to the data obtained with sectioning. Once sliced, the cross-sectional data can then be interpreted and compared to natural case studies. Furthermore, it can be digitised and then investigated in 3D; this reconstruction process has greatly improved visualisation of complex fault geometries (Sugan et al. 2014).

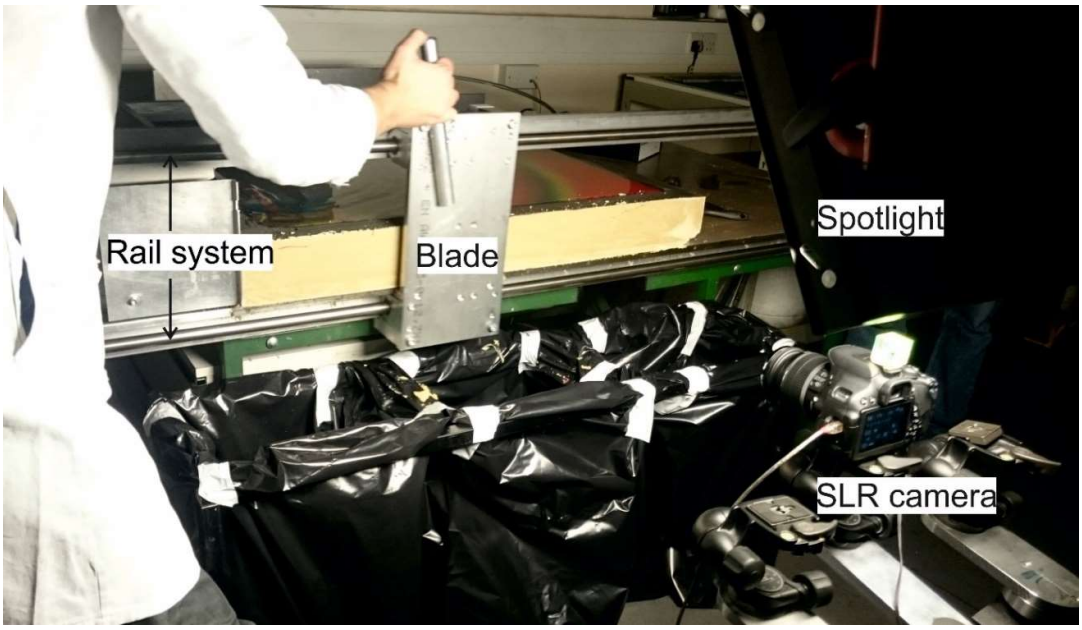

Figure 3.9: Image showing sectioning of a completed sandbox model. The incremental thickness to be sectioned is pushed over the edge of the table using a stepper motor. Then a blade (located behind the safety plate) is pulled along a rail-system which precisely cuts the overhanging thickness. Images are then recorded using the SLR camera.

3.2 Numerical Modelling

3.2.1 Overview

This section provides a brief outline of numerical stratigraphic forward modelling, specifically of marine carbonates, including an overview of the natural parameters/processes which are replicated within modern stratigraphic forward modellers. Work contained within this thesis entirely uses the stratigraphic forward modeller 'CarboCAT' (Burgess 2013). Specific details pertaining to the functionality of CarboCAT are included within subsequent chapters.

Stratigraphic forward modelling is a powerful tool for two primary reasons:

1. Generated models can provide a predictive representation of the subsurface, petrophysical properties from which are applicable to oil & gas exploration, groundwater exploitation/remediation or geothermal endeavours.

2. Models improve understanding of how sedimentary accumulations vary in both time and space in response to external (e.g. tectonics or eustasy) and internal (e.g. compaction or isostatic adjustments) driving factors in response to ongoing sedimentation and tectonic loading.

Computer-based stratigraphic forward modelling is a comparatively emergent field versus that of analogue sandbox modelling. Through time the number of geological processes encompassed by the modelling software (e.g. the complexity of physics governing sediment transport or ecological controls of carbonate productivity) are increasing as more computational power is available. An overview of early advances in models through time is given by Paola (2000) and specifically focussing on carbonate platforms and reefs by Dalmasso et al. (2001). Early carbonate models aimed to simply replicate larger-scale behaviour observed in nature, representing systems tracts and investigating the relationship between available accommodation

and subsequent accumulation. Over time, model complexity has increased to account for additional factors:

- Biological (biotic producers and their interactions)
- Chemical (salinity)
- Physical (hydraulic regime, temperature, light intensity)

Combinations of these have been included within more recent models (Pomar and Hallock 2008; Lanteaume et al. 2018; Burgess et al. 2019).

Numerous numerical stratigraphic forward models have simulated large-scale characteristics of carbonate stratal architectures (Bosence and Waltham 1990, Figure 3.9; Aurell et al. 1995; Williams et al. 2011), justifying the use of CarboCAT within this project to calculate basin-scale sedimentation patterns.

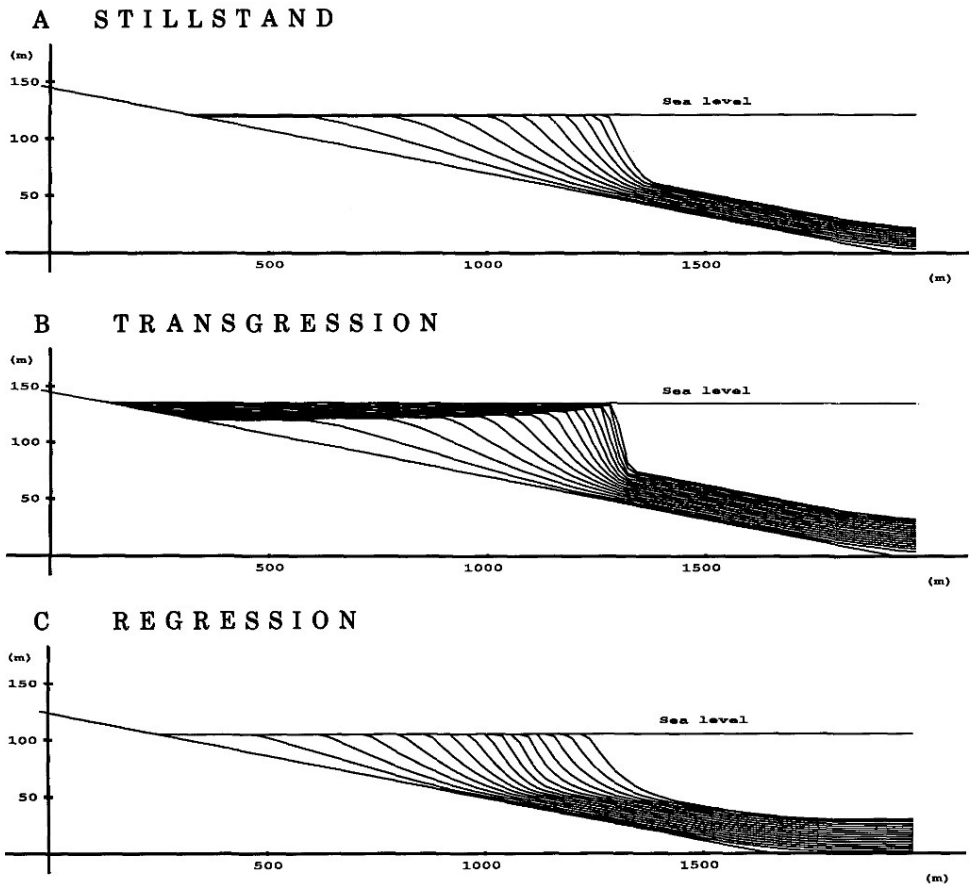

Figure 3.10: Example of an early stratigraphic forward model (Bosence and Waltham 1990). 2D computer-generated profiles of evolving carbonate platforms. A: Stillstand sequence. B: Transgressive sequence with sea level rising at 0.1m/ky. C: Regressive sequence with sea level falling at 0.1m/ky. All production values and initial slope geometry remain constant throughout the models.

Carbonate production is driven by different modes of precipitation, being divided into separate 'factories' by Schlager (2000). These are the Tropical factory (Shallow euphotic carbonates), Cool-water factory (deep euphotic carbonates) and Mud-mound factory (aphotic factory). Historically, modelling work has focussed on the tropical factory, likely due to the relative abundance of subsequent accumulations and role within petroleum systems often found in passive margin settings. Interplay of processes including; light intensity, temperature, salinity, carbonate concentration within the water column, energy and subsidence, determines which of the modes of precipitation will dominate.

3.2.2 Carbonate Production

Water depth regulates three main factors of carbonate precipitation; light intensity, temperature and salinity. As a result, most models use a depth-dependent production curve to determine the production rate of carbonate in a euphotic system. This relationship determines production at a given depth based upon the interplay of the aforementioned factors. Largely these apply a similar trend, but variations are demonstrated below (Figure 3.11):

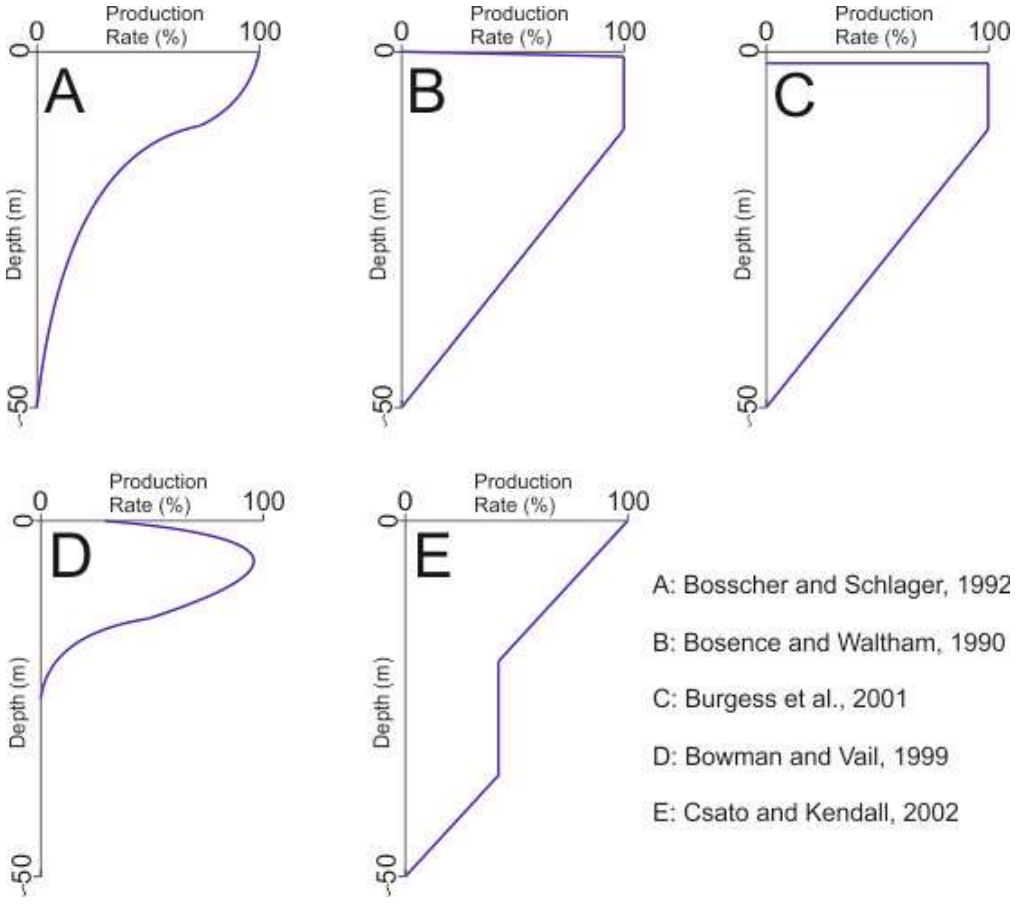

Figure 3.11: Example carbonate production curves which have been applied in different stratigraphic forward models

Some models have a decrease (B, C & D) in production close to the surface to incorporate the effect of turbidity and suspension of sediment, reducing transmission of light, a process referred to as 'poisoning' of carbonate systems (Bowman and Vail 1999).

The most prevalent production curve (A), also used within CarboCAT (Burgess 2013), is derived from Bosscher and Schlager (1992). It adapts the dependence of photosynthetic activity with light intensity through:

$$g_{(w)} = g_m \times tanh \frac{I_o e^{-kw}}{I_k}$$

- $g_{(w)}$: growth rate at depth w
- g_m: maximum growth rate
- $k_{e:}$ extinction coefficient of light
- I_o: surface light intensity
- I_k: saturating light intensity.

The growth rate derived from the above formula is then translated into production and accumulation rates for use within stratigraphic forward models. Production is simply the amount of carbonate material being generated, whereas accumulation is a representation of combined natural processes, determined by the production and subsequent transport, dissolution and compaction of carbonate (i.e. fraction of produced carbonate that remains in-situ). Models commonly assume a direct correlation between production and accumulation.

Depth also controls the energy within the water column; determining entrainment and transport within carbonate platforms being affected by water velocity. Though not used within the CarboCAT models of this project; production rate can be lowered or disabled at particularly low water depths to account for platform exposure due to tides.

3.2.3 Interactivity

Most stratigraphic forward models use one carbonate production curve to calculate the generation of carbonate lithofacies in either 2D/3D. Other models such as CarboCAT (Burgess 2013) or CARBONATE3D (Warrlich et al. 2002) use multiple types of carbonate production, of which each will have a different production profile. As a result, there needs to be methodology applied to determine which type of carbonate can produce at a given point and subsequent interactions between them.

A widely-used system is the application of cellular automata (CA), which has been successfully applied to carbonate models (Drummond and Dugan 1999; Burgess and Emery 2004; Burgess 2013). It consists of a discrete regular grid of cells, each in a finite number of states which can be entirely deterministic in their calculation and, with a series of defined input rules, enable output of predictable results, such as particular stratal geometries.

CA models can be applied to biological concepts of space, competition and population dynamics, justifying their application to investigate natural systems in many different disciplines (Drummond and Dugan 1999). The complexity of CA models can vary considerably, however there are three core features they all share:

- A grid of cells, each assigned a value representing its state.
- Structured networks between the cells.
- Computational algorithms that govern the nature of the networks.

The application these three core features within CarboCAT (Burgess 2013) is as follows:

Cell state is determined with reference to surrounding cells, the scale of which is based on the ‘radius’ extending outwards from each cell, which determines the cell’s ‘neighbourhood’. The states of the cells in the surrounding neighbourhood

determine the specific state of a cell at the next iteration, the possible states being either one of a finite number of carbonate 'factories', or empty.

The rules which govern this variation are an approximate representation of the principles of spatial competition and resource availability, determining minimum and maximum thresholds of population size required for survival, but as such are rather poorly constrained due to sparse data on competition (Burgess 2013).

A cell remains in its current state (survival rule) when (X = number of cells in the neighbourhood with identical factory type) $4 \leq X \leq 10$, becomes empty when $X \leq 3$ or $X \geq 11$ and, if empty, is recolonized (triggering rule) when $6 \leq X \leq 10$.

To circumvent bias, the factory type which occupies an empty cell is continuously varied. The rules are applied for each model timestep, determining the state of the cell for that specific timestep. These are applied to constrain the principles of spatial competition and resource availability; and resulting minimum and maximum thresholds of population size.

By relying solely on cellular automata rules to govern model evolution results in a wholly deterministic forward model of carbonate strata. This contrasts with stochastic approaches (e.g. Parcell 2003) due to the generation of pseudo random numbers, meaning the laws imitating nature which govern model evolution do not have full influence over the outputs.

3.2.4 Transport

Sediment transport is a natural process that strongly influences the geometrical development of carbonate platforms, being both current-driven and gravity-driven. Williams et al. (2011) classifies this feature into three distinct parts:

- Erosion of consolidated / entrainment of unconsolidated material
- Transport of the material over a distance either as bed-load or in suspension, depending on the relationship between flow velocity and grain size

- Deposition of material at a new position

Geometrical models are a widespread method to calculate transport of sediment (e.g. Bosence et al. 1994). Transported material is either estimated from natural examples of erosion, simply a fraction of the produced volume or any excess production that would take the platform above the point of sea level. Transport then follows simple rules such as the steepest descent pathway and beginning deposition once the gradient falls below a threshold value.

CarboCAT uses a geometric style of modelling transport (e.g. Bosence et al. 1994), occurring when model slope is over a threshold value (i.e. always occurs downslope) and the volume is simply derived as a fraction of the total produced, if available within a given cell. Deposition of material then initiates in adjacent cells downslope, depositing half of the transported material into the subsequent cell (Figure 3.12). This process then continues, distributing produced material downslope. Additional input of clastic material can also be defined at either a point or as a linear feature.

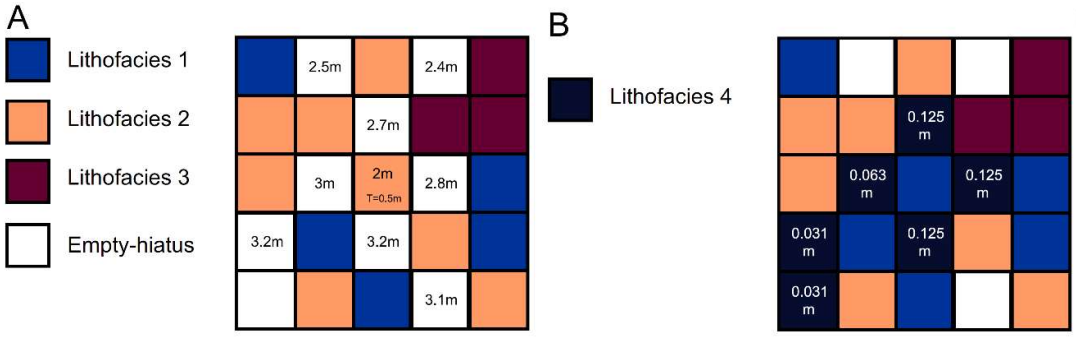

Figure 3.12: Diagrams demonstrating method of transport of sediment within CarboCAT (Burgess 2013), numerical values in white cells indicate water depth. (A): Within this model, the central cell is acting as the source of material, with a thickness of 0.5m available for transport (T) at a depth of 2m. Only unoccupied adjacent cells can accept the transported material, of which there are 4 immediately adjacent, which each receive 25% of the available thickness. Transport then continues to any adjacent, lower elevation cells. (B) shows the outcome of transport. 3 of the adjacent cells to the centre still retain their 25% portion of the initial thickness as they cannot transport it any further. Whereas in the bottom left of the model the thickness has been divided up multiple times.

3.2.5 Subsidence

Tectonic subsidence rates have been commonplace within carbonate stratigraphic forward models, as they are frequently investigating the relationship between water depth and subsequent sequence stratigraphic development. Alternative stratigraphic forward models which incorporate tectonic subsidence are SEDSIM (Griffiths et al. 2001), SEDPAK (Csato and Kendall 2002) and DIONISOS (Aschoff and Rountree 2012), with a comparison of these three models given in Shafie and Madon 2008.

Tectonic subsidence applied to stratigraphic forward models is typically linear (Bosence and Waltham 1990; Aurell et al. 1995), with even comparatively basic effects such as differential subsidence as a control on platform architecture only being investigated recently by Kozlowski (2017) using CarboCAT. Within CarboCAT a subsidence field is generated prior to the model run, consisting of values either constant or varying through time, which is used to calculate the subsidence value affecting every model grid cell, at every iteration during the model run (Burgess 2013). SEDSIM, SEDPAK and DIONISOS apply simple subsidence maps, which can be spatially variable, but are not temporally variable.

However, subsequently generated sedimentation patterns are not imparting a loading effect on the model, influencing tectonic subsidence rate, and certainly not impacting the model through generation of tectonic deformation in the form of faulting.

Numerical models that are capable of dynamically calculating and applying tectonic deformation are in their advent, for example Furuichi et al. (2018) scripted a ‘numerical sandbox’, digitally representative of a compressional analogue experiment. Though numerical models have some clear advantages over traditional analogue methods; primarily replicating a truly identical setup and running repeat experiments permitting a systematic investigation of the impact of variables, currently these numerical models are far too computationally demanding to be widely accessible.

4 Development of apparatus to yield mechanically homogeneous sandpacks for use in analogue experiments simulating variable syn-rift sedimentation

Abstract

This study presents a new cellular approach for the deposition of mechanically homogeneous sand layers with user-defined spatial and temporal thickness variations for use in scaled analogue experiments, enabling the simulation of more realistic stratigraphic architectures.

Current analogue syn-kinematic sedimentation methods are inconsistent with natural stratigraphic development, which involves diverse volumes of sediment being delivered to/developed in-situ on different areas of an evolving surface. Given that the loading effect of sedimentation during kinematic evolution affects strain localisation, invoking the tectonic response in the form of fault development; the potential for more accurate sedimentation patterns delivered using this apparatus would produce a meaningful tectonic response, determining future accommodation development.

Apparatus is developed which permits loading of variable amounts of sand into a grid of cells. Once complete, sand is passed through an array of individual tubing lengths to maintain desired cellular heterogeneity, permitting incremental deposition of sand layers with user-defined spatial thickness variations. The distance of fall determines the packing arrangement of sand grains when they settle on the underlying model surface, determining the mechanical properties.

The cellular sedimentation device is used to produce a variety of sandpacks, demonstrating the capability to evolve into 3D structures over successive layers. Results are statistically analysed using topographic surface data, demonstrating that the apparatus repeatedly deposits sand layers with both accurate translation of heterogeneous volumes and suitable mechanical properties critical for consistent scaling relationships between model and nature.

4.1 Introduction

Granular materials are a well-established tool to simulate brittle deformation processes in scaled analogue models (McClay and Ellis 1987; Lohrmann et al. 2003) as their flow exhibits a comparable deformation to brittle rocks in the upper crust (Marone 1998). Brittle deformation and granular flow both are characterised by complex, non-linear deformation processes, consisting of pre-failure distributed deformation and spontaneous shear localization (Adam et al. 2005). Consequently, analogue experiments consisting of dry silica loose sand are capable to simulate brittle tectonic deformation process and the kinematic evolution of upper crustal to basin-scale systems.

Syn-kinematic sedimentation is a technique employed in the field of scaled analogue sandbox experiments; depositing granular materials during syn-tectonic evolution of a model to replicate the loading effect of deposition through time for kinematic (both compressional and extensional) experiments (Duerto and McClay 2009; Adam et al. 2012; Burliga 2012). This process has been demonstrated to strongly influence tectonic evolution in both nature (Bialas and Buck, 2009) and models (Barrier et al. 2013; Zwaan et al. 2018), by the gravity-loading controlling the strength of underlying material and fault development, governing accommodation for subsequent deposition. However, currently, models produced using this by-hand method cannot accurately exhibit intricate stratigraphic evolution; sandbox models commonly fill all available accommodation and have the top surface scraped flat. Whilst fill-to-spill grabens are common in the stratigraphic record, Ravnås and Steel (1998) demonstrate that half graben sedimentary evolution is a complex, continuous process and thus cannot be adequately simulated by uniformly filling the available accommodation at regular, pre-defined time intervals.

An improvement to the process of syn-kinematic sedimentation would be achieved by permitting a more precise sedimentation procedure that better reflects natural stratigraphic development in both time and space. This will in turn invoke a tectonic

response from the analogue model, governing future accommodation for later sedimentation intervals, permitting studies to improve understanding of tectono-sedimentary evolution in sedimentary basins.

Apparatus is required that is capable of depositing variable sand volumes within a single layer input to the model, mimicking natural stratigraphic development. Furthermore, to achieve suitable model scaling; cohesion and density of deposited sandpacks are required to be sufficiently similar to those produced by traditional, by-hand sedimentation methods which are used to produce pre-kinematic layering in sandbox experiments. When depositing granular materials, dependent upon the velocity upon contact with model surface, the sand grains will produce different arrangements, affecting both the density and cohesion. There are two main methodologies in use to deposit sand, pouring and sifting (also referred to as sprinkling). Observed in both extensional sandbox experiments and ring-shear tests, dependent upon the method of deposition, the coefficient of internal friction will vary (Krantz 1991; Schellart 2000; Lohrmann et al. 2003). This differentiation occurs as a result of dissimilar packing arrangement; specifically, sifted grains have higher densities than materials which are poured. Due to this tighter packing in sifted materials, the grains have less ability to be rearranged by shearing forces, manifesting as a higher internal friction coefficient.

Given that grains must fall a certain distance to achieve suitable packing and model scaling; if variable volumes are to be deposited synchronously within a single layer, there needs to be a physical barrier to maintain the desired depositional pattern. A cellular array of tubing lengths would permit heterogeneous volumes to be deposited adjacent to each other in a synchronous manner, whilst maintaining desired homogeneous mechanical properties within the deposited layer.

Approach involved initial testing to determine the required tube length, investigating the potential impact of falling friction against the tube sides and fall distance to achieve desired density and cohesion in the sandpack, quantified using a ring-shear tester. Based on parameters derived from initial testing, a prototype apparatus is constructed and then used to produce a series of models to

demonstrate the apparatus' capability to replicate the desired spatial and volume distribution and generate 3D structures with successive layering.

4.2 Methods & Materials

4.2.1 Material - BL60 sand

All testing conducted within this work utilised "BL60" sand, a well sorted, high purity silica sand (>99.7% SiO2) with a median grain size of 180µm (Figure 4.1). Maximum diameter of any grains measured during testing was still significantly smaller than any apparatus sieve openings to prevent any possible build-up of sand grains, inhibiting flow. All work follows scaling principles that permit results to be quantitatively compared to nature (Hubbert 1937). A geometric scaling of 10^{-5} (1cm model = 1km nature) was used.

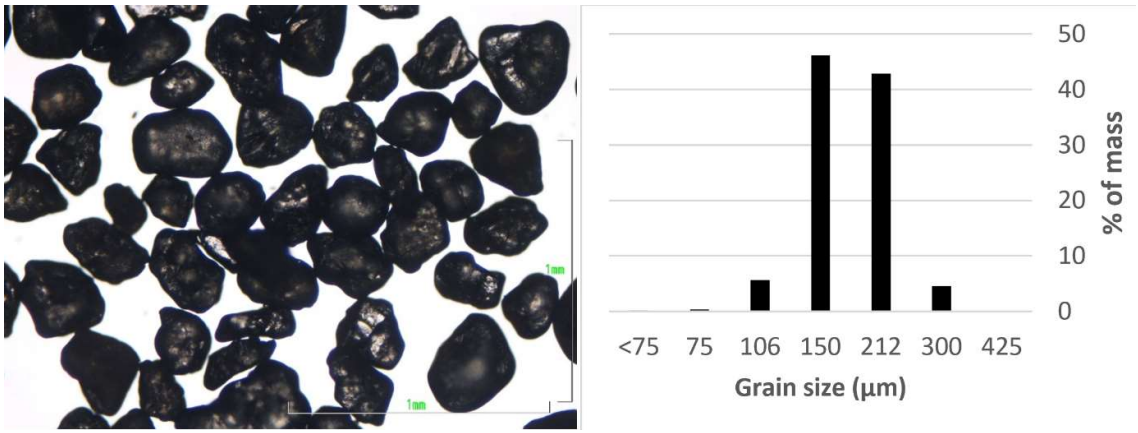

Figure 4.1: Microscope image of BL60 silica sand and its corresponding grain-size distribution

4.2.2 Ring Shear Testing

The frictional properties of the BL60 sand were analysed using a dynamic ring-shear tester to demonstrate comparable behaviour to that exhibited by experimentally deformed rocks, representing brittle deformation of upper crustal processes to be modelled. Testing delivers computer-controlled measurements of the granular material's flow properties and permits calculation of angle of internal friction and cohesion. Output is a stress-strain or material curve showing the evolving material strength in a shear zone with increasing strain.

It is conducted by filling a cell with the desired material, which is then subjected to confining pressure as a set normal stress (a range of normal stresses from 400 to 2400Pa were tested). Increasing shear stress is then applied to the cell and recorded by software. The early period is characterised by an initial elastic strain, superseded by plastic strain-hardening prior to failure known as 'peak friction/strength', at which the material begins to flow. The material then achieves equilibrium in a state known as 'dynamic friction' or 'residual strength' at the minimal force required to keep the body flowing. The shearing force is then stopped, and the sand body returns to rest, at which point the shear forces are reapplied in order to test the 'static strength' (Panien et al. 2006).

4.2.3 Digital Image Correlation (DIC)

To investigate the variability observed of deposited surfaces, stereoscopic DIC (Digital Image Correlation) was used. Primarily this tool captures time series data, monitoring deformation and surface flow in high resolution, which permits calculation of 3D displacement fields, fully quantifying deformation at all scales within experiments (Adam et al. 2005). Within this work, static 3D surfaces were captured at sub-millimetre scale. Statistical analysis was then conducted on this data to explore the variability in surface expression.

4.3 Results 1: Determining prototype specification

4.3.1 Density measurements

Results (Figure 4.2) indicate that confined fall distance (i.e. what proportion of the total drop distance occurs within the tubing) has no effect on the obtained sandpack density, with different tube lengths (10 and 30cm) commonly providing identical averages for the same cumulative drop. The implication of this is that tube length can be chosen at discretion, based upon the desired falling pattern, with longer tube lengths better confining sand volumes within the target area (i.e. same footprint as the tube itself).

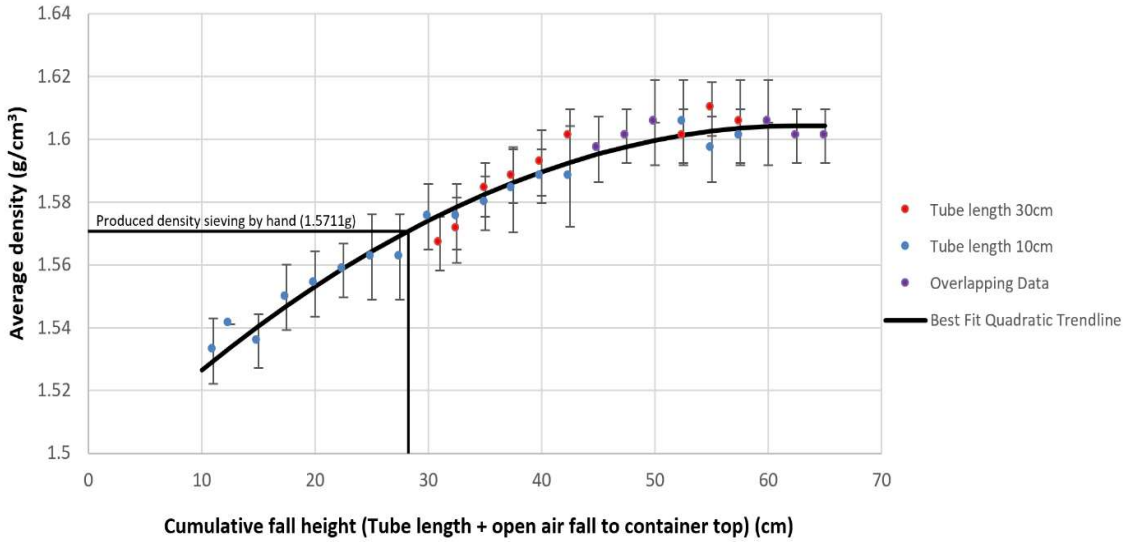

Figure 4.2: Graph of cumulative fall height vs. produced sandpack density utilising either 10cm or 30cm tubing lengths and variable distances to surface

The graph plateau implies a maximum obtainable density, which is correlated to terminal velocity of the sand grains (Krantz 1991). However, current by-hand deposition is conducted from a height of 30cm which yielded an average density of 1.571g/cm^3 when tested, lower than that of the plateau at around 1.605g/cm^3. To produce a coherent density when flowing sand through tubing, a total fall height of approximately 28cm is to be used (As shown by the intercepts on Figure 4.2). The explanation for the shorter distance with the mechanical approach, than with hand-sifting, is that it has a more consistent, slower deposition rate, whereas when

depositing by hand, certain motions can cause larger volumes to be sporadically deposited, increasing the density in localised areas.

4.3.2 Internal friction measurements

Based upon the relationship between density and internal friction, a total fall height of 28cm when flowing sand through tubing should also yield suitable frictional properties of the sandpack. Using tubing of length 25cm, a cumulative drop of 28cm was used to fill a ring-shear test cell to conduct investigative measurements. Measurements were taken for both passing sand through tubing and sifting by hand to compare results.

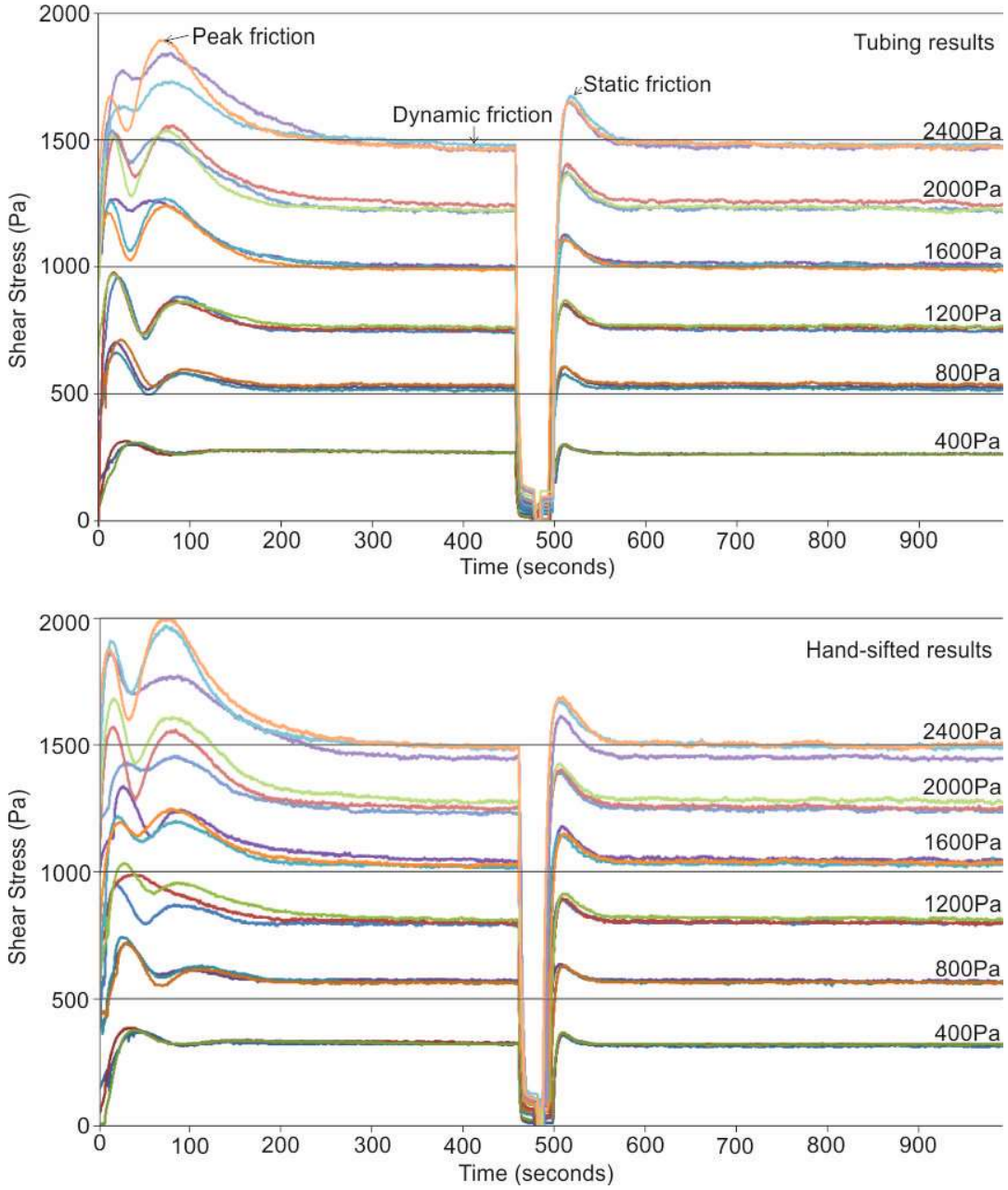

Figure 4.3: Material testing profiles produced from ring-shear testing, measuring peak, static and dynamic friction (Example measurement positions indicated) achieved at a series of applied normal stresses (annotated on right-side of profiles) for sandpacks produced by both hand sieving and passed through tubing.

The cumulative drop of 28cm using tubing produces sandpacks with an average internal friction and cohesion visually, very similar to that of hand-sifted sand at 30cm. Furthermore, the coherency is much better in the mechanical approach than the hand-sifted results, as demonstrated by the trendlines more accurately intercepting the points (Figure 4.4). Both methods of deposition demonstrate

expected linear Navier-Coulomb behaviour, have similar angles of friction and exhibit very low cohesion.

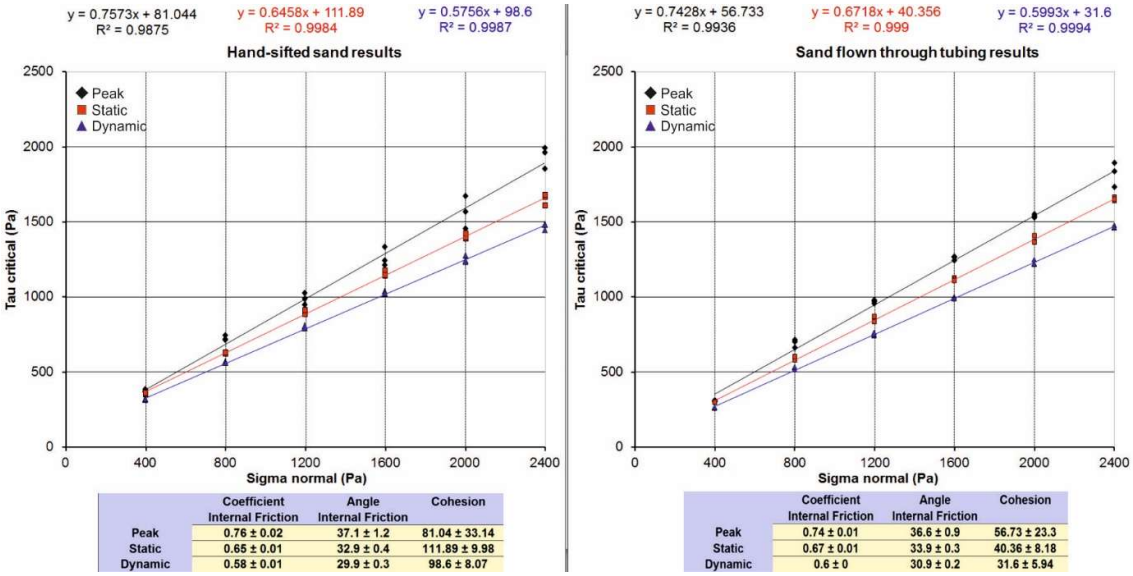

Figure 4.4: Plots of ring shear testing results comparing peak, static and dynamic shear stresses achieved at a series of applied normal stresses for sandpacks produced by both hand sieving and flown through 25cm tubing. Values for coefficients of internal friction, angles of internal friction and cohesions are also presented.

Applied normal load (Pa)	Method of deposition and shear stress measurement (Pa) (Averages)					
	Tube Peak	Hand Peak	Tube Static	Hand Static	Tube Dynamic	Hand Dynamic
400	308.178	376.351	298.839	361.409	261.951	314.715
800	692.001	725.620	595.812	630.365	519.234	557.056
1200	969.362	1024.460	858.2309	903.056	765.310	796.128
1600	1261.664	1272.871	1119.715	1153.335	990.374	1021.659
2000	1543.695	1481.125	1394.275	1390.539	1227.578	1224.309
2400	1835.063	1866.815	1652.024	1645.487	1456.377	1455.910

Table 4.1: Peak, static and dynamic friction coefficients recorded at a range of applied normal stresses (400-2400Pa) for sandpacks constructed by flowing sand through appropriate length tubing and by hand-sifting.

4.4 Apparatus Construction and Setup

A prototype cellular sedimentation apparatus was constructed based upon the desired characteristics from section 4.4.1 & 4.4.2, capable of depositing heterogeneous sandpacks of appropriate density (1.57g/cm^3) and frictional properties. A grid of 10x10 cells, each 4cm^2 (2x2cm) overlies a series of corresponding 25cm aluminium tubing lengths (Figure 4.5). Cell area is a compromise between precision and time taken to load in each layer.

This apparatus is then emplaced within a box, with an internal area of just over 20x20cm. Within this it was then used to generate different sandpacks made up of multiple layers. Lateral spacers permit the apparatus to be adjusted upwards to maintain a consistent fall distance to the model surface as sand layers are incrementally deposited beneath it. Two removable Perspex walls enable the model to be saturated with a gelatine solution and removed from the box to undergo cross-sectional analysis.

Aluminium was used for the construction due to its high strength and its resistance to build-up of static charge on the insides of the tubing. Another material investigated was plastic; however static charge resulted in sand grain build-up within tubing lengths. This would mean inaccurate sand volumes due to collection on tubing interiors. Alternatively, it may influence falling velocities, producing different densities and packing arrangements, affecting peak internal friction.

Above the tubing lengths, there is a grid of cells to enable the different sediment volumes to be fully loaded prior to deposition; beneath this is an aluminium plate. As shown in the cross-section in Figure 4.5, the countersunk holes direct the loaded sediment into position above the tubing lengths. They direct it away from the edges to prevent any possible deposition on the flat tubing tops or contamination into other tubing lengths. The aluminium plate is removed manually once the configuration is set-up over the analogue surface and deposition is to begin. A key feature is that it enables near-synchronous deposition across the model surface, with only a short time lag between deposition at opposite model sides.

Since the discrete cellular nature of the layer needs to be preserved, it was decided that tube length should cover almost the entire fall distance. The heterogeneous surfaces being deposited onto will result in different open-air fall distances for various cell. Therefore, to minimise potential spread of sediment during deposition, a length of 25cm was chosen. This enables a fluctuation in open-air fall distances, whilst maintaining coherent mechanical properties with pre-kinematic layers produced by standard manual preparation techniques, with acceptable values being produced for cumulative drops between approximately 25-30cm.

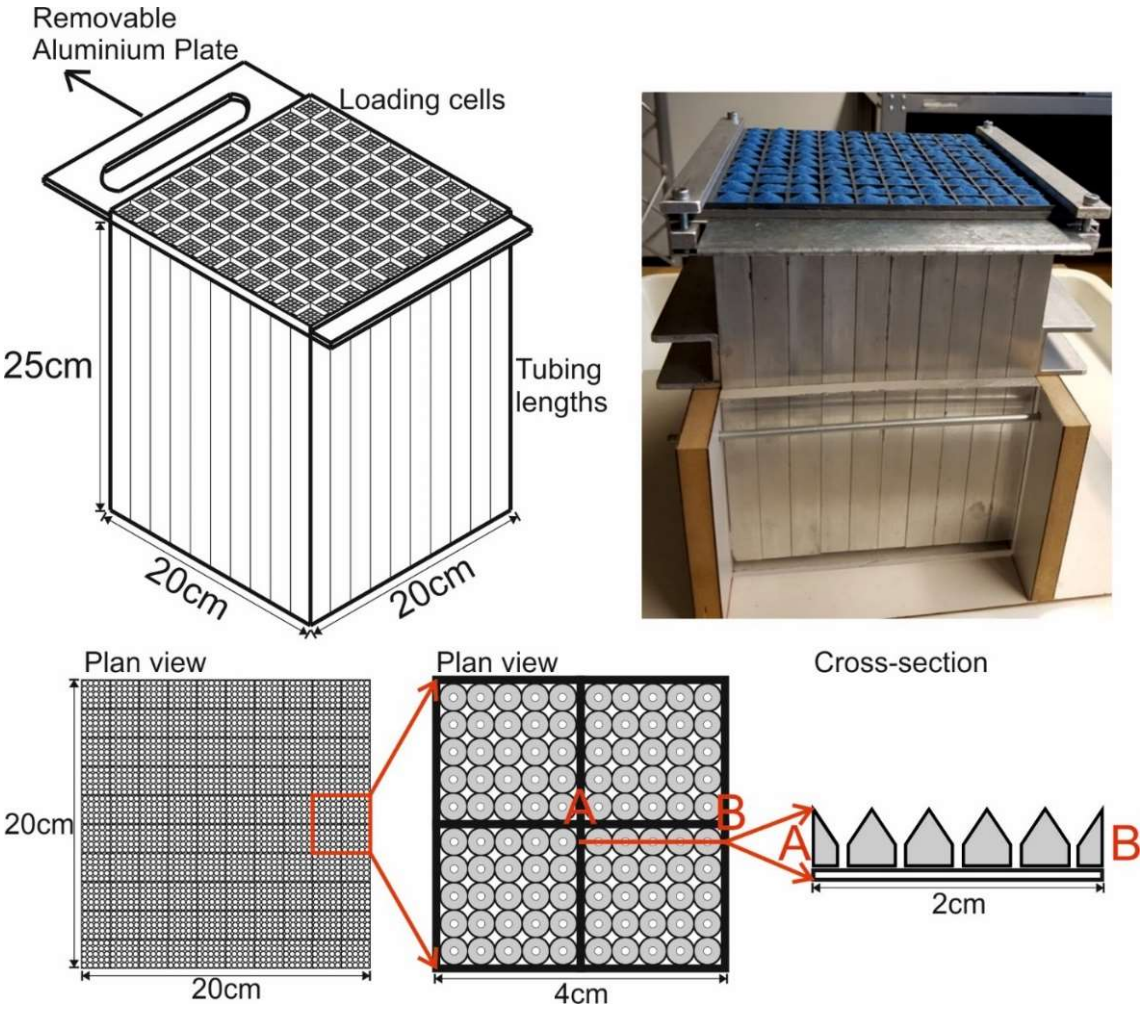

Figure 4.5: Upper left: Schematic of the 10x10 sieving device. Upper right: Apparatus is placed in a confined box within which layers can be deposited, constructing sandpacks/analogue models beneath it. Sand is in the loading cells and ready to be deposited, flow is being inhibited by the steel plate protruding outwards. Below: Schematic representation of the cellular loading tray in plan-view and x-section.

4.5 Results 2: Demonstration of prototype apparatus

Once produced, the test configuration was utilised to construct 3 models to explore repeatability and how effectively the cellular deposition translated onto the model surface. Investigation involved capturing static surfaces using 3D stereo DIC and conducting cross-sectional analysis of completed models in 3mm increments.

Cell loading was conducted using measuring spoons for the sand which were levelled flat. Each spoon holds approximately either 0.632g, 1.264g or 2.528g of bulk density BL60 sand. When passed through the apparatus and deposited with the correct density, these weights deposit vertical thicknesses of 1, 2 and 4mm within their 2x2cm cell, respectively.

Measured weights using the spoons (Table 4.2) were averaged from 5 readings. Actual vertical thicknesses deposited by the spoons were calculated by using the predicted density (1.57g/cm^3) of sand when using the sieving apparatus and the precise target cell size of 2x2cm. Given that the sand has potential to spread laterally and physically cannot form exact columns as would be derived from the numerical model, the precision of the weights being loaded by the spoons is satisfactory.

Spoon size (tsp)	Target vertical thickness	Measured weight of sand	Actual thickness deposited	Percentage versus target thickness
(1/4)	**4mm**	2.4467g	3.90mm	97.5%
(1/8)	**2mm**	1.2770g	2.03mm	101.5%
(1/16)	**1mm**	0.5934g	0.95mm	95%
(1/32)	**0.5mm**	0.2919g	0.47mm	94%

Table 4.2: Comparison of target thicknesses and actual thicknesses deposited when using spoons to manually load the sand into the sieving apparatus.

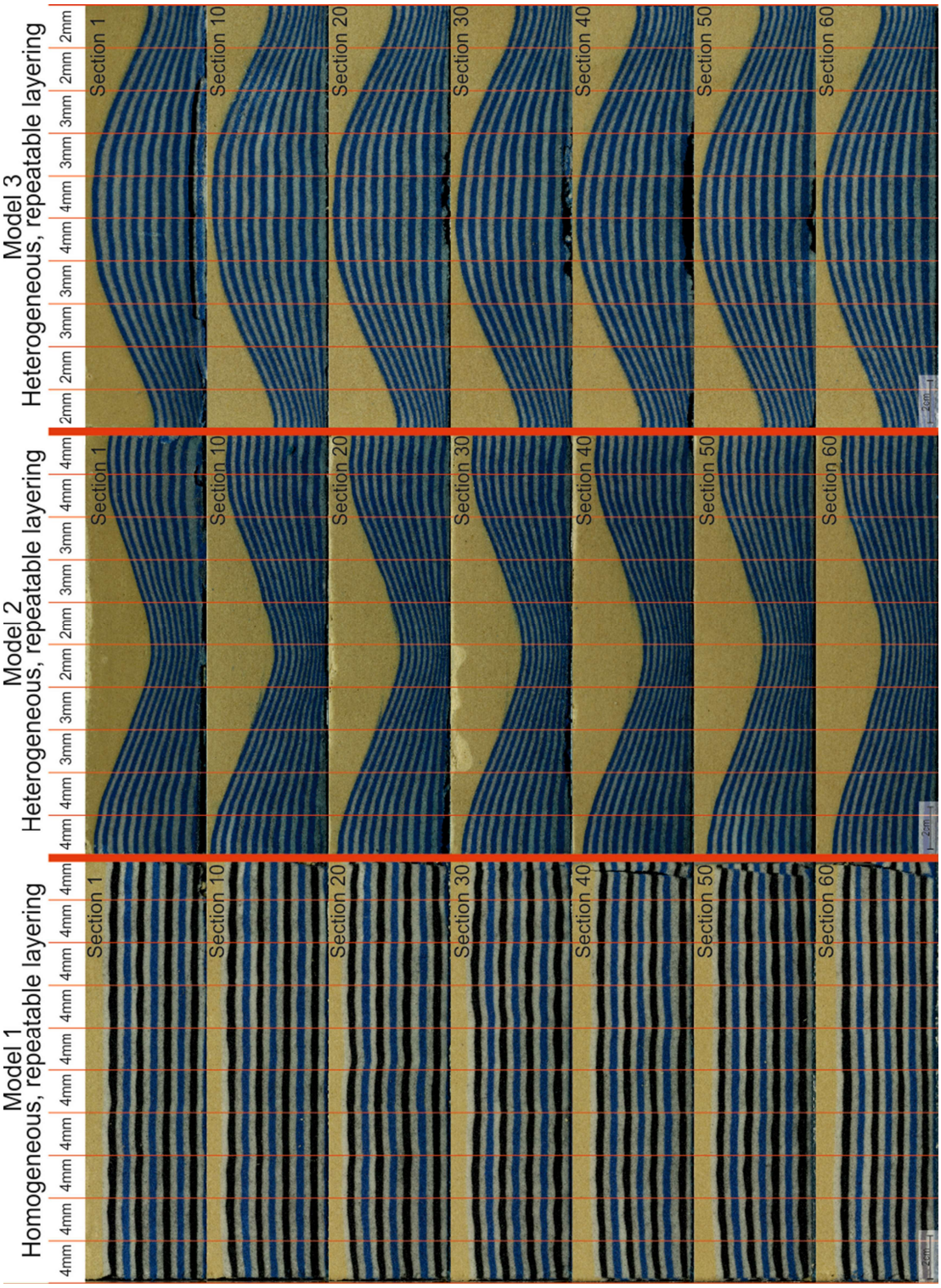

Figure 4.6: Composite cross-sections of the three experiment sandpacks produced using the apparatus. Superimposed on the image are lines demonstrating the layout of the 10-wide tubing arrangement that overlay the model. Each cell had a constant thickness deposited within it for each layer in that model.

4.5.1 Horizontal layering

Repeatability of deposited sandpacks is essential to ensure validity of experiment outcomes when using the mechanical sieving device. To test this, an experiment consisting of uniform sedimentation in all cells for 16 total layers was run, as shown in Figures 4.7 & 4.8, to demonstrate consistent volumes being deposited in three dimensions.

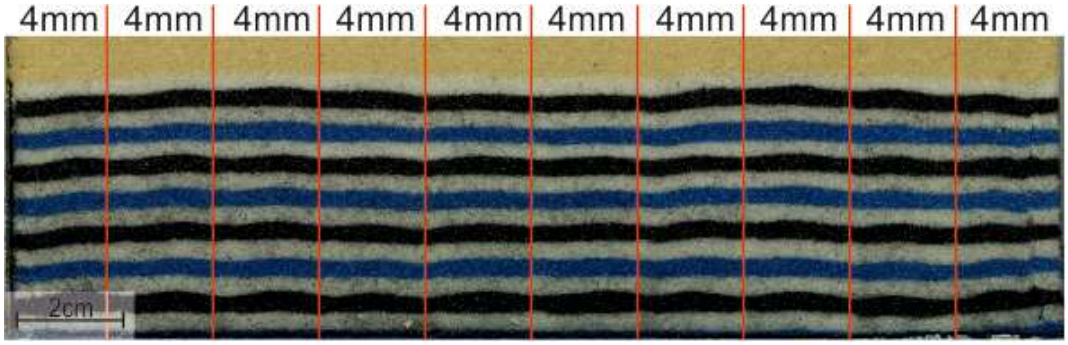

Figure 4.7: Central cross-section (section 30 in Figure 4.6) of the flat-layering experiment sandpack, 16 layers. Each layer had a constant thickness deposited, indicated above.

Black sand layers appear to exhibit a higher cohesion than the white/blue layers (Figure 4.6, 4.7). Consequently, the black sand was removed from any future experiment runs.

To investigate the observed surface variations in more depth, DIC imaging was used. Separate models were run, consisting of a single homogeneous layer deposited onto a flat surface and subsequently imaged. The surface was then cleared, and the process repeated, producing 6 example images (Figure 4.8):

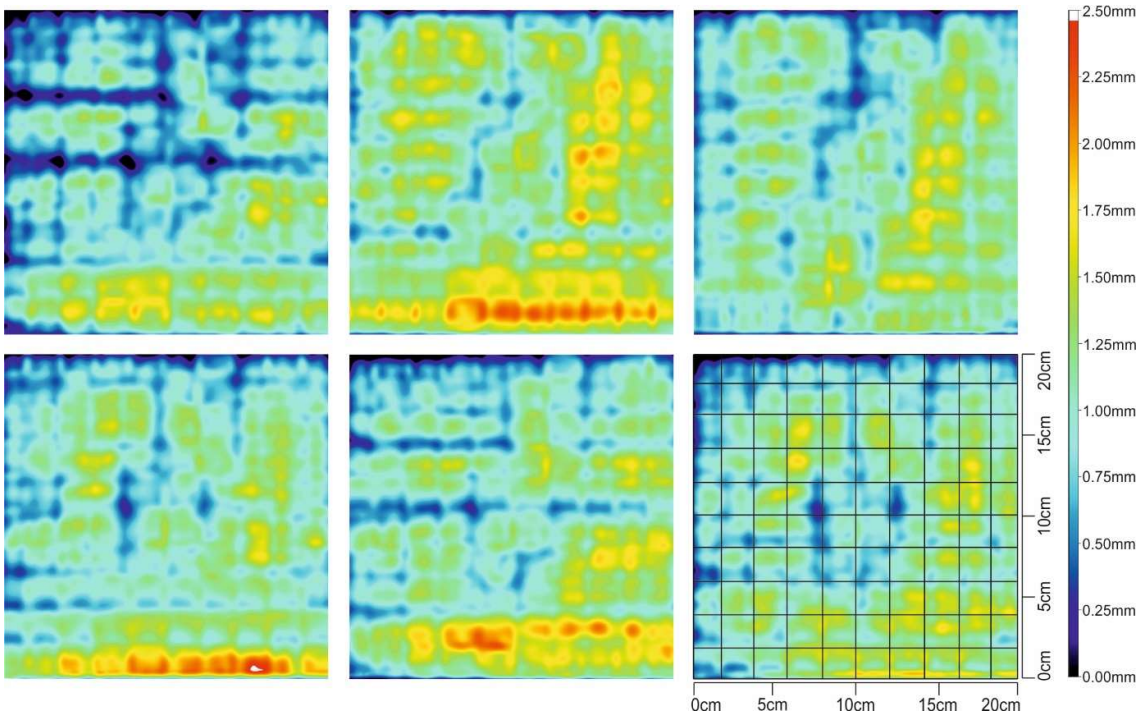

Figure 4.8: DIC topographic images showing six separate, initial surfaces formed by depositing an identical thickness into each cell. Bottom-right image is overlain with a grid denoting the relative positions of the 10x10 cell arrangement.

The data gathered from these six separate, initial layers was statistically analysed to determine the average thicknesses, as well as the variance observed within each layer. Calculated variances for individual layers are being inflated by the horizontal ridges, observed at base of most examples. This structure is formed when there is a spike in deposited sand volumes at the moment when the aluminium plate is entirely removed from the apparatus.

Experiment run (surfaces shown in Figure 4.8)	Average thickness (mm)	Thickness variance
1	3.233	1.175
2	3.618	1.104
3	3.421	0.928
4	3.375	1.138
5	3.456	1.013
6	3.404	1.000

Table 4.3: Average thicknesses and variance of individual layers constructed using identical input sediment volumes

4.5.2 Heterogeneous layering

The novel feature of the sieving device is to permit deposition of heterogeneous sand volumes within individual layers, which have the potential to evolve into cumulative features as successive layering is deposited. To test this, two sandbox models were constructed (Figure 4.9, also seen in Figure 4.6). Volumes of sediment per cell were kept constant throughout each of the models and were equivalent to the values shown over the corresponding location on the figures.

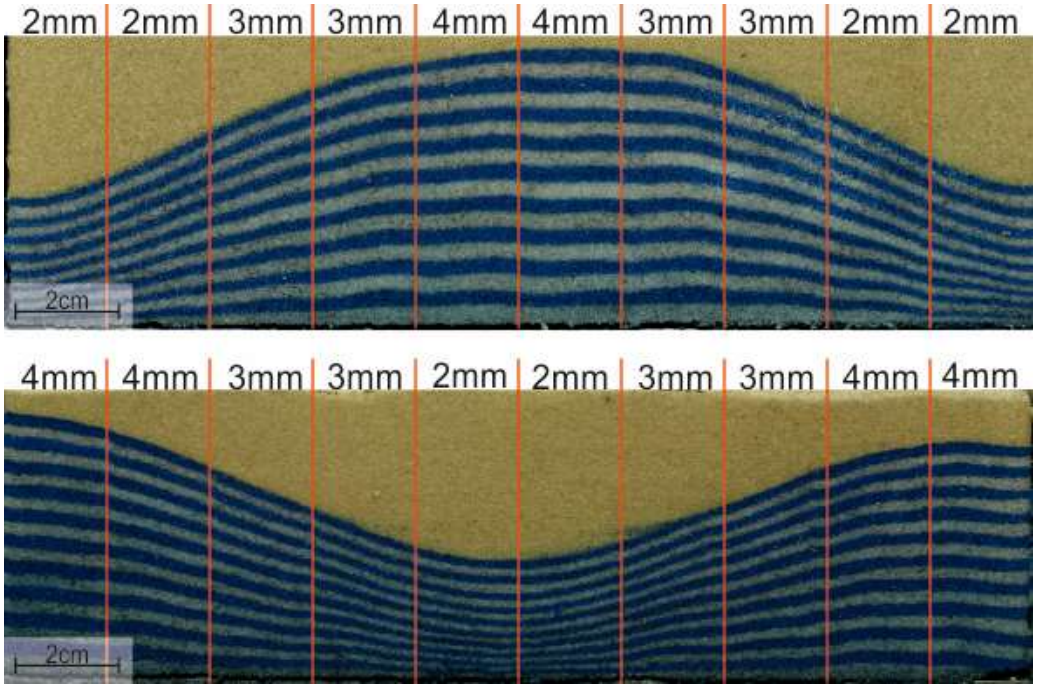

Figure 4.9: Central cross-sections of the heterogeneous 'mound' experiment sandpack (18 layers) and heterogeneous 'basin' experiment sandpack (20 layers). Each position with a model had a constant thickness deposited for each layer, indicated above.

Both models achieve development of 3D architectures, though there is some minor transport of material downslope occurring. Identical replication of deposited amounts onto the analogue model would generate vertical-sided columns, which cannot be achieved using granular materials. Due to kinetic energy from falling and angle of repose the sand spreads out, producing a smoothed topography. These models also demonstrate good repeatability of the sedimentation device based upon the symmetry observed in both models.

4.5.3 Surface Spread

Surfaces being deposited onto using the apparatus may be heterogeneous in their expression, meaning there will be different lengths from the end of the tubing to the model surface at different locations. This may potentially result in different dispersions of the sand based on the distance to model surface once sand is beyond the confines of the tubing, affecting the desired cellular output. DIC imaging was used to display the variation in spread due to different falling heights (Figure 4.10). This was setup by having a homogeneous, flat layer initially laid down, then depositing four isolated, identical volumes (0.8cm^3 per cell) onto it. This was done for 1, 3 and 5cm unconfined fall heights.

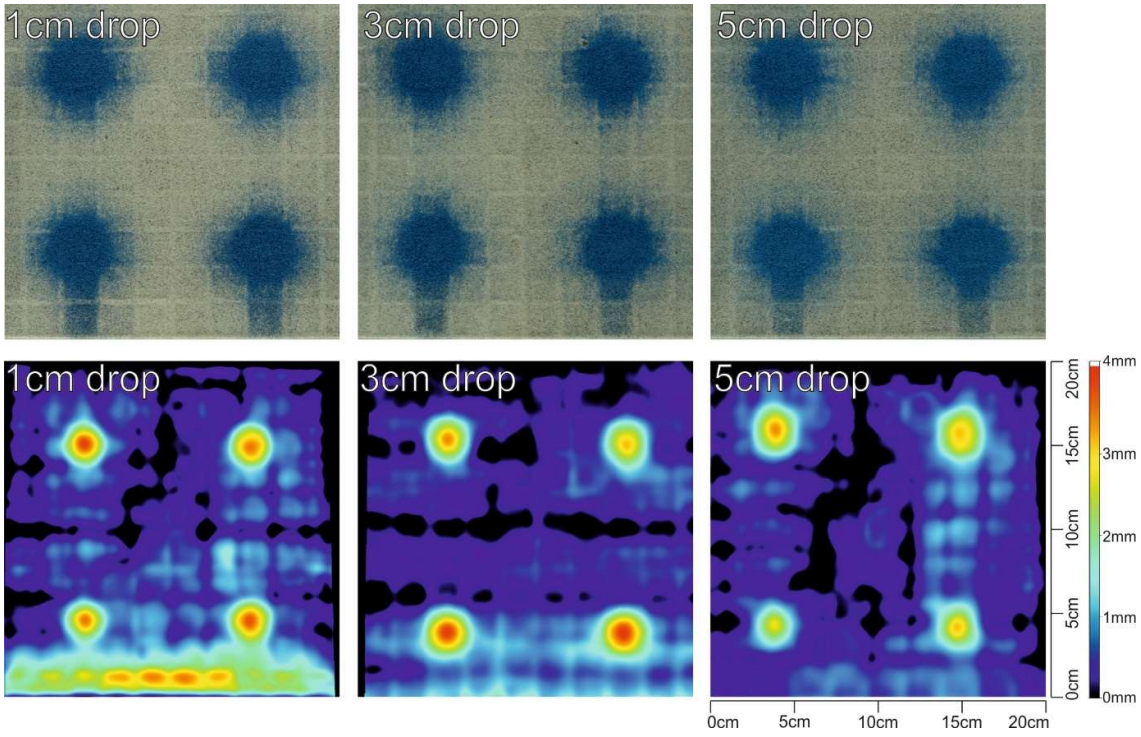

Figure 4.10: Top: SLR photos, below: DIC topographic images showing surface spread of 4 individual sediment depositions with different unconfined falling distances (1,3 and 5cm), deposited onto a pre-existing sandpack.

Unconfined fall distance	Average mound diameter (mm)	Percentage relative to 1cm
1cm	29.500	100.0
3cm	30.125	102.1
5cm	30.625	103.8

Table 4.4: Average mound diameters for results shown in Figure 4.10

4.6 Discussion

As shown by the flat layering experiments (4.6.1), there is good repeatability exhibited by the sieving device. Individual layers produce an average variance of 1.06mm, approximately a 31% variation of average thickness (3.418mm). Given the small unconfined fall distance (1cm) which will lead to a more laterally compact structure and grain size being 0.18mm, a variance equal to 6 stacked sand grains is acceptable.

Heterogeneous sandpacks (4.6.2) demonstrate that with continued deposition of heterogeneous sand layers onto an initially flat surface, 3D structures can be developed. Both models run also exhibit a high degree of repeatability, confirmed by the symmetry of the models, both in a single section and at opposite edges when sliced.

When investigating the variability of deposited sandpacks; 1, 3 and 5cm unconfined falling distances have only a minor impact on the deposited sediment structure. Investigated in section 4.6.3, the deposited mounds only exhibit a 3.8% growth in diameter when increasing the unconfined distance from 1 to 5cm. Although, shown by the regular SLR images (Figure 4.10), there is a wider dispersion of some of the sand resulting in the mounds not reaching the same height. When depositing entire layers, the variance will decrease, if unconfined falling height is increased whilst the average thickness remains consistent. This is expected, as the same volume of

sediment is being given more time to distribute laterally and mix with adjacent cells.

Observed within the results (Figures 4.6, 4.7); black sand layers appear to exhibit a higher cohesion than the white/blue layers. Dyes used in granular material production have previously been demonstrated to influence mechanical behaviour (Gomes et al. 2010), however within this work there is a distinct difference observed between dye colours. The black grains produce a doming effect towards the centre of the cell locations, which is gradually smoothed out over the subsequent white and blue layers. Differences in the volume of doming observed within different layers is likely due to a slight difference in depositional origin (i.e. different observable part of the mounds in that layer), with layers not being deposited directly above one another. Consequently, the black sand was removed from the two later heterogeneous experiment runs and the sand layers within those experiments demonstrate a much higher consistency.

Another issue is the effect of initiating sand deposition. For all the DIC images, the tray initially blocking sediment flow was removed towards the bottom of the image. Due to the flexibility of the plate, there is a small gap between the top of the plate and base of the cell loading unit and, because of this, sediment can collect on the plate. This rapidly builds up initially, leading to a lack of sediment volume towards the top of the model, with greater volumes being deposited towards the base of the model (Figure 4.10). This collection of sediment on the plate is also responsible for the horizontal ridges observed towards the base of the model (Figure 4.8). When nearing the end of removal (i.e. depositing over the bottom 20% of the model) the plate tended to become stuck. This abrupt stopping resulted in a portion of the sediment built up on the plate edge to be deposited at the base of the model.

4.7 Conclusions and Future Work

When depositing granular sandpacks consisting of near-pure quartz sand the apparatus has been shown to yield the mechanical properties (density and internal friction profile) required to successfully replicate brittle-frictional behaviours observed in the upper crust. Furthermore, it has a strong repeatability and the added advantage of enabling heterogeneous deposition within individual layers. This approach also involves near synchronous deposition across the entire model, with adjacent cells being filled at overlapping intervals, preventing unwanted model evolution which may be caused because of sporadic, unequal deposition synonymous with hand sieving methods.

The capability to deposit heterogeneous sandpacks permits this workflow to mimic realistic sedimentation patterns. If suitably applied to kinematic sandbox experiments, this should produce a more in-depth tectonic response from the model. Within extensional settings, such as rift basins, the interaction of sedimentation and tectonic processes exert a strong control upon the evolution of sedimentary basins, however the relationship and subsequent feedback mechanisms between the two are poorly understood. The tectonic response exhibited by realistic sedimentation patterns will determine future accommodation, different to that produced with current syn-kinematic depositional methods. Therefore, this workflow may produce markedly different extensional architectures, providing valuable insights for exploration geologists.

5 Application of cellular stratigraphic forward modelling software to permit quantitative simulation of carbonate depositional systems in analogue sandbox experiments

Abstract

This study presents a novel integration of cellular stratigraphic forward modelling (SFM) software with a basin-scale analogue sandbox experiment, permitting dynamic calculation and deposition of complex sedimentation patterns, with the evolving sandbox surface influencing subsequent deposition. This fully quantitative application of sedimentation input to an analogue experiment is not something presently achievable with existing manual techniques.

The dynamic topography of the sandbox is monitored by high-resolution stereo Digital Image Correlation (DIC) techniques, yielding a digital input surface for the SFM. This is then run, in combination with a series of production parameters and subsidence rate, to calculate the depositional pattern for the sandbox for a given time interval. The spatially heterogeneous depositional output is then deposited as a mechanically homogeneous incremental sand layer onto the experiment surface using a custom-made cellular array of tubes.

Experiment results demonstrate that the workflow is capable of translating sandbox surface data into the SFM to act as a scaled input, as well as depositing subsequent SFM calculated outputs back onto the analogue model which have the capacity to develop into complex 3D depositional architectures with required mechanical properties. Model evolution is also entirely deterministic, being governed solely by feedback between the initial parameters of both the analogue and numerical models.

Given that sedimentation has been demonstrated to influence tectonic evolution, both in sandbox models and nature, governing future accommodation; this methodology has potential to provide a more detailed insight into feedback mechanisms between sedimentation and tectonic deformation, as accurate

simulation of them will now be achieved with a single integrated workflow. Non-tectonic controls such as sea level or climate can also be investigated in more detail.

5.1 Introduction

Syn-tectonic depositional sequences are controlled by basin geometry, active tectonic structures, subsidence, sediment supply and sea-level fluctuations (Leeder and Gawthorpe 1987; Schlische 1991). In turn, the loading effect from ongoing sedimentation affects fault strength and strain localisation, governing future tectonic evolution (Bialas and Buck 2009). Feedback mechanisms between sedimentation and tectonic processes are known, but as of yet have not been investigated in detail using analogue modelling techniques.

Scaled analogue sandbox models develop realistic, basin-scale fault architectures and tectonic subsidence patterns, including fault localisation, segmentation, linkage and displacement, producing meaningful tectonic-subsidence (McClay and Ellis 1987). However, syn-kinematic sedimentation within analogue sandbox experiments is a process almost exclusively conducted manually in a conceptual, qualitative manner. Consequently, even when geological constraints like sedimentation rates and available accommodation are considered (e.g. Adam et al. 2012), the methodology is still somewhat basic, being restricted to gross first-order sedimentation patterns. In contrast, syn-kinematic sedimentary evolution of natural half-grabens within extensional settings is highly complex (Ravnås and Steel 1998), so it is argued that current analogue methods cannot adequately simulate sedimentation patterns and thus are not invoking a representative tectonic response within the model.

In this study a new workflow is presented, employing cellular stratigraphic forward modelling (SFM) software to calculate realistic volumes and distributions of sediments to be input to analogue experiments for given time intervals. This

process uses Stereo-DIC (Digital Image Correlation) methods to derive a high-resolution digital elevation model of the analogue experiment as an input for the SFM. Incrementally generated volumes are then deposited using a cellular array of tubes onto their relevant locations on the sandbox surface. The tubing apparatus has been specifically designed to yield sand layers with homogeneous mechanical properties (Chapter 4), whilst depositing heterogeneous volumes within individual layers. An outline of the workflow is shown in Figure 5.1.

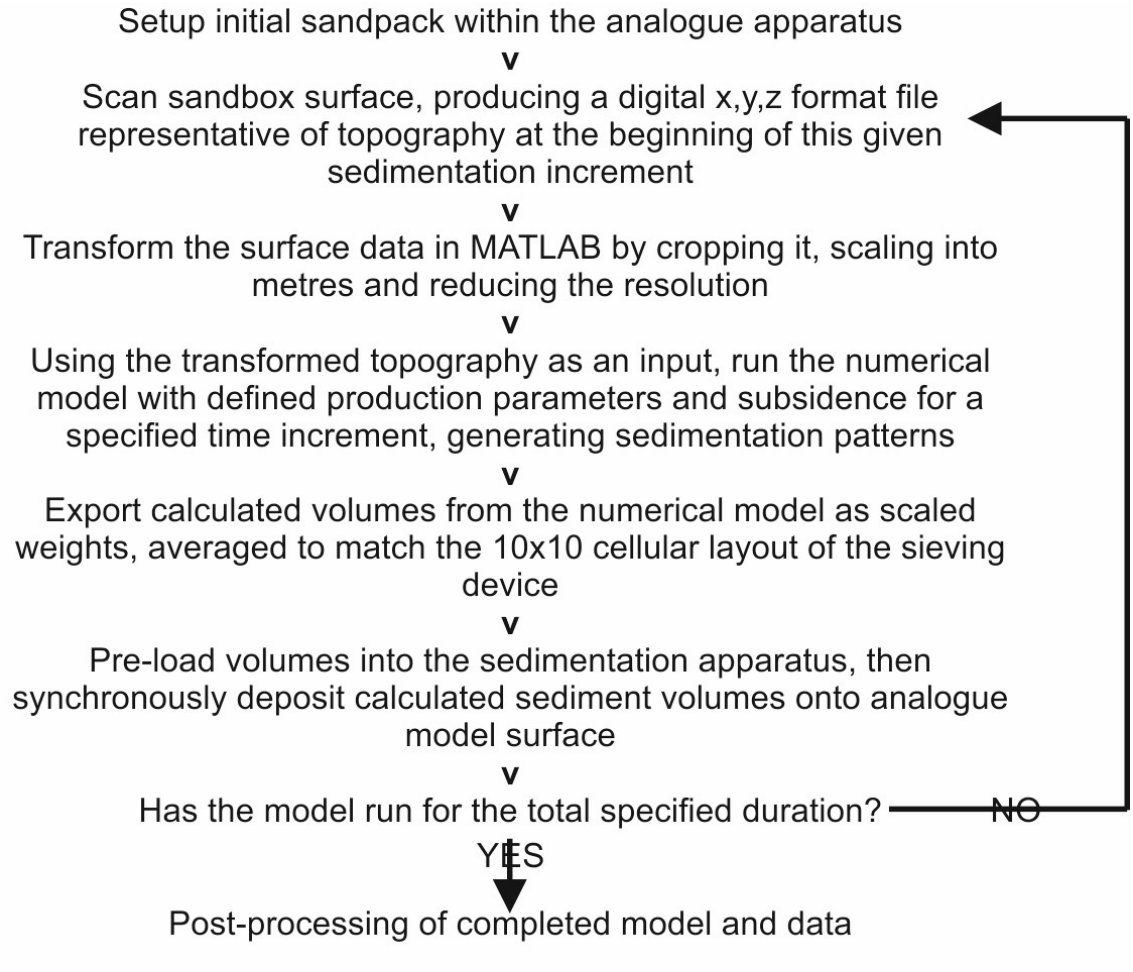

Figure 5.1: Flow chart documenting the integrated workflow procedure between analogue and numerical models

5.2 Methods

5.2.1 Analogue scaling and modelling materials

All models contained within this paper were constructed entirely from a high purity (>99.7% SiO_2), well sorted, silica sand with a median grain size of 180μm. The granular flow characteristics of dry, near-cohesionless, granular materials are well-suited to simulate brittle upper-crustal deformation in scaled analogue experiments (Lohrmann et al. 2003). Material parameters derived by ring-shear testing showed an internal angle of friction of 30-37°, peak internal friction coefficient of 0.76, dynamic internal friction coefficient of 0.58 and static internal friction coefficient of 0.65. The dynamically scaled sandbox experiments have a geometrical scaling factor of 10^{-5} (1cm in model = 1km in nature), derived from density and cohesion ratios of model and natural materials (Hubbert 1937; Lallemand et al. 1994).

5.2.2 Analogue sieving device

The sedimentation apparatus (Figure 5.2, described in more detail in Chapter 4) is a 10x10 cellular array of aluminium tubes, each 2x2cm wide and 25cm in vertical length, which is placed in a fixed position above the analogue surface and permits incremental deposition of heterogeneous sand volumes within a single layer, whilst maintaining homogeneous mechanical properties. A discrete grid of cells sits above the tubes, supported by an aluminium plate. Discrete volumes are loaded into the cells, with their position overlying the relevant position on the experiment surface. Once all required cells are filled the aluminium plate is withdrawn, allowing near-synchronous deposition of the heterogeneous sand volumes onto the experiment surface.

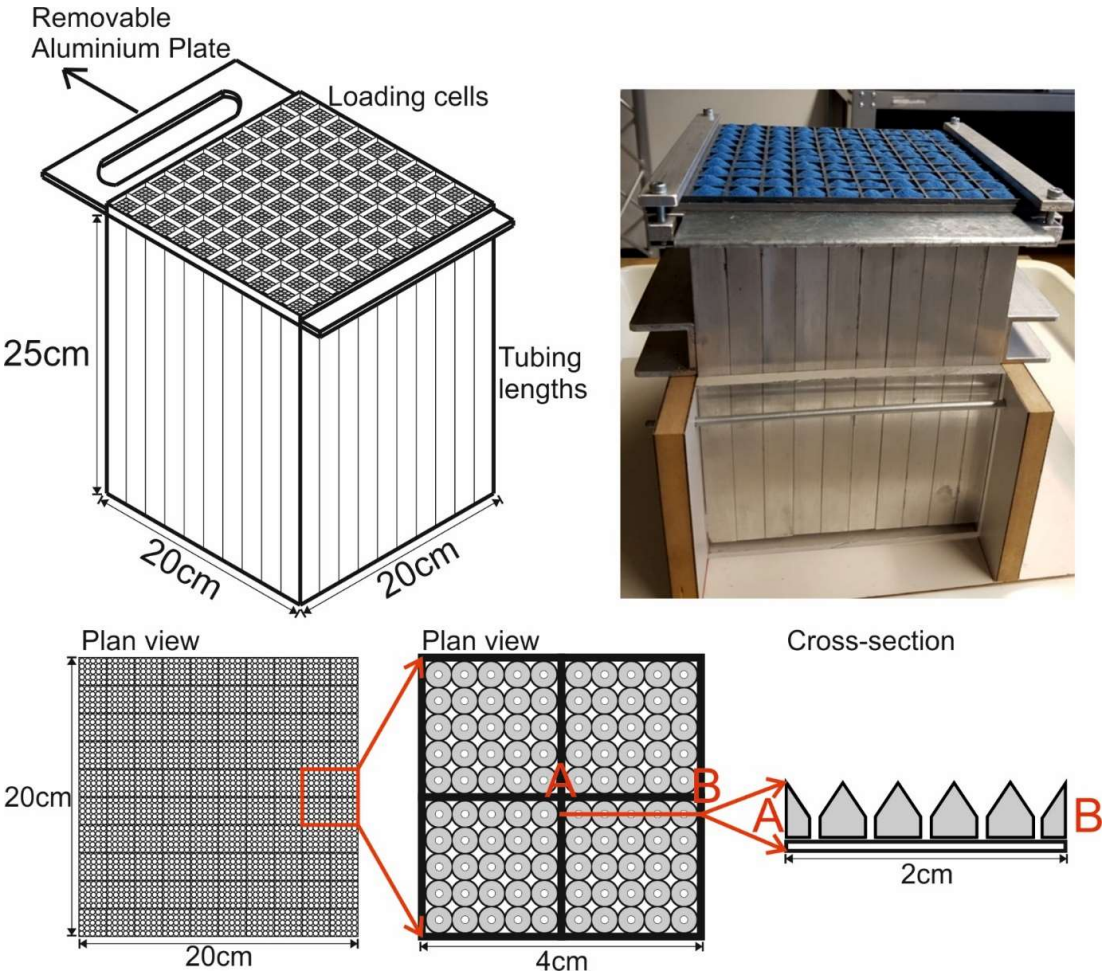

Figure 5.2: Images of the 10x10 sieving device. Upper left: 3D diagram of the device. Upper right: Sand volumes are loaded and ready to be deposited, flow is being inhibited by the steel plate protruding outwards. Below: 2D diagram of the cellular loading tray in plan-view and x-section.

5.2.3 Experiment surface recording – Stereo Digital Image Correlation

Sandbox surface topography is recorded using two high-resolution charge-coupled device cameras in a stereo setup. Digital Image Correlation (DIC) (Adam et al. 2005) is a tool typically used to capture time series data, monitoring deformation and surface flow in analogue deformation experiments at sub-millimetre resolution. For this study, Stereo-DIC is solely being employed to capture stereo images to derive incremental static digital elevation data from, each of which provides a high-resolution topographic data input for the use with the SFM.

5.2.4 Stratigraphic Forward Modelling – CarboCAT

The cellular stratigraphic forward modelling software used in this work is CarboCAT (Burgess 2013). Written in MATLAB, it functions using m-files to calculate carbonate lithofacies distributions in three dimensions based upon user-defined input parameter files. CarboCAT models enable reproduction of genuine carbonate architectures, displaying intricate stratal patterns such as interfingering. Large scale carbonate architectures have previously been successfully replicated by SFM (Bosence and Waltham 1990; Williams et al. 2011). CarboCAT has been demonstrated to handle complex basin subsidence patterns and provide a response of carbonate deposystems (Kozlowski 2017), making it suitable for coupling with basin-scale analogue sandbox experiments to yield realistic sedimentation patterns.

Central to CarboCAT's functionality is the use of cellular automata (CA), a discrete regular grid of cells, each in a finite number of states. They can be entirely deterministic in their calculation and, with a series of defined input rules, enable output of predictable results, such as particular stratal geometries. CA models can be applied to biological concepts of space, competition and population dynamics, justifying their application to investigate natural systems in many different disciplines (Drummond and Dugan 1999). The complexity of CA models can vary considerably, however there are three core features they all share:

- A grid of cells, each assigned a value representing its state.
- Structured networks between the cells.
- Computational algorithms that govern the nature of the networks.

By relying solely on cellular automata rules to govern model evolution, CarboCAT is a wholly deterministic forward model of carbonate strata. This contrasts with stochastic approaches (e.g. Parcell 2003) due to the generation of pseudo random numbers, meaning the laws imitating nature which govern model evolution do not have full influence over the outputs.

In CarboCAT, cellular automata are used to determine the distribution of lithofacies in two dimensions, which over time evolves into 3D. Cell state is determined with reference to surrounding cells, the scale of which is based on the 'radius' extending outwards from each cell, which determines the cell's 'neighbourhood'. The states of the cells in the surrounding neighbourhood determine the specific state of a cell at the next iteration, the possible states being either one of a finite number of carbonate 'factories', or empty. Carbonate factories are a concept derived from Schlager (2005) representing different groups of carbonate producing organisms, which occur at a characteristic range of water depths, temperature and seawater chemistry conditions. Three different factory types are applied within this work to represent the close spatial juxtaposition of three different groups of tropical carbonate producing organisms.

- Facies 1: Restricted to very shallow water production
- Facies 2: Production extends to greater depths
- Facies 3: Carbonate material is produced at a lower rate but near-independent of water depth.

A cell remains in its current state (survival rule) when (X = number of cells in the neighbourhood with identical factory type) $4 \leq X \leq 10$, becomes empty when $X \leq 3$ or $X \geq 11$ and, if empty, is recolonized (triggering rule) when $6 \leq X \leq 10$. To circumvent bias, the factory type which occupies an empty cell is continuously varied. The rules are applied for each model iteration, determining the state of the cell for that specific timestep. These are applied to constrain the principles of spatial competition and resource availability, and resulting minimum and maximum thresholds of population size.

The CA ruleset (Table 5.1) is then run together with a suite of geological processes, including; tectonic subsidence, water depth-dependent carbonate production rates and basic sediment transport. These inputs are then run for a predefined total time length, calculated by a number of timesteps of set length, generating sediment volumes and distribution.

Facies	Radius size	Minimum neighbours for survival	Maximum neighbours for survival	Minimum neighbours to trigger colonisation	Maximum neighbours to trigger colonisation	Triggers colonisation of which facies
1	2	4	10	6	10	1
2	2	4	10	6	10	2
3	2	4	10	6	10	3

Table 5.1: Cellular Automata rules used in CarboCAT scripting

Carbonate accumulation for a given cell is calculated by:

$$g_{(w)} = g_m \times tanh \frac{I_o e^{-kw}}{I_k}$$

- $g_{(w)}$: growth rate at depth w
- g_m: maximum growth rate
- $k_{e:}$ extinction coefficient of light
- I_o: surface light intensity
- I_k: saturating light intensity.

Tectonic subsidence is input as a grid of values, the same dimensions as the CarboCAT model itself. Each cell has a value which represents the tectonic subsidence / vertical adjustment for each increment. For example, 200m total subsidence would be achieved by having a subsidence value of 10 for 20 model iterations.

Sediment transport occurs whereby a pre-defined proportion of the accumulated carbonate material of a given timestep is transported and in this instance is given a separate facies assignment. CarboCAT uses a geometric style of modelling transport (e.g. Bosence et al. 1994), occurring when model slope is over a threshold value (i.e. always occurs downslope) and the volume is simply derived as a fraction of the total produced, if available within a given cell. Deposition of material then initiates in adjacent cells downslope, depositing half of the transported material into the subsequent cell. This process then continues, distributing produced material downslope.

5.3 Experiment Workflow

The static analogue sandbox model is setup with an inclined surface, area measuring 20x20cm (identical to the area covered by the sieving device), 1cm elevation difference between the top and base of the ramp (Figure 5.3). To produce this, sand was sifted into a u-shaped wooden box with a horizontal base. Two inclined acrylic blocks at are placed at the edges and then their tops are scraped flat to provide a smooth, angled surface. Following this, two more, taller, flat blocks are placed at the edges to confine later sand deposition within the model.

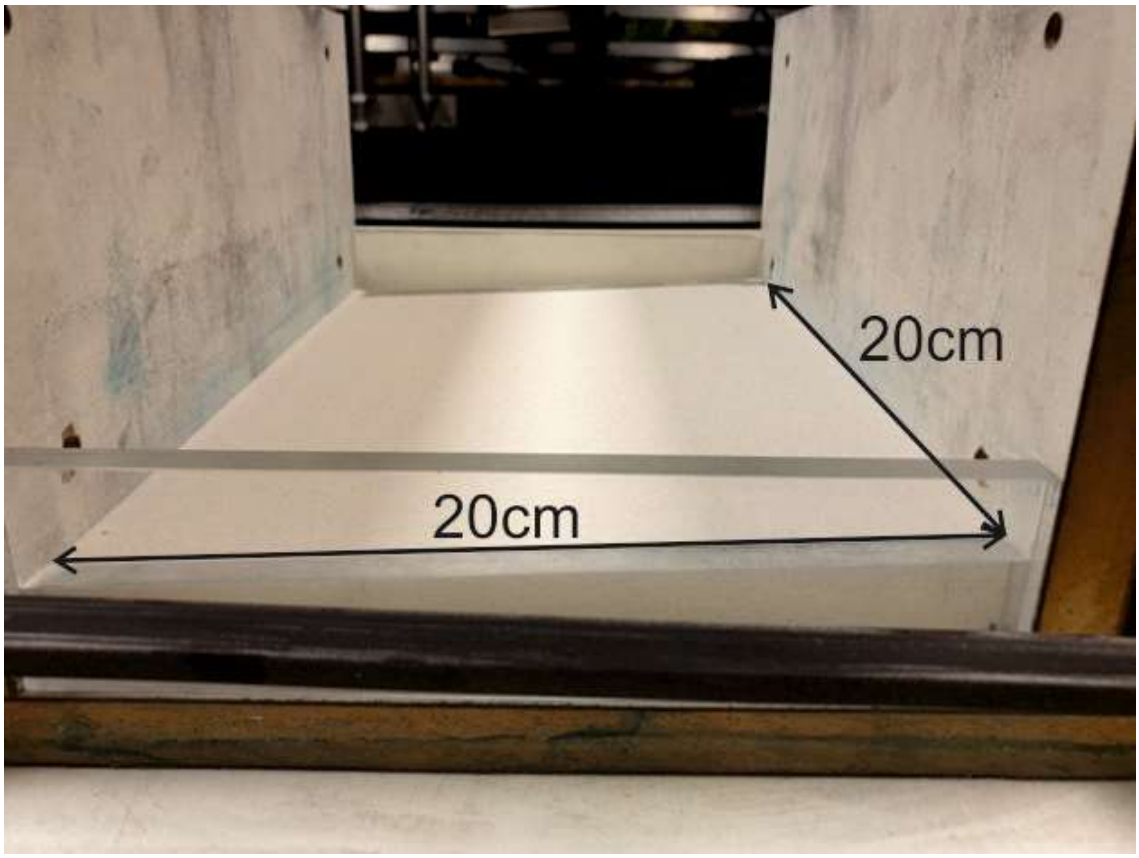

Figure 5.3: Experiment setup with initial sandpack of 3° degree inclination, experiment area is 20x20cm

Once set up, the surface is recorded using Stereoscopic DIC (Digital Image Correlation) yielding a digital format (TECPLOT) of the topography at sub-millimetre scale, with each data point being recorded as an x, y and z value (Figure 5.4). Minimal areal coverage is unable to be captured from the outermost edges because of incident angles of the cameras.

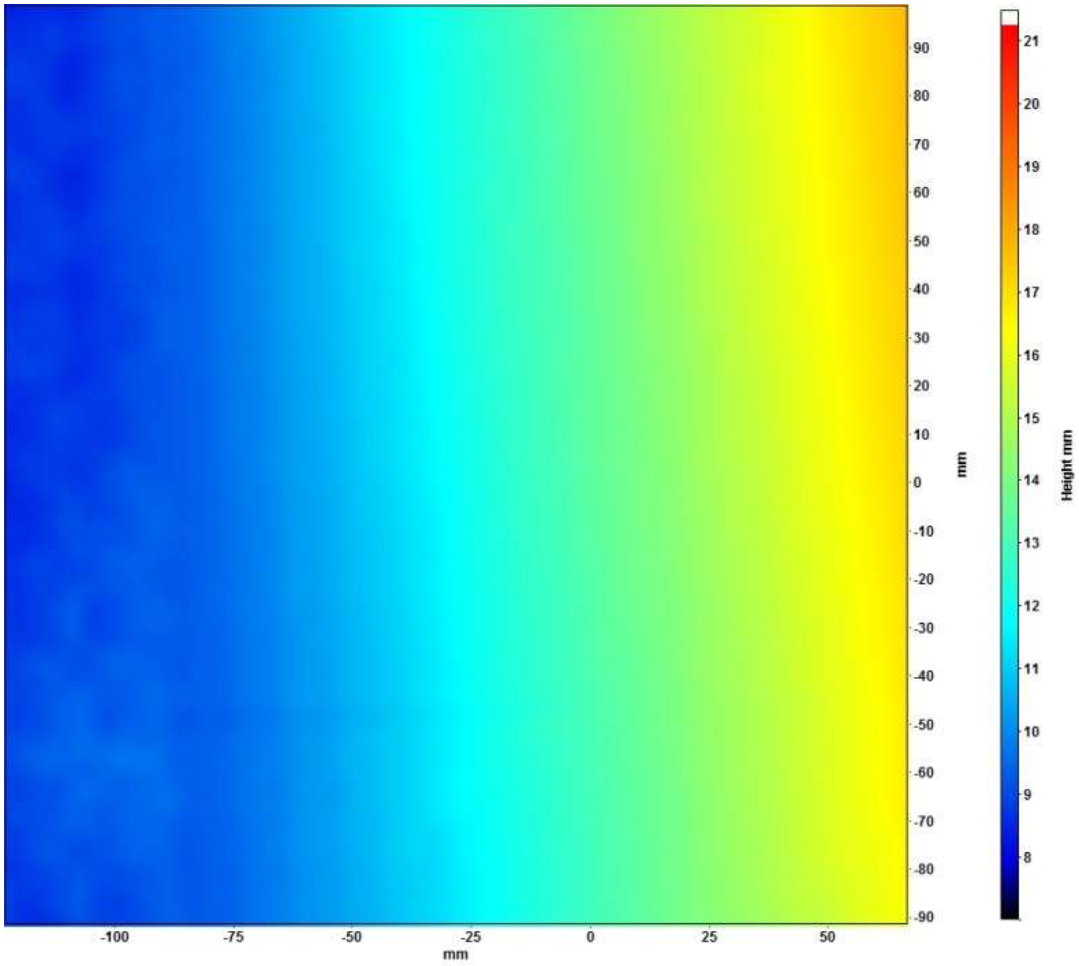

Figure 5.4: Elevation map of initial experiment surface derived from stereo images with DaVis™ software (version 8.4, LaVision)

The raw topographic data is exported to MATLAB and suitably cropped (leaving the 20x20cm surface), re-scaled (mm to metres), has sea-level applied at a pre-defined point near the base of the ramp (0m elevation) and reduced in resolution to an appropriate complexity (100x100 data points, each representing an area of 200x200m in nature). Any missing areal coverage from the cameras required to produce a representative 20x20cm input is extrapolated across from the adjacent data points at that edge. (Figure 5.5).

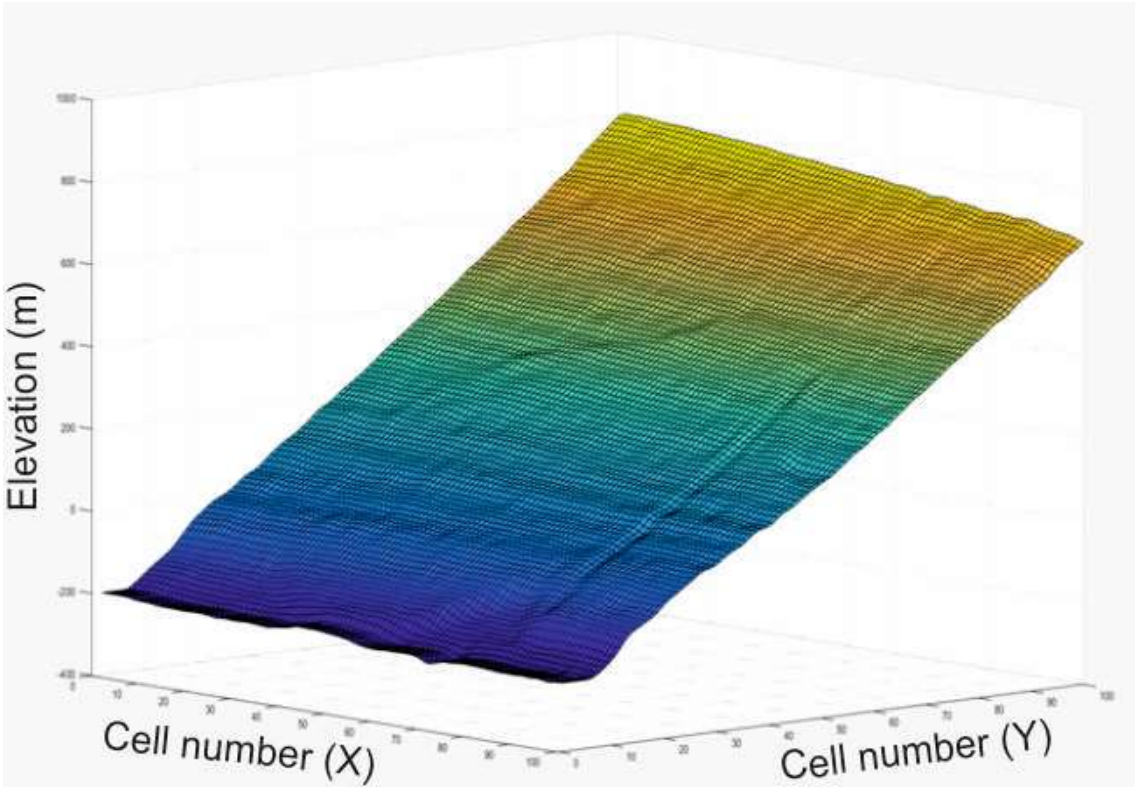

Figure 5.5: Digital elevation data of the initial experiment surface imported and visualised within MATLAB to form the input surface for the SFM.

The SFM (CarboCAT) calculates a sedimentation pattern of carbonate lithofacies distribution in 3D (Figure 5.6). This uses the formatted topography of the experiment surface as an input, which is run with a series of parameter files (Table 3); including subsidence rate, carbonate production rates and length of time.

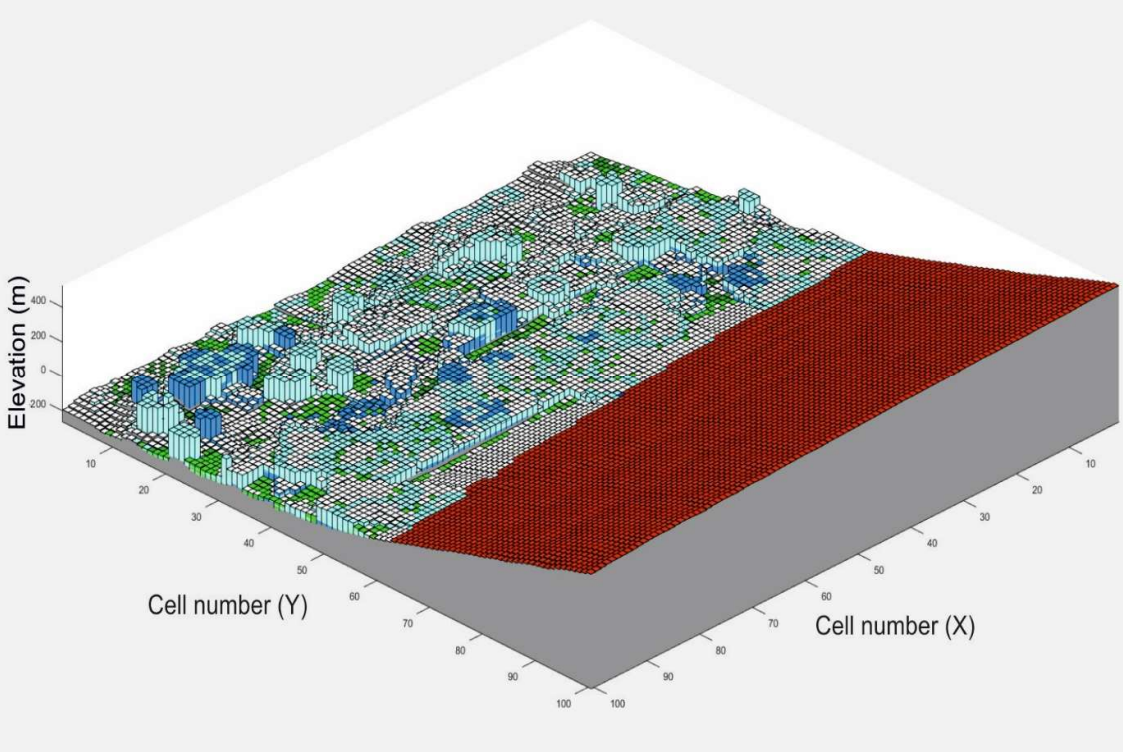

Figure 5.6: CarboCAT output displaying carbonate generation across the input topography. Each cell is in a discrete state; blue (actively producing carbonate lithofacies), green (transported carbonate material), white (unoccupied). Different shades denote the different lithofacies.

Calculated output volumes are averaged, transforming the 100x100 cell output from CarboCAT to 10x10, which mirrors the sieving device layout.

The sieving apparatus is able to deliver a minimum layer thickness of 0.5mm increments. Any surplus volumes remaining from SFM input, which would be unaccounted for by deposition, are transformed into a digital matrix and added onto the next input surface. These volumes are also combined with next output, as they still need to be deposited onto the sandbox. Generated volumes are loaded into their cells by hand, using levelled measuring spoons (Figure 5.7).

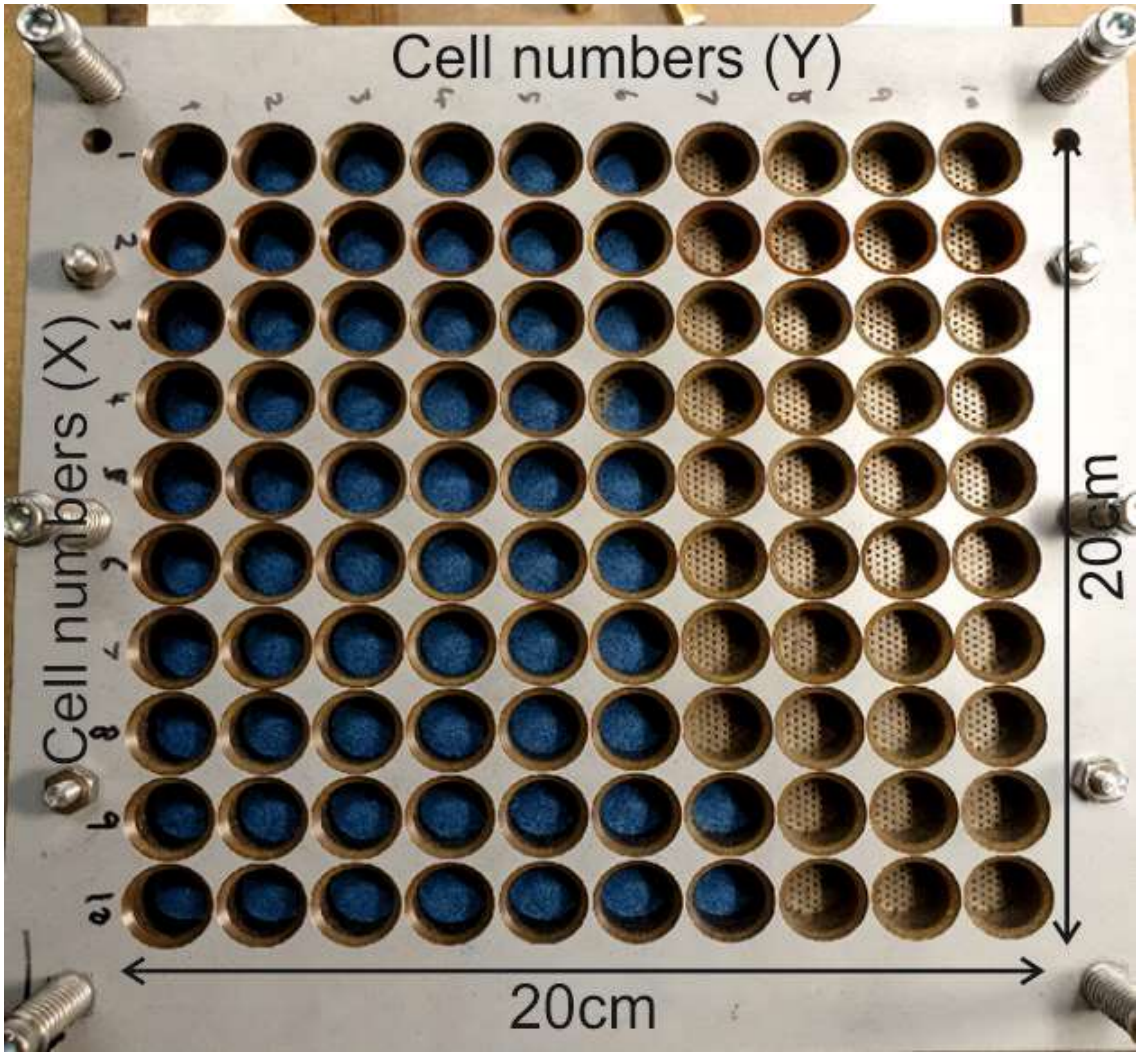

Figure 5.7: Calculated, scaled sand volumes from the SFM which are loaded into the sieving apparatus, awaiting deposition.

Once all the required cells are loaded, the aluminium retaining plate is withdrawn from beneath and the sand falls to the model surface through the network of tubes, maintaining the spatial distribution of material derived from the numerical model (Figure 5.8).

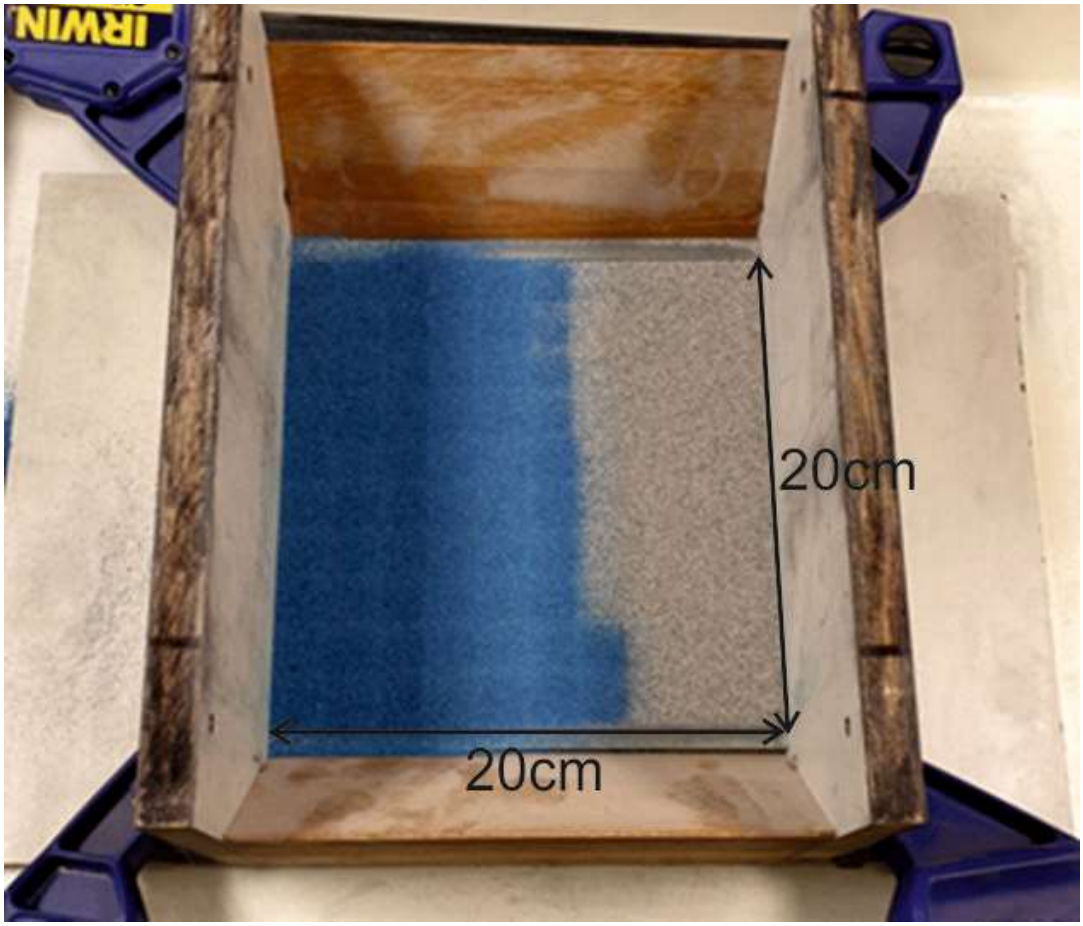

Figure 5.8: Heterogeneous volumes calculated by the SFM which have been deposited onto the sandbox surface in their relevant locations, whilst maintaining homogeneous mechanical properties with the rest of the sandpack.

The workflow is then repeated for a pre-defined number of sedimentation intervals. Within the numerical model, subsidence is cumulatively applied, starting at the position where it ended with the previous increment. This incrementally submerges the model surface when imported to the SFM, generating an ongoing source of accommodation.

Once complete, the finished model is covered with a protective sand cover, gelled and serially sectioned along strike in 3mm intervals and digitally photographed.

5.4 Results

Within this work three different models were conducted representing different initial surfaces and/or SFM parameters (Table 2). This was to demonstrate the functional integration of the analogue and numerical modelling steps, and to show that the model outcome is entirely deterministic; with only the experiment initial setup of the sandbox or SFM parameters independently determining the experiment evolution and result. Each model was subject to six discrete sedimentation intervals lasting 2My and having a nominal 200m of subsidence applied (12My time length and 1.2km subsidence total per model). Sea-level initiated near the base of the ramp and incrementally covers the entire initial model surface.

Model Parameter	Model 1	Model 2	Model 3
Experiment Surface	Ramp	Ramp	Incised Ramp
Carbonate production	Standard	Increased	Increased

Table 5.2: Key features of the three models

Numerical model parameters for each of the 3 models are outlined in the following table:

Model Parameter	**Model 1**	**Model 2**	**Model 3**
Total iterations	2000	2000	2000
Time step (My)	0.001	0.001	0.001
Subsidence rate (m My^{-1})	100	100	100
Eustasy	N/A	N/A	N/A
Lithology 1 carbonate production rate (m My^{-1})	500	5000	5000
Lithology 1 Surface light intensity (µE m^{-2} s^{-1})	2000	2000	2000
Lithology 1 extinction coefficient	0.1	0.1	0.1
Lithology 1 saturating light (µE m^{-2} s^{-1})	200	200	200
Lithology 1 transport product facies	5	5	5
Lithology 1 transported fraction of total production	0.1	0.1	0.1
Lithology 2 carbonate production rate (m My^{-1})	400	400	400
Lithology 2 Surface light intensity (µE m^{-2} s^{-1})	2000	2000	2000
Lithology 2 extinction coefficient	0.05	0.05	0.05
Lithology 2 saturating light (µE m^{-2} s^{-1})	300	300	300
Lithology 2 transport product facies	6	6	6
Lithology 2 transported fraction of total production	0.1	0.1	0.1
Lithology 3 carbonate production rate (m My^{-1})	100	100	100
Lithology 3 Surface light intensity (µE m^{-2} s^{-1})	2000	2000	2000
Lithology 3 extinction coefficient	0.005	0.005	0.005
Lithology 3 saturating light (µE m^{-2} s^{-1})	300	300	300
Lithology 3 transport product facies	7	7	7
Lithology 3 transported fraction of total production	0.1	0.1	0.1

Table 5.3: Numerical SFM parameters for the three models

5.4.1 Model 1

Model 1 was designed as a baseline experiment to demonstrate the functional integration of deriving experiment surface data into the numerical modeller, calculating relevant sediment input for the given time interval and depositing calculated sediment patterns with correct volumes and locations back onto the experiment surface. Results show the generation of a typical flat-topped carbonate platform produced over the six sedimentation intervals (Figure 5.9). A steep platform edge is generated, with repeated drowning of production down-dip and primarily transported material from the platform top being deposited beneath the platform in subsequent layers.

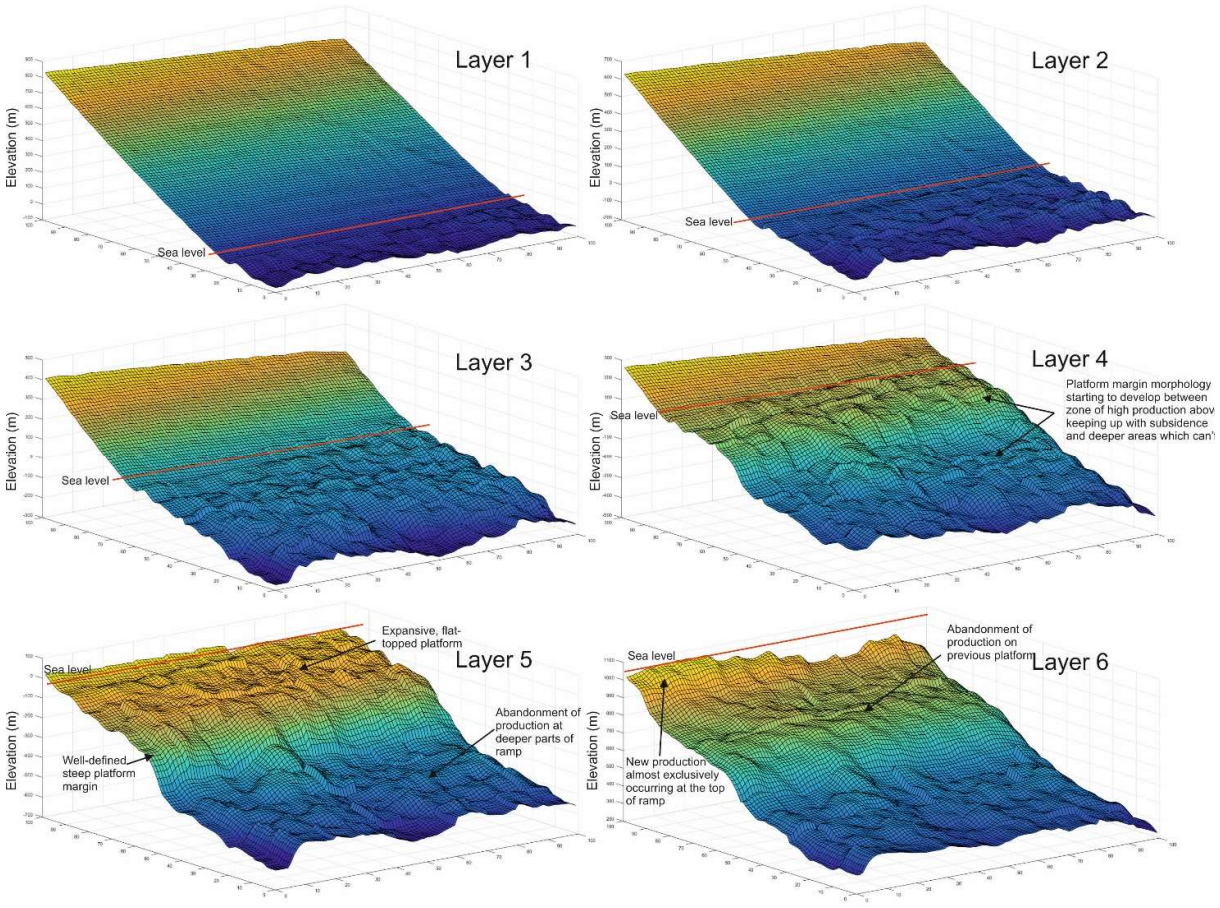

Figure 5.9: Model 1: Scaled 3D topographic input surfaces visualised in MATLAB showing model evolution over the 6 sedimentation intervals.

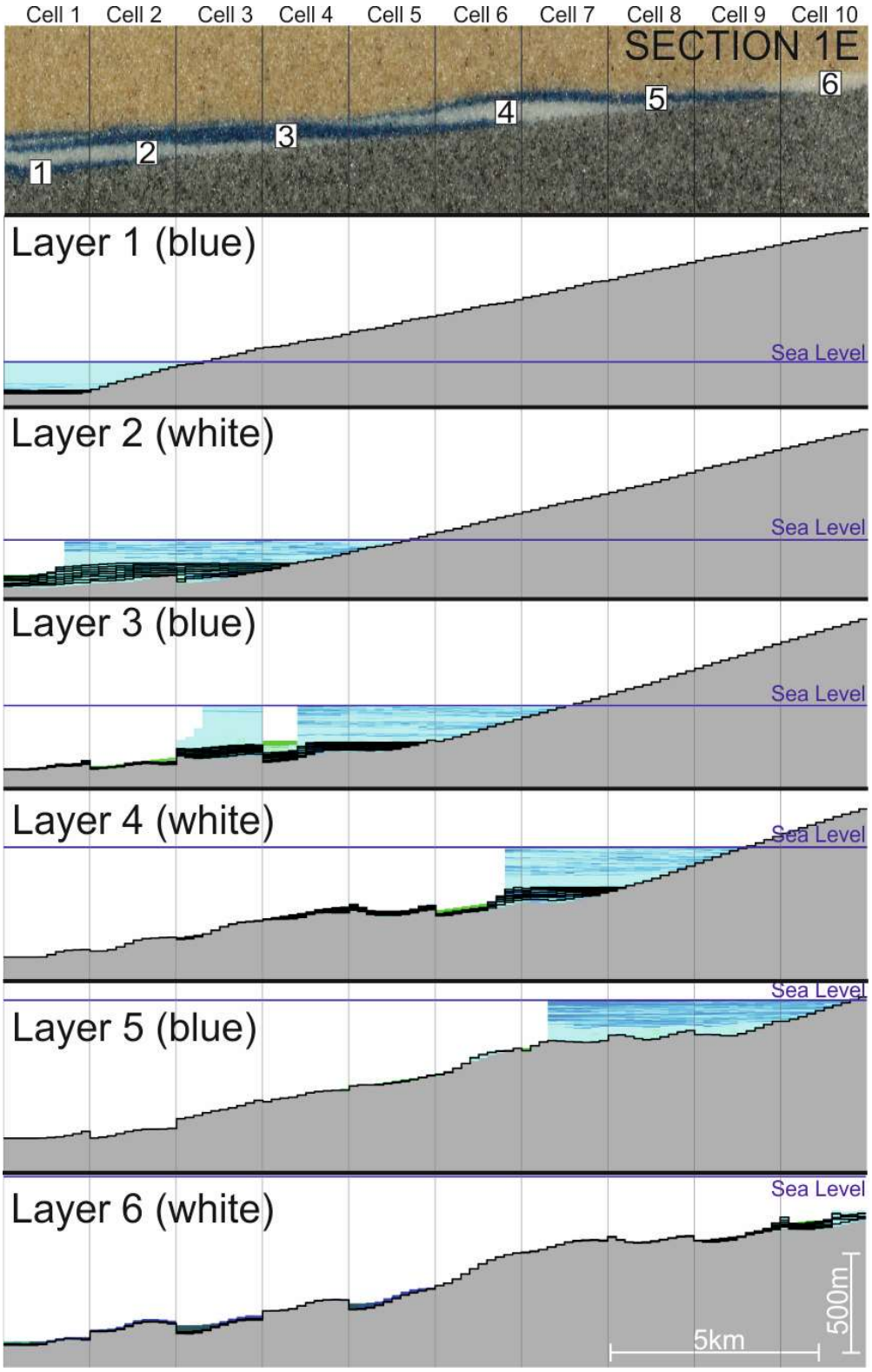

Figure 5.10: Top: A vertically exaggerated (2:1) cross-section taken from the centre of the finished sandbox model 1 (exact position indicated in Figure 5.14), showing the 6 sedimentation intervals. Below: The 6 individual calculated sedimentation intervals shown in CarboCAT. Numerical cross-sections are taken from the same relative position as the sandbox section. Overlain are the positions of the 10 analogue cellular depositional areas which correspond to the 100 cells in the numerical model which are averaged.

Within Figure 5.10, some minor differences are observed between the sections showing calculated carbonate volumes and 2D extent of deposited sand representing them above. This is due to the numerical model representing the cross-section of a single model cell, whereas the sand volume deposited is calculated from an average of 10 numerical cells in both X and Y directions. Addition of omitted sedimentation from a previous interval also accounts for some of the observed differences between numerical model and sandbox section. In layer 4 many cells below the platform margin were close to having an additional 0.5mm of sand added. Material transported downslope from the platform top in the following increment 5 meant many cells crossed the threshold for a 0.5mm resulting widely pervasive deposition of the blue layer, despite minimal sedimentation occurring in cells below the platform margin.

To verify that the correct volumes are being translated from the numerical model onto the analogue surface; deposited thicknesses were measured from section 1E (Figure 5.10) and compared with the calculated output from the numerical model. Layer thicknesses were measured at the centre of each of the 10 cell areas indicated on section 1E. Vertical thicknesses calculated from the numerical model are indicated in Table 5.4.

Cell no.	Layer 1 (blue)			Layer 2 (white)			Layer 3 (blue)		
(Y-axis)	Target (mm)	Actual (mm)	Difference (mm)	Target (mm)	Actual (mm)	Difference (mm)	Target (mm)	Actual (mm)	Difference (mm)
1	1.50	1.31	-0.19	2.00	1.69	-0.31	1.00	0.80	-0.20
2	0.50	0.73	0.23	2.00	1.68	-0.32	1.00	1.07	0.07
3	0.00	0.00	0.00	1.50	1.33	-0.17	2.00	1.87	-0.13
4	0.00	0.00	0.00	1.00	0.93	-0.07	2.00	1.73	-0.27
5	0.00	0.00	0.00	0.00	0.00	0.00	1.50	1.33	-0.17
6	0.00	0.00	0.00	0.00	0.00	0.00	1.00	1.00	0.00
7	0.00	0.00	0.00	0.00	0.00	0.00	0.00	0.00	0.00
8	0.00	0.00	0.00	0.00	0.00	0.00	0.00	0.00	0.00
9	0.00	0.00	0.00	0.00	0.00	0.00	0.00	0.00	0.00
10	0.00	0.00	0.00	0.00	0.00	0.00	0.00	0.00	0.00
Cell no.	**Layer 4 (white)**			**Layer 5 (blue)**			**Layer 6 (white)**		
(Y-axis)	Target (mm)	Actual (mm)	Difference (mm)	Target (mm)	Actual (mm)	Difference (mm)	Target (mm)	Actual (mm)	Difference (mm)
1	0.50	0.53	0.03	1.00	0.93	-0.07	0.50	0.27	-0.23
2	0.50	0.60	0.10	0.50	0.60	0.10	0.00	0.00	0.00
3	0.00	0.27	0.27	0.50	0.53	0.03	0.00	0.00	0.00
4	0.50	0.40	-0.10	0.00	0.27	0.27	0.50	0.40	-0.10
5	1.00	1.07	0.07	0.50	0.40	-0.10	0.50	0.27	-0.23
6	2.00	1.87	-0.13	1.00	0.93	-0.07	0.50	0.27	-0.23
7	2.00	1.87	-0.13	1.50	1.27	-0.23	0.50	0.27	-0.23
8	1.00	0.59	-0.41	1.00	1.27	0.27	0.50	0.40	-0.10
9	0.00	0.00	0.00	1.00	1.27	0.27	1.00	0.93	-0.07
10	0.00	0.00	0.00	0.00	0.00	0.00	2.00	2.00	0.00

Table 5.4: Comparison of thicknesses calculated by the numerical model (Target) and observed translation into the sandbox experiment (Actual) in Figure 5.10. Each layer is split into the 10 cells that are deposited within it for that orientation.

Results demonstrate that the apparatus achieves accurate scaled translation of calculated thicknesses onto the analogue surface. The majority of differences are around or within the thickness of a single grain of sand (average grain size = 0.18mm).

Generally, thicknesses deposited are slightly lower than calculated, this is likely attributed to some sand being lost within the apparatus and lateral spread upon deposition, particularly in isolated cells where spread is not being inhibited laterally by deposition in adjacent cells.

5.4.2 Model 2

Model 2 illustrates the impact of changing a parameter within the numerical model. The model has increased production rates of carbonate lithology 1 (5000m My^{-1}) versus Model 1 (500m My^{-1}). The aim was to observe how the increased production rate affects the developed platform architecture and how much more of the available accommodation is filled over the 6 sedimentation intervals, as the production rate should now comfortably outpace the subsidence rate (100m My^{-1}). This was largely achieved, with a homogeneous appearance to the platform, covering the majority of the sandbox (Figure 5.11). The model still retains a distinct steep margin, primarily at model edges, where production ceased.

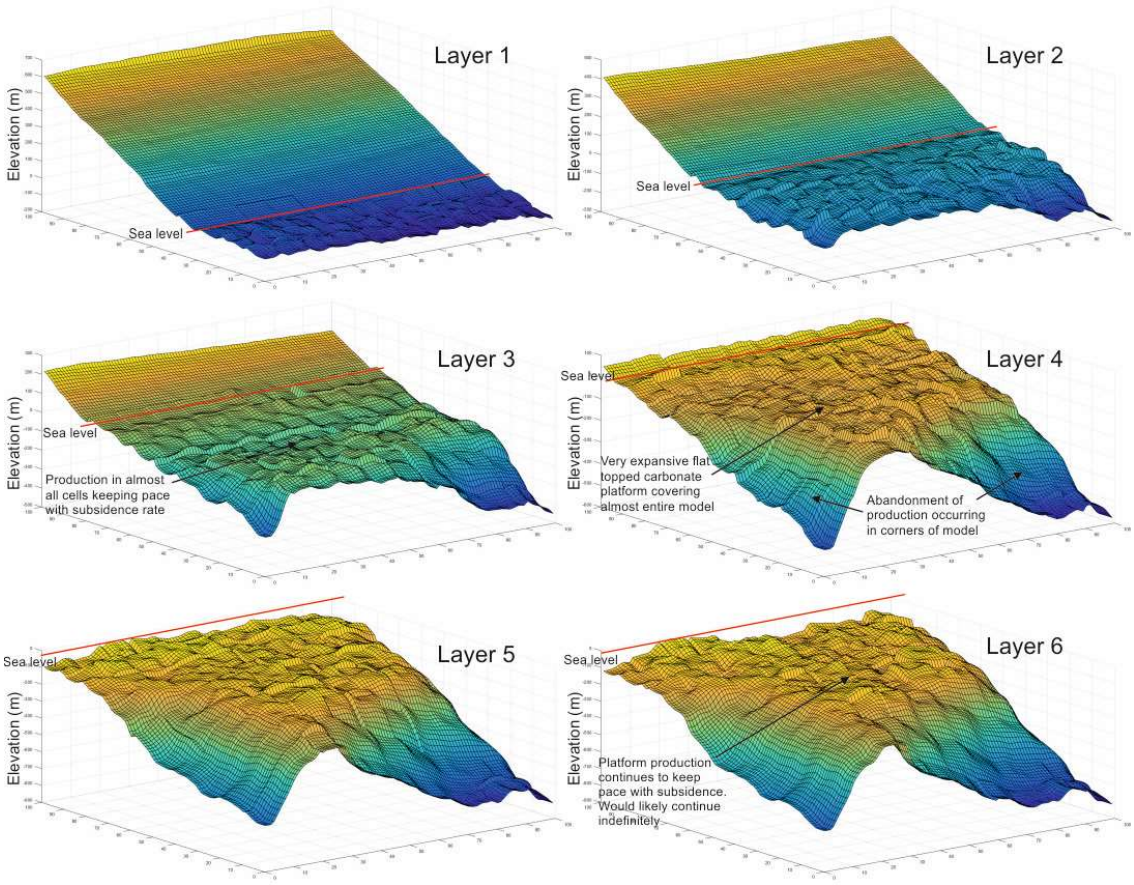

Figure 5.11: Model 2: Scaled 3D topographic input surfaces visualised in MATLAB showing model evolution over the 6 sedimentation intervals.

5.4.3 Model 3

Model 3 was to illustrate the impact of changing the initial experiment surface geometry, whilst keeping numerical parameters identical to model 2. It had the initial sandpack incised, forming structural highs and lows. Initially the model has carbonate lithofacies being deposited into the canyons, whilst maintaining the structure of the lobe-like highs and having no deposition occurring on top of them, until a later stage in the model at which point subsidence transitions the tops below sea-level and sedimentation occurs on top of them (Figure 5.12).

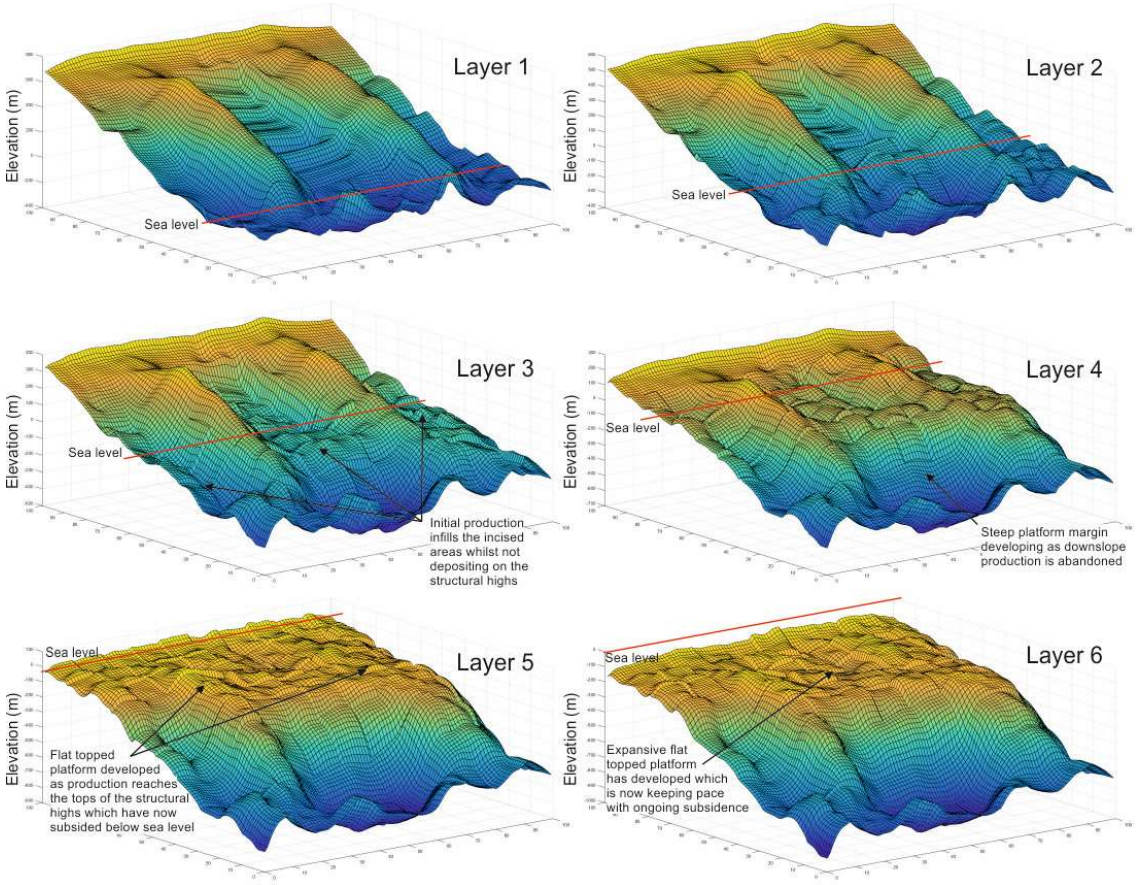

Figure 5.12: Model 3: Scaled 3D topographic input surfaces visualised in MATLAB showing model evolution over the 6 sedimentation intervals.

5.4.4 Results Overview

An overview of the three scaled experiments is given below, illustrating experiment evolution with a combination of digital topographic surfaces and plan-view SLR photos (Figure 5.13), and suites of experiment sections (Figure 5.14).

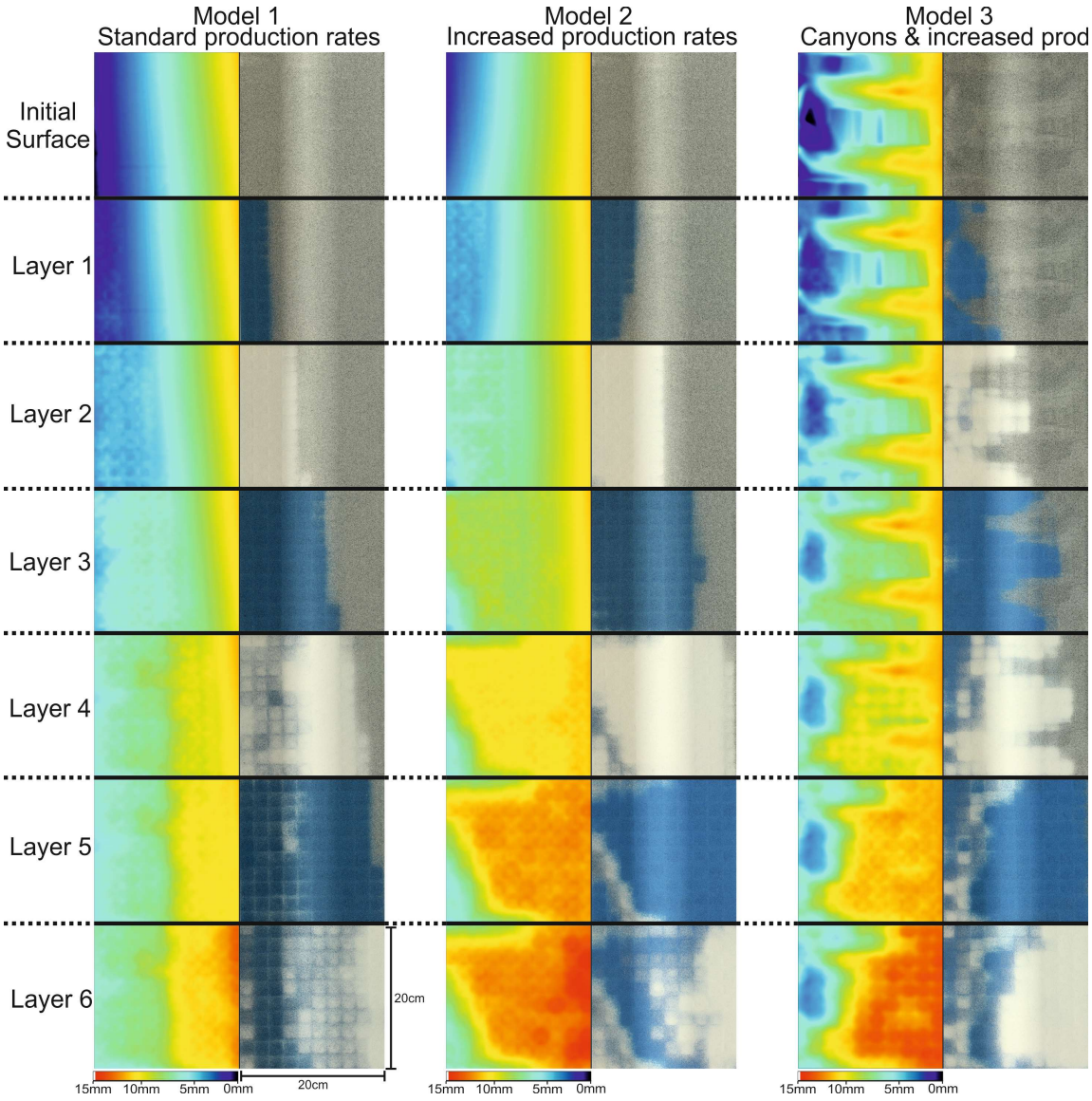

Figure 5.13: Composite diagram showing the incremental evolution for each of the 3 models. Left-hand images are plan-view digital topographic data shown in DaVis™ software (version 8.4, LaVision). Right-hand images are plan-view photos of the same surface.

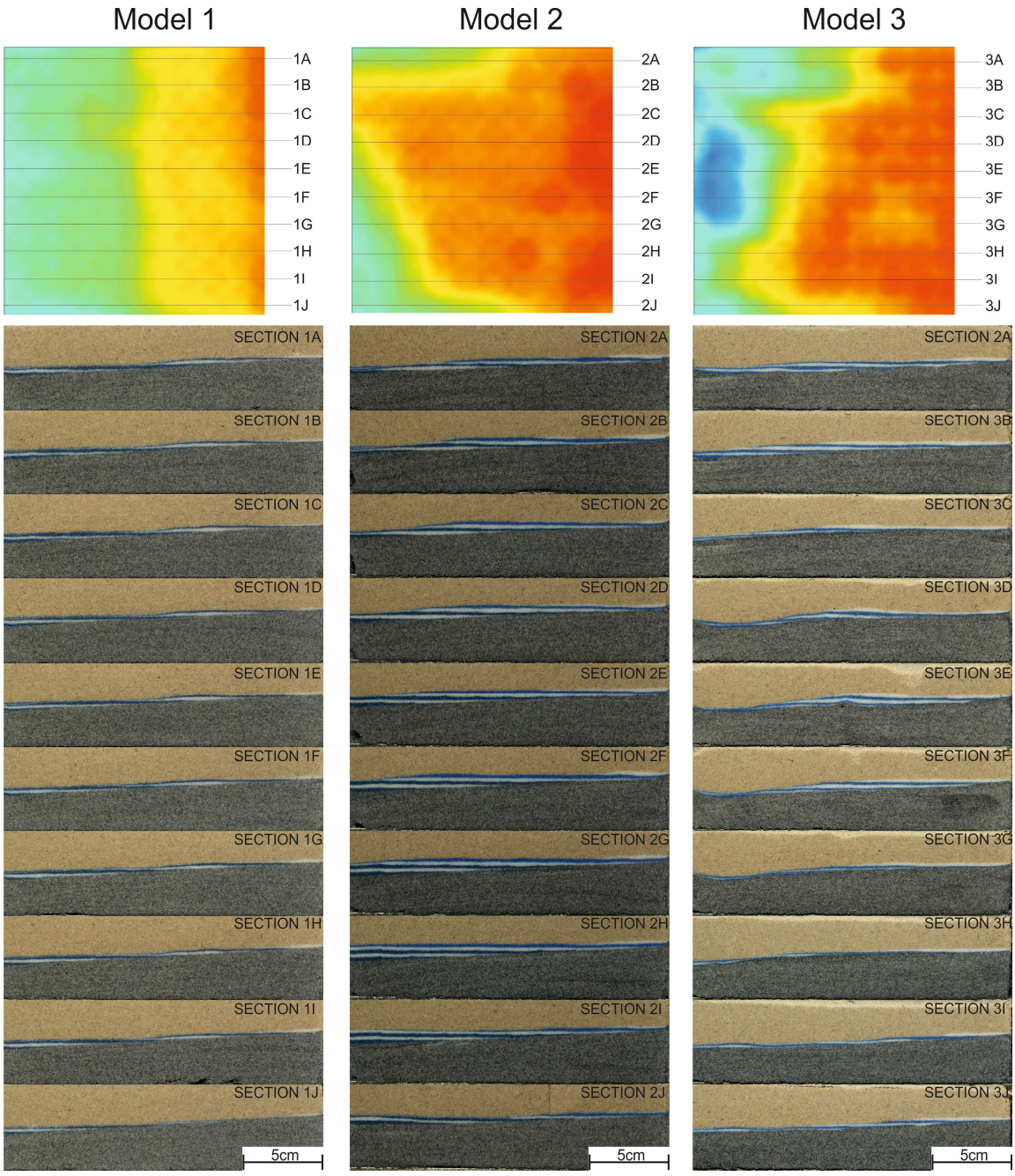

Figure 5.14: Cross-section data taken from the finished sandbox models. Relative positions of each section are indicated on the final topographic surface image above.

5.5 Discussion

Results from the three models demonstrate that calculated sedimentation volumes and patterns differ (Figure 5.13 and Figure 5.14); being determined by initial experiment topography and numerical modelling parameters, which can be reliably reproduced in the analogue experiment. Consecutive sedimentation intervals deposit complex patterns which evolve into 3D structures deterministically, with carbonate production in later intervals being dependent upon the existing sandbox topography to provide a surface to colonise. As typical flat-topped, steep-margin carbonate platforms are developed, the actively producing area expands for each model, resulting in a greater volume of carbonate being produced and subsequently transported downslope, blanketing previously deposited layers.

Model 1 successfully demonstrates a working integration between analogue and numerical modelling in a novel workflow, with numerically calculated volumes being accurately translated onto the analogue surface, influencing subsequent evolution.

Model 2 achieved its goal of proving that changing input numerical parameters, whilst starting with the same inclined analogue surface, will produce a different final result. The role of increased carbonate production meant a far greater amount of available accommodation was filled, with thicker sand layers being deposited throughout. This resulted in a much more expansive platform being developed compared to Model 1 (Figure 5.13).

Model 3 maintained the numerical parameters from model 2, but used a different initial topography. Sedimentation patterns deposited were the most complex, varying both down-dip (as with previous models) but also along strike, being affected by the presence of the canyons/lobes (Figure 5.14). Canyons were filled over the 6 sedimentation intervals, whereas production onto the lobes could only begin in later intervals once they were subsided below sea-level. Their appearance is preserved in the final model with the two lobes protruding beyond the otherwise

straight platform margin where production has continued on top of their pre-existing topography.

A feature observed in all three models over time is abandonment of down-slope production, which occurs somewhat unexpectedly in models 2&3, even despite the vastly increased production rates which should comfortably outpace subsidence. A contributing factor is possibly that translated volumes are not perfectly accurate. The sand, when deposited within a given cell, has potential to spread laterally beyond the confines of the 2x2cm target area, as well as sand being lost within the apparatus as it provides a thin coating on the surface of the aluminium plate when withdrawn. These two factors are resulting in deposited sand layers being slightly thinner than desired. Given the geometric scaling, 0.5mm in the sandbox represents 50m within the numerical model (nature), this distance is sufficient to reduce the primary carbonate producing lithology (1), and only one able to keep-up with subsidence, to zero, resulting in cessation of production within these cells. Thus, as indicated in Table 5.4, even when cell thicknesses are being accurately deposited, they may be as little as 0.18mm lower than expected (median grain size). This distance of 18m in nature still somewhat reduces the production of a given cell due to the production profile of carbonates, indicating quite a high sensitivity within the model.

Another potential cause is the smoothing of outputs from CarboCAT to the sieving apparatus. Models are calculated at a 100x100 resolution, however when translated into volumes to be deposited, they are averaged to a 10x10 resolution. A single cell at this coarser resolution may overlap zones of both high and low production from the numerical model. As a result, when volumes are averaged to provide the single value for that depositing cell, it will be lower than desired for the actively producing area, thus negatively that those cells will be incapable of continuing to produce and keep-up with subsidence in latter sedimentation intervals.

5.6 Conclusions and Future Work

The workflow outlined in this paper has been demonstrated to successfully integrate the two processes of analogue sandbox modelling and numerical stratigraphic forward modelling in a novel approach. Final models are entirely deterministic and evolution is governed purely by interaction between the analogue and numerical modelling techniques. This has been achieved by:

- Digitally adapting surface data derived from analogue experiments to represent a scaled topographic input for numerical modelling software.
- Using a sieving apparatus to successfully deposit the complex, spatially variable volumes calculated from the numerical modeller onto the analogue sandbox, whilst maintaining a sandpack with homogeneous mechanical properties.

Previous work (Chapter 4) has demonstrated that the sedimentation device will yield correct mechanical properties in the deposited sandpack to simulate brittle-frictional behaviours observed in the upper crust, permitting its use within dynamically-scaled sandbox experiments with ongoing tectonic deformation. Given that stereo-DIC techniques are capable of monitoring sandbox surface evolution through time, permitting derivation of vertical displacement (i.e. subsidence); if this data were suitably captured and scaled, it could act as an input for the numerical model. This would permit the SFM to undergo a near identical tectonic evolution (subsidence history) to the analogue surface whilst it is calculating the sediment accumulations.

Successfully completing this step means the workflow would be uniquely capable of accurate simulation of both regional tectonic processes and spatially variable depositional patterns within a single integrated model.

6 Combining stratigraphic forward modelling software and an extensional analogue sandbox experiment to permit both quantitative simulation of depositional systems and dynamically-scaled tectonic deformation within a single integrated model

Abstract

This work documents the application of stratigraphic forward modelling (SFM) software to a kinematic analogue sandbox experiment. Sedimentation patterns are dynamically calculated in the numerical model based upon input data derived from extensionally-driven tectonic subsidence within the sandbox which determines accommodation creation.

Sandbox topography and subsidence of a domino-style basement fault system is captured using high resolution Digital Image Correlation (DIC) techniques, yielding a scaled digital input surface and subsidence rate data for the SFM, which then calculates realistic sedimentation patterns by running the data in combination with geologically reasonable production parameters for carbonate sedimentation. These heterogeneous volumes are then scaled to the analogue model and deposited onto the sandbox surface at their relevant positions using a cellular array of tubes within a single sand layer.

Previous work has shown that the workflow accurately achieves scaled translation of SFM calculated sedimentation patterns onto the analogue surface, which have the capacity to develop into complex 3D structures with repeated layering, whilst depositing a sandpack with required, homogeneous mechanical properties. Model evolution is also entirely deterministic, being governed by the numerical production parameters and surface evolution of the analogue model.

Given that sedimentation affects tectonic evolution, both in sandbox models and nature, governing future accommodation; this methodology has potential to provide a more detailed insight into feedback mechanisms between sedimentation and tectonic deformation, as accurate simulation of them will now be achieved with

a single integrated workflow. Non-tectonic controls such as sea level or climate can also be investigated in more detail, showing how they influence model evolution.

6.1 Introduction

Syn-tectonic depositional sequences are controlled by basin geometry, active tectonic structures, subsidence, sediment supply, base level and sea-level fluctuations (Leeder and Gawthorpe 1987; Schlische 1991). In turn, the loading effect from ongoing sedimentation affects fault strength and strain localisation, governing future tectonic evolution (Bialas and Buck 2009; Barrier et al. 2013; Zwaan et al. 2018). Feedback mechanisms between sedimentation and tectonic processes are known, but as of yet have not been investigated in detail using analogue modelling techniques.

Scaled analogue sandbox models develop realistic, basin-scale fault architectures and tectonic subsidence patterns, including fault localisation, segmentation, linkage and displacement, producing meaningful tectonic-subsidence (McClay and Ellis, 1987). This governs accommodation evolution in both time and space.

Syn-kinematic sedimentation within analogue sandbox experiments is currently a process almost exclusively conducted manually in a conceptual, qualitative manner. Consequently, even when geological constraints like sedimentation rates and available accommodation are considered (e.g. Adam et al. 2012), the methodology is still somewhat basic, being restricted to gross first-order sedimentation patterns. In contrast, syn-kinematic sedimentary evolution of natural half-grabens within extensional settings is highly complex (Ravnås and Steel 1998), so it is argued that current analogue methods cannot adequately simulate sedimentation patterns and thus are not invoking a representative tectonic response within the model.

This work seeks to apply a previously demonstrated workflow (Chapter 5) to a kinematic basin-scale analogue experiment. This workflow was shown to calculate realistic sediment distributions using cellular stratigraphic forward modelling (SFM)

software based upon the topography derived from an analogue sandbox surface, geologically-constrained carbonate production parameters and user-defined subsidence patterns. Computer-calculated volumes are then accurately scaled and deposited onto the analogue surface at their relevant positions using a sieving apparatus (Chapter 4) capable of yielding mechanically homogeneous sandpacks with variable volume distribution within a single layer.

For this study a stereo-DIC camera setup is used to monitor surface deformation during incremental kinematic evolution in an extensional analogue apparatus simulating a pair of domino-style half grabens. The high-resolution images of surface topography are transformed to produce input data representing both topography and subsidence rate for the SFM, permitting dynamic calculation of depositional systems. By applying the subsidence history, for a given extension increment, to the surface geometry at the beginning of it; the numerical model will undergo a near-identical tectonic evolution to the analogue sandbox whilst dynamically-calculating realistic 3D sedimentation patterns.

Changing the length of individual iterations within the SFM determines the length of time to calculate sedimentation patterns for (1000 iterations of either 1, 2 or 4ky). As the distance of extension is kept constant between models, the extension rate of the analogue model can be varied and appropriately scaled within the SFM. Incrementally generated accumulations are then deposited onto their relevant locations on the sandbox surface before resuming model extension and repeating the process.

An outline of the workflow is shown in Figure 6.1, with a detailed description of most steps in Chapter 5. Within this Chapter there is an explanation of the additional steps; the kinematic extension of the model and subsequent monitoring using a stereo-DIC setup. Then, from this data, calculating a scaled subsidence rate to be used by the SFM, enabling the numerical model to undergo an identical tectonic evolution to the analogue sandbox.

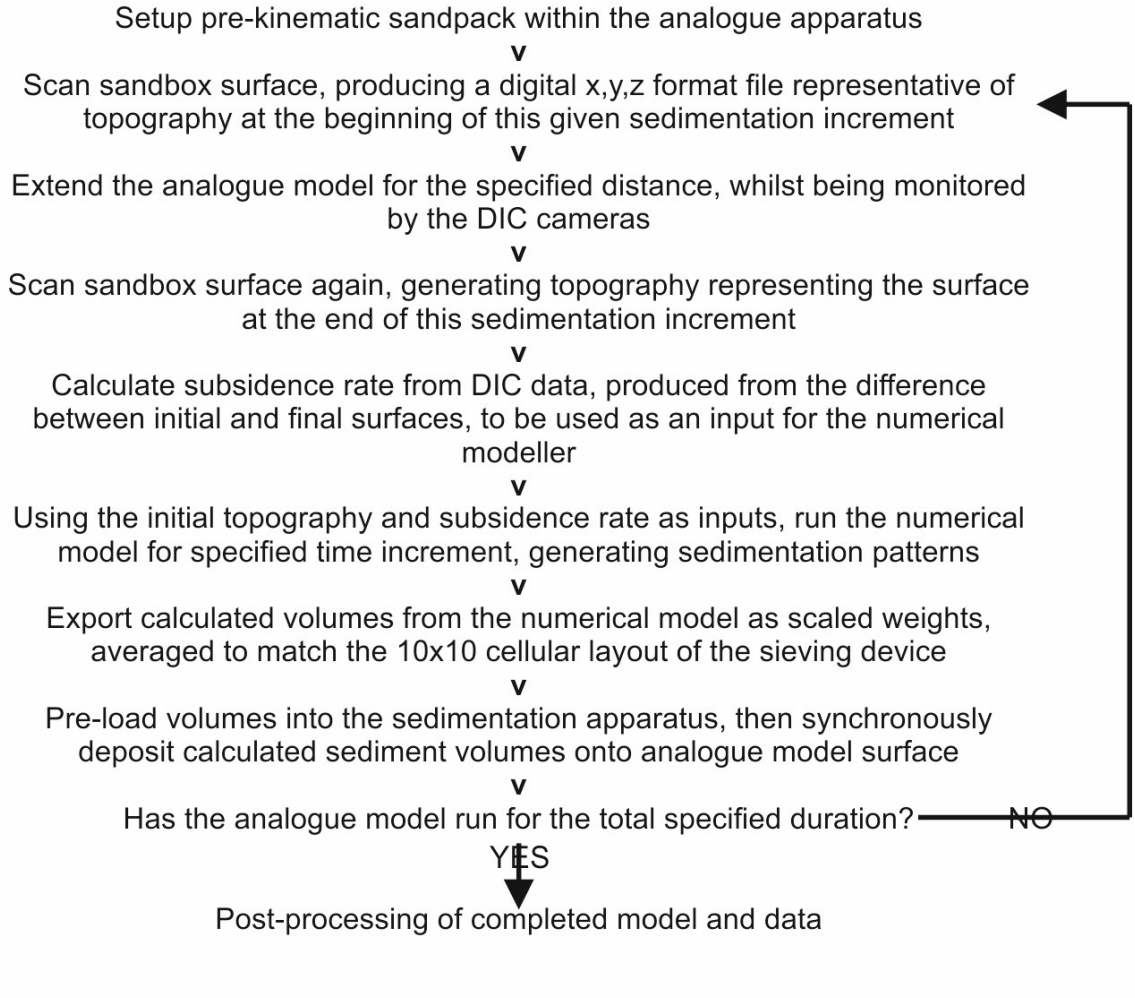

Figure 6.1: Flow chart documenting the integrated workflow procedure between analogue and numerical models when applied to an extensional sandbox experiment

6.2 Methods and Materials

6.2.1 Analogue scaling and modelling materials

(As in Chapter 5): *All models documented were constructed entirely from a high purity (>99.7% SiO_2), well sorted, silica sand with a median grain size of 180µm. The granular flow characteristics of dry, near-cohesionless, granular materials are well-suited to simulate brittle upper-crustal deformation in scaled analogue experiments (Lohrmann et al. 2003). Material parameters derived by ring-shear testing showed an internal angle of friction of 30-37°, peak internal friction coefficient of 0.76, dynamic internal friction coefficient of 0.58 and static internal friction coefficient of 0.65. The dynamically scaled sandbox experiments have a geometrical scaling factor of 10^{-5} (1cm in model = 1km in nature), derived from density and cohesion ratios of model and natural materials (Hubbert 1937; Lallemand et al. 1994).*

6.2.2 Analogue sieving device

(As in Chapter 5): *The sedimentation apparatus (Figure 6.2, described in more detail in Chapter 4) is a 10x10 cellular array of aluminium tubes, each 2x2cm wide and 25cm in vertical length, which is placed in a fixed position above the analogue surface and permits incremental deposition of heterogeneous sand volumes within a single layer, whilst maintaining homogeneous mechanical properties. A discrete grid of cells sits above the tubes, supported by an aluminium plate. Discrete volumes are loaded into the cells, with their position overlying the relevant position on the experiment surface. Once all required cells are filled the aluminium plate is withdrawn, allowing near-synchronous deposition of the heterogeneous sand volumes onto the experiment surface.*

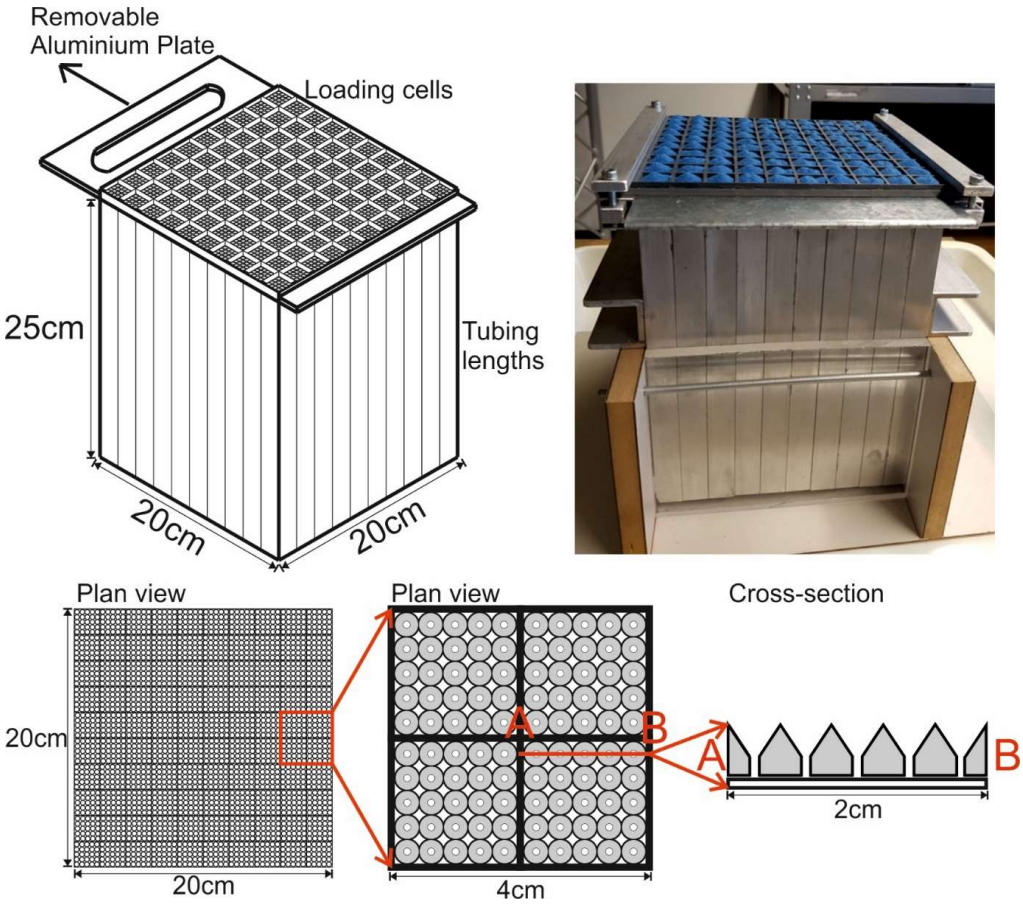

Figure 6.2: Images of the 10x10 sieving device. Upper left: 3D diagram of the device. Upper right: Sand volumes are loaded and ready to be deposited, flow is being inhibited by the steel plate protruding outwards. Below: 2D diagram of the cellular loading tray in plan-view and x-section.

6.2.3 Experiment surface recording – Stereo Digital Image Correlation

The actively deforming sandbox surface topography is recorded using two high-resolution charge-coupled device cameras in a stereo setup. Digital Image Correlation (DIC) (Adam et al. 2005) is a tool typically permitting capture of time series data, monitoring deformation and surface flow in analogue deformation experiments at sub-millimetre resolution. For this study, stereo-DIC is being employed to capture surface images to derive incremental digital elevation data from. The sandbox surface is being recorded during each extension interval, permitting quantification of the surface evolution, which can be used to replicate the development in the SFM.

6.2.4 Stratigraphic Forward Modelling – CarboCAT

(As in chapter 5): *The cellular stratigraphic forward modelling software used in this work is CarboCAT (Burgess 2013). Written in MATLAB, it functions using m-files to calculate carbonate lithofacies distributions in three dimensions based upon user-defined input parameter files. CarboCAT models enable reproduction of genuine carbonate architectures, displaying intricate stratal patterns such as interfingering. Large scale carbonate architectures have previously been successfully replicated by SFM (Bosence and Waltham 1990; Williams et al. 2011). CarboCAT has been demonstrated to handle complex basin subsidence patterns and provide a response of carbonate deposystems (Kozlowski 2017), making it suitable for coupling with basin-scale analogue sandbox experiments to yield realistic sedimentation patterns.*

Within this Chapter, subsidence applied to the SFM is not being user-defined, but instead is derived from the analogue experiment. Input data recorded from the stereo-DIC surfaces, representing the beginning and end of each extension interval, are used to calculate the elevation difference (i.e. subsidence).

This is done by importing the raw topographic data to MATLAB; where both surfaces are suitably cropped (leaving only the 20x20cm target surface), re-scaled (mm to metres), have sea-level applied at a given point and reduced in resolution to an appropriate complexity (100x100 data points, each representing an area of 200x200m in nature). The vertical displacement (subsidence) is then isolated by calculating the elevation difference between the two surfaces. This provides a 100x100 matrix where each cell has its own subsidence value. The subsidence rate is calculated by dividing each value in the matrix by the total number of increments (1000) for each calculated sedimentation interval.

By applying this subsidence rate to the scaled input surface representing the beginning of the extension interval, for the correct number of increments, it will undergo a near-identical tectonic evolution to that observed within the analogue sandbox whilst calculating realistic, spatially-variable sedimentation patterns.

6.3 Experiment Setup

All experiment runs documented within this work used an extensional analogue apparatus simulating a series of domino-style half-grabens (Figures 6.3 and 6.4). It has been previously used to investigate inversion of the domino-style basement fault system (Jagger and McClay 2018), where syn-kinematic sedimentation was applied for both extensional and contractional phases, pouring and levelling alternating layers of the sand, exactly filling available accommodation.

This area modelled within this work overlies the middle of fault blocks 2 & 3; this was defined by the areal extent of the sieving device (20x20cm).

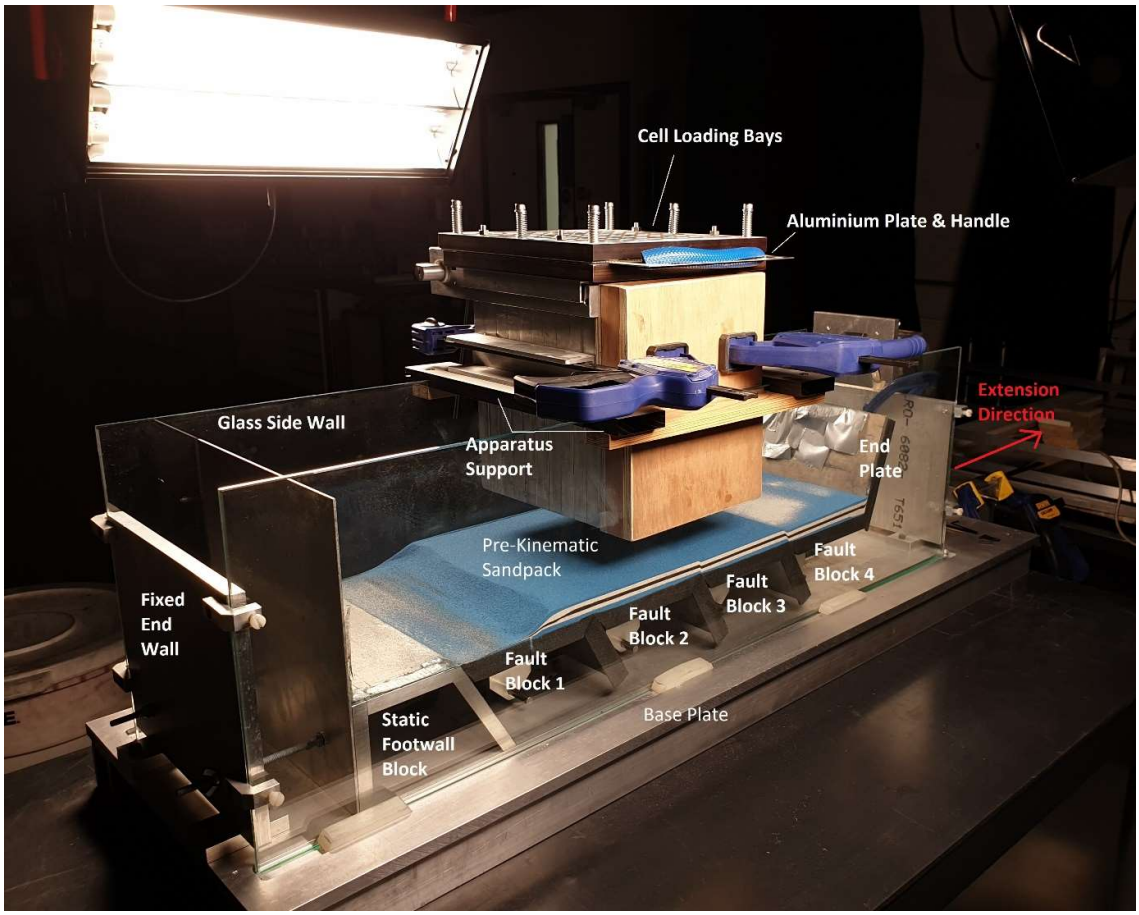

Figure 6.3: Photo of apparatus at the point of being ready to deliver the first sedimentation increment to the slightly deformed pre-kinematic sandpack.

The apparatus (Figure 6.4) uses four angled metal plates simulate rigid domino-style basement fault blocks. These are attached to an underlying trellis system which permits rotation of the, initially horizontal topped, fault blocks by a motor-driven worm screw, decreasing their inclination.

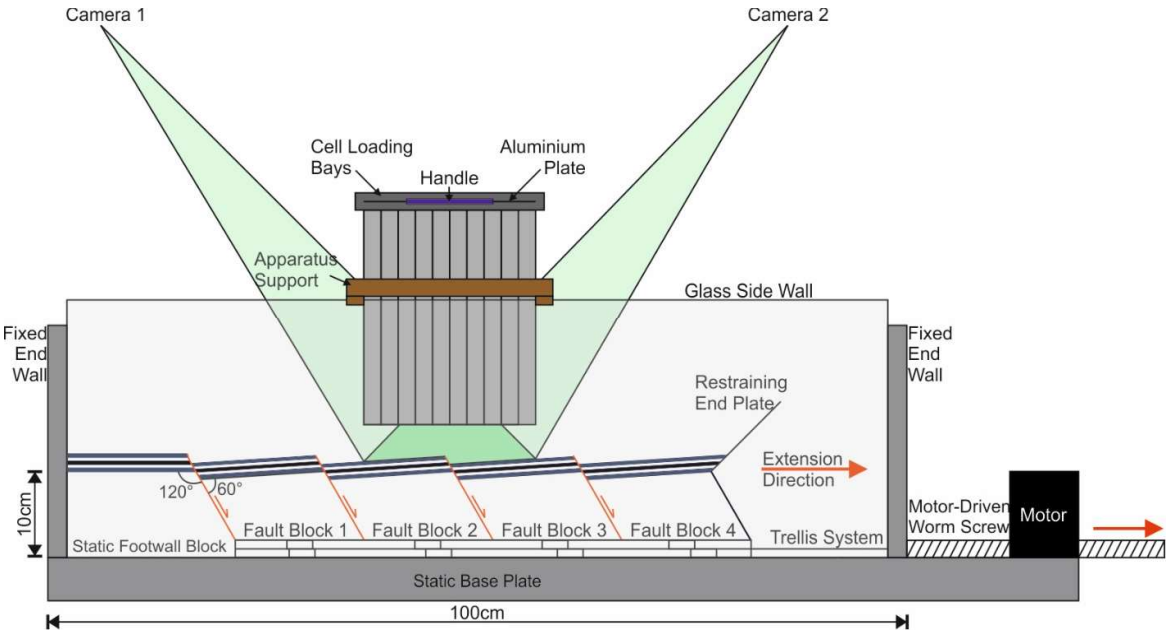

Figure 6.4: Schematic of the extensional apparatus used to model the domino-style basement fault system.

Pre-kinematic layering was deposited above the basement fault system (when flat) by sifting and levelling alternate layers of the BL60 sand (blue, white and black) to 2cm in thickness (5 layers, 0.4mm thickness each). Once the pre-kinematic sandpack is constructed, the cameras begin surface monitoring and the model is extended for a set distance, producing slip on the faults and generating accommodation by block rotation. Recorded camera data is then transformed and applied within the SFM to yield input topography and subsidence rate. Sedimentation patterns are then calculated using this data as an input. These volumes are then scaled and loaded into the sieving apparatus which is placed above the model surface overlying the target area. The calculated syn-kinematic sedimentation volumes are then deposited onto the model (red, white, black) and the sieving device removed. The process is then repeated for subsequent layers.

Within this work three separate experiment runs were conducted to demonstrate the influence of different sandbox-derived subsidence rates on the calculated sedimentation patterns. Each model was subject to five discrete extension intervals, each of which applied 1cm of horizontal extension (5cm total). Extension rates were discretionary and chosen to ensure subsidence did not outpace carbonate production. They were calculated based upon the amount of time simulated by the numerical model for a given increment. All models consisted of 1000 iterations (per sedimentation increment) but had the length of each SFM iteration (timestep) changed to represent different total production times.

Scaled extension rates were as follows:

- Model 1: 0.25km/My (Each SFM increment: 1000 timesteps of 0.004ky)
- Model 2: 0.5km/My (Each SFM increment: 1000 timesteps of 0.002ky)
- Model 3: 1km/My (Each SFM increment: 1000 timesteps of 0.001ky)

Numerical modelling parameters were kept constant for each of the 3 models and are outlined in Table 6.1, cellular automata rulesets used for all models run are identical to those outlined in Chapter 5.

Model Parameter	**Value**
Lithology 1 carbonate production rate (m My^{-1})	500
Lithology 1 Surface light intensity (µE m^{-2} s^{-1})	2000
Lithology 1 extinction coefficient	0.1
Lithology 1 saturating light (µE m^{-2} s^{-1})	200
Lithology 1 transport product facies	5
Lithology 1 transported fraction of total production	0.1
Lithology 2 carbonate production rate (m My^{-1})	400
Lithology 2 Surface light intensity (µE m^{-2} s^{-1})	2000
Lithology 2 extinction coefficient	0.05
Lithology 2 saturating light (µE m^{-2} s^{-1})	300
Lithology 2 transport product facies	6
Lithology 2 transported fraction of total production	0.1
Lithology 3 carbonate production rate (m My^{-1})	100
Lithology 3 Surface light intensity (µE m^{-2} s^{-1})	2000
Lithology 3 extinction coefficient	0.005
Lithology 3 saturating light (µE m^{-2} s^{-1})	300
Lithology 3 transport product facies	7
Lithology 3 transported fraction of total production	0.1

Table 6.1: Numerical SFM parameters for the three models runs described in the paper

6.4 Results

Differences between the three models are immediately apparent when compared (Figures 6.6 and 6.7), with the influence of extension rate and resulting subsidence markedly affecting the accumulated volumes.

Model 1, which has the lowest extension rate (0.25km/My), produces the thickest syn-kinematic layering. This is because the production time in the numerical model is longer (4My per increment), thus it has a far greater ability to keep-up with the rotational subsidence. It develops a flat-topped platform that is expansive on both the foot-wall and hanging-wall block and strongly homogeneous along strike. There is some tapering observed towards the glass walls where deposited volumes are spreading laterally, resulting in thinner layers which inhibit the ability to keep building upwards in subsequent intervals.

Models 2 and 3 display a trend, with the increased extension rates resulting in smaller accumulations of syn-kinematic volumes. Model 2 initially produces layers only slightly thinner than Model 1, however this deeper bathymetry means that in subsequent layers the carbonate production is less able to keep-up with subsidence and results in an earlier backstepping of the carbonate platform.

Model 3 (highest extension rate, 1km/My) has very little sedimentation at all, with subsidence outpacing production near-instantaneously, thus effectively negating its effect to produce any significant volumes.

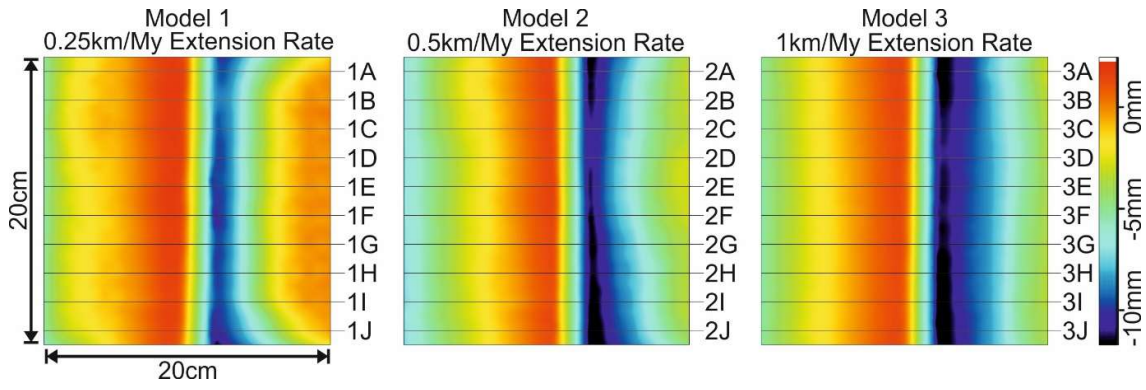

Figure 6.5: Relative positions of each cross section shown in Figure 6.6. Extension direction is to the right

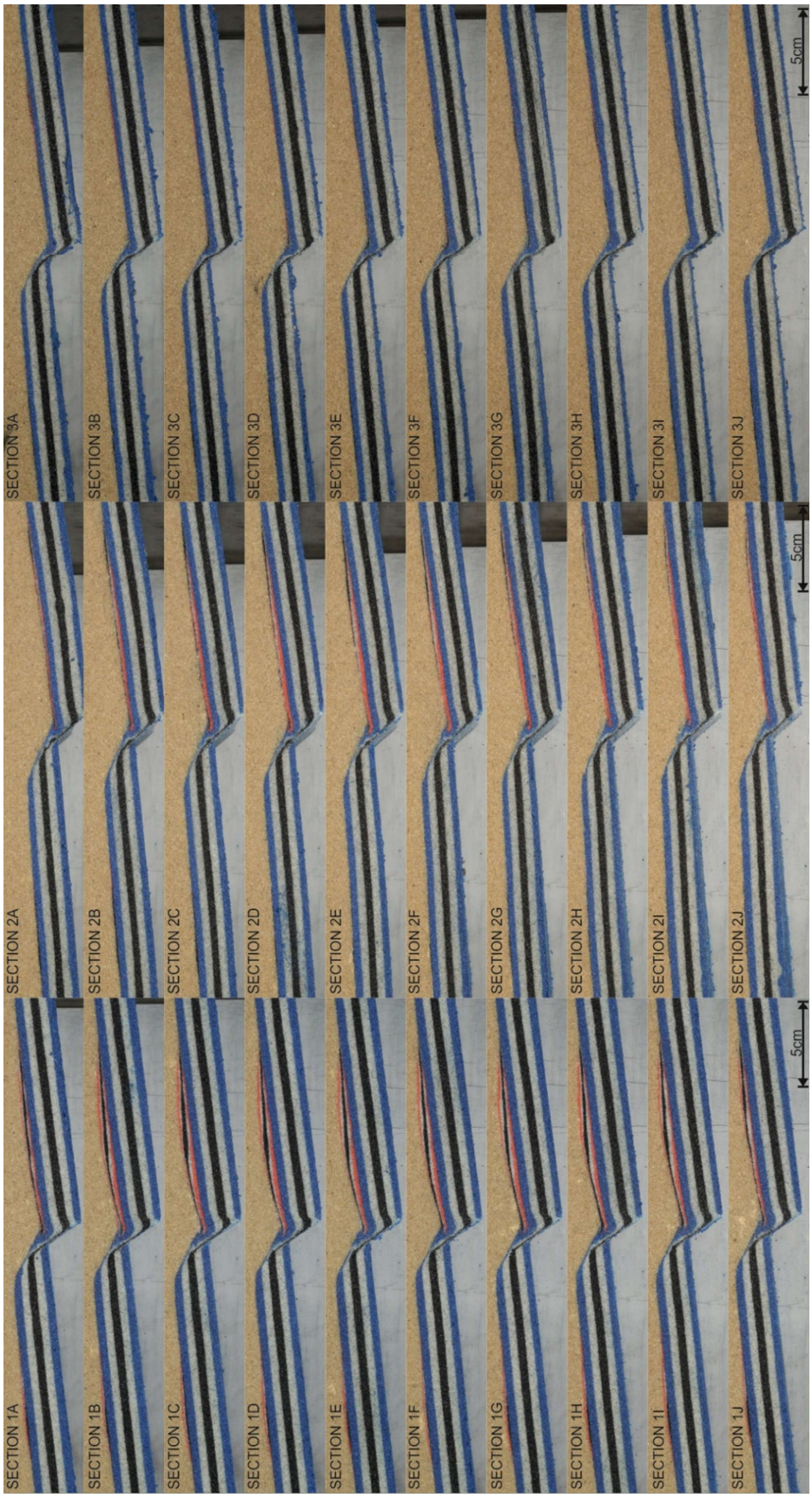

Figure 6.6: Cross-section data taken from the finished sandbox models. Figure 6.5 indicates relative positions.

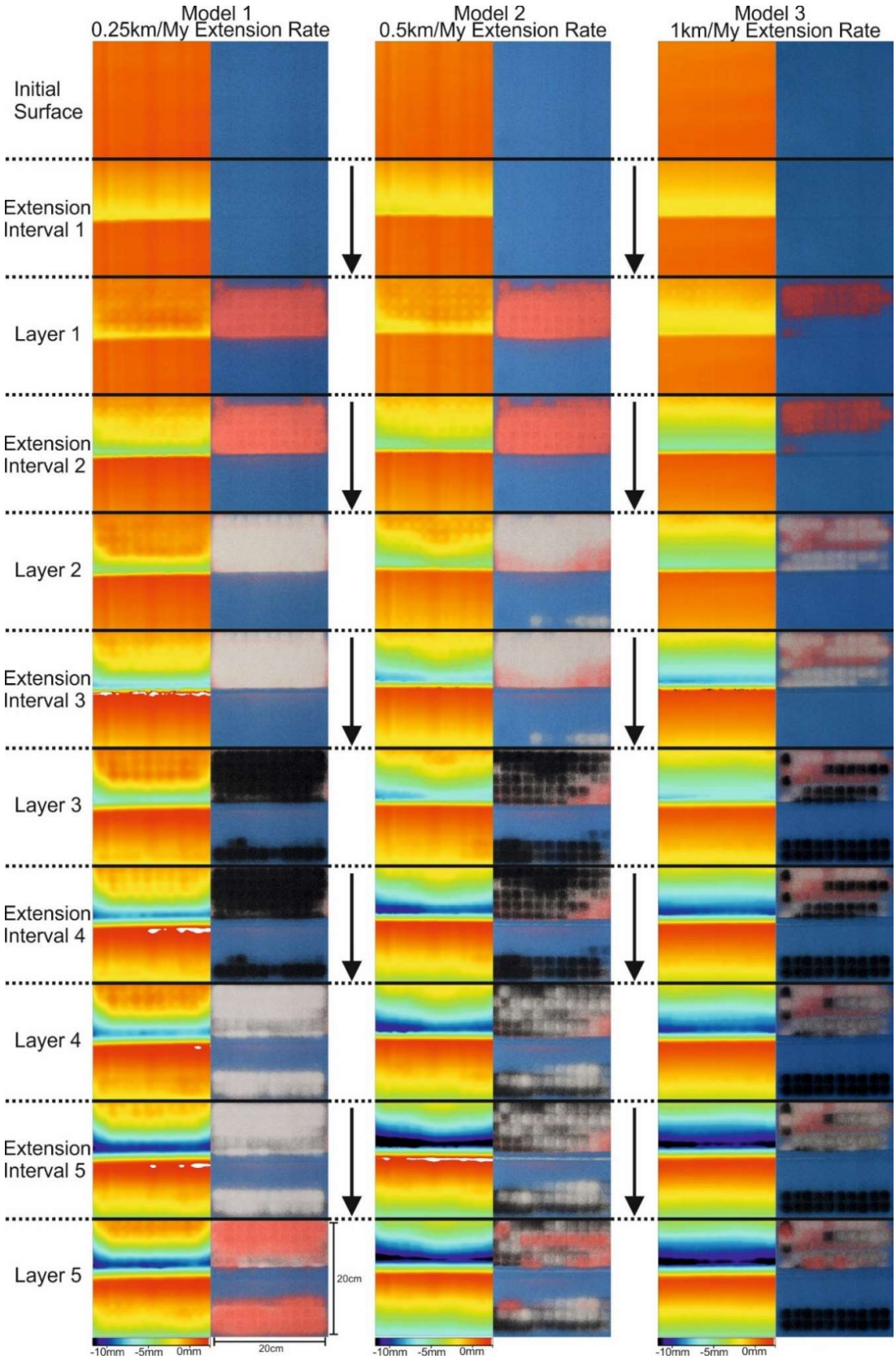

Figure 6.7: Incremental evolution for each of the 3 models, showing stages of extension and layer deposition. Left-hand images are plan-view digital topographic data shown in DaVis™ software (version 8.4, LaVision). Right-hand images are plan-view photos of the same surface. Extension direction is downwards.

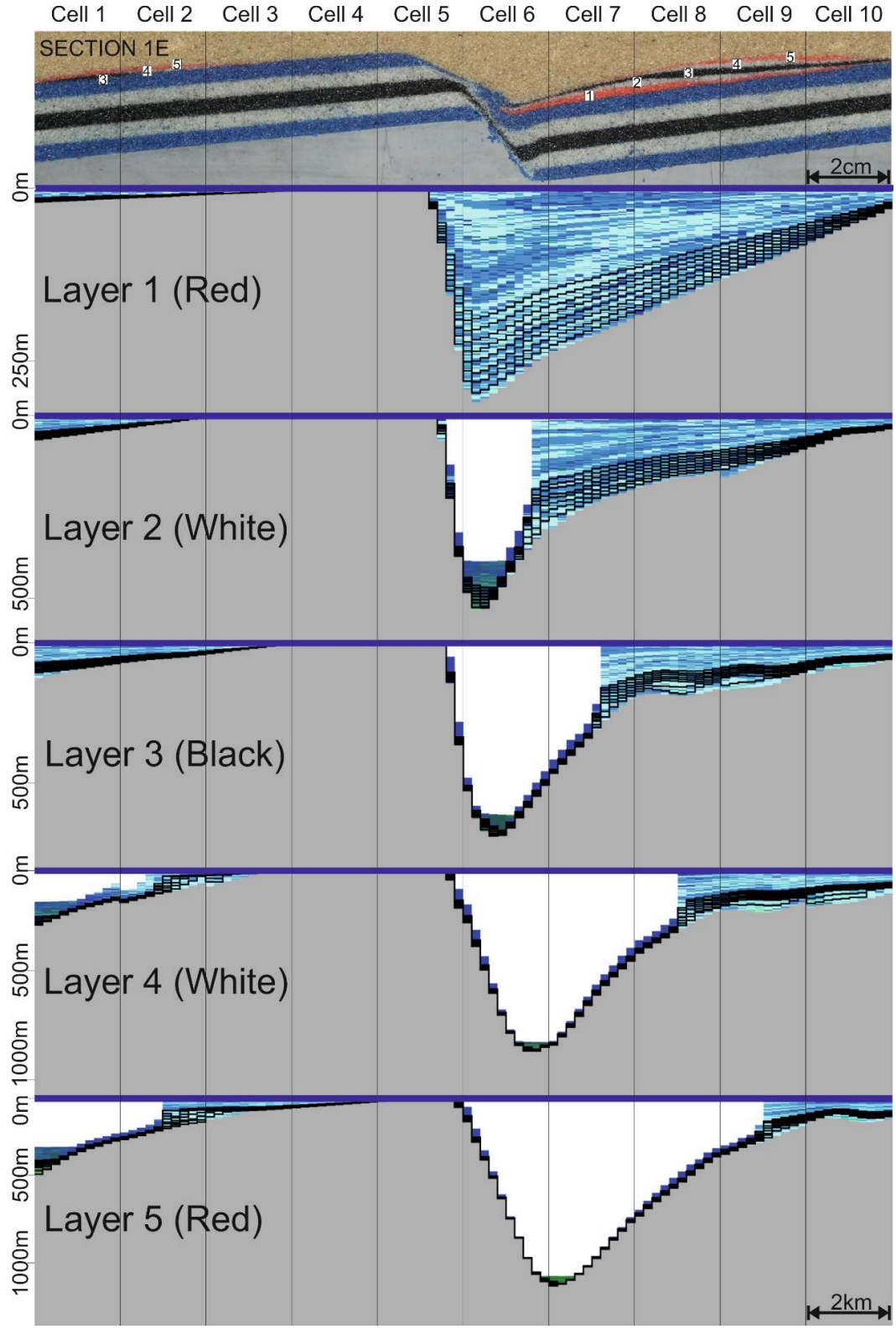

Figure 6.8: Top: Cross-section taken from the centre of the finished sandbox model 1, showing the 5 sedimentation intervals. Below: The 5 individual calculated sedimentation intervals shown in CarboCAT. Numerical cross-sections are taken from the same relative position as the sandbox section. Overlain are the positions of the 10 analogue cellular depositional areas which correspond to the 100 cells in the numerical model which are averaged. Grey (input topography), blues (carbonate accumulation), greens (transported). *NB vertical scale of numerical models is variable and shows a progressive vertical displacement by the fault.

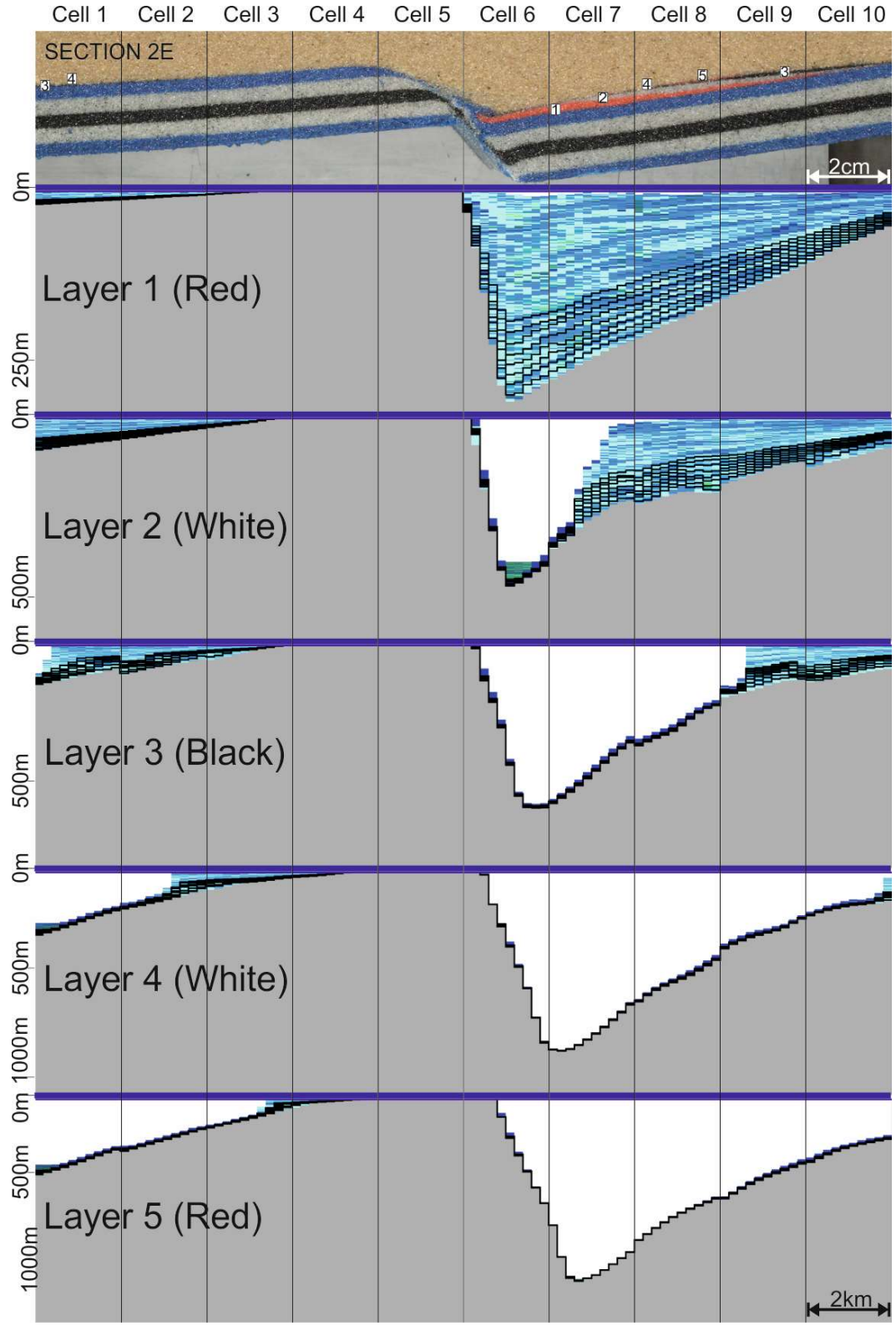

Figure 6.9: Top: Cross-section taken from the centre of the finished sandbox model 2, showing the 5 sedimentation intervals. Below: The 5 individual calculated sedimentation intervals shown in CarboCAT. Numerical cross-sections are taken from the same relative position as the sandbox section. Overlain are the positions of the 10 analogue cellular depositional areas which correspond to the 100 cells in the numerical model which are averaged. Grey (input topography), blues (carbonate accumulation), greens (transported). *NB vertical scale of numerical models is variable and shows a progressive vertical displacement by the fault.

6.5 Discussion

As demonstrated by previous models (Bosence and Waltham 1990) subsidence (determining water depth) governs carbonate production and parasequence development. Carbonates need to remain within their narrow production window (Schlager 2005) and outpace subsidence to maintain production at a given point. The models presented follow this relationship, with an increase in extension rate, and subsequent increase of subsidence rate, lowering total accumulations.

Subsidence at the base of the fault (deepest part of the model) outpaces production in all three models. To fill all accommodation and produce syn-kinematic sequences similar to those presented in Jagger and McClay (2018) would require an even slower extension rate. Though this may not purely be as a result of the relationship between subsidence and accumulation. There is a minor loss of sand occurring between the fault blocks, which will lower the surface elevation slightly. Furthermore, there is transport of sand grains downslope towards the fault (analogue sections in Figures 6.8 and 6.9). Transport is a feature already being accounted for in the numerical model, therefore this additional transport is further lowering the position of the actively producing platform. As a result, the surface elevation is lower than expected, which will potentially end production in these deeper cells prematurely and begin backstepping of the platform.

Within Figure 6.7 there is a slight offset of deposited volumes (i.e. they do not stack perfectly on top of one another). This is due to area being scanned and deposited onto remaining static while the model is extending outwards. The model growth, particularly the deeper parts, means that deposited thicknesses are being spread out and subsequently thinning. Also previously deposited volumes at the edge of the model will be being transported slightly beyond the target area and will not impact further depositional intervals.

A feature observed in the analogue cross-sections (Figure 6.6), but not the plan-view images (Figure 6.7), is production beginning on the deepest part of the footwall block in first numerical interval; however, it does not accumulate enough

thickness to cross the 0.5mm depositional threshold until layer 3 is deposited. This should not have impacted the model evolution as these thicknesses are being accounted for digitally and added onto the next input topography until they cross the threshold thickness for deposition (detailed in Chapter 5).

Carbonate development against the fault scarp is common in nature (Dorobek 2008). However, within the models presented, there is a combination of a steeply dipping fault and an analogue depositional cell size which can cover the full vertical extent of the fault exposure. As a result of this, the accumulation calculated by the 100 numerical cells which make up this small area, will be unlikely to cross the minimum threshold value for deposition to occur (as subaerially exposed cells and particularly deep cells, will contribute near-zero production). Combined with the granular sands tendency to flow towards the base of the fault, it is not possible to get detailed carbonate platform development against the fault itself using the current workflow. This is largely caused by the model scaling and could potentially be remedied if modelling took place at a different scale.

6.6 Conclusions and Future Work

A novel integrated workflow has been successfully demonstrated; applying numerical stratigraphic forward modelling to dynamically calculate basin-scale sedimentation patterns for input to an extensional sandbox experiment.

Work has shown that the procedure is deterministic, with a difference in extension rate producing markedly different sedimentation patterns. (Previous work, Chapter 5, has already demonstrated the impact of changing either production parameters in the numerical model or the initial surface geometry of the sandbox experiment).

The integrated workflow has now been demonstrated to be capable of:

- Digitally adapting data derived from analogue experiments to represent both a scaled topographic input and subsidence rate for use with the stratigraphic forward modelling software.

- Deterministic calculation of complex sedimentation patterns which are governed by both the derived sandbox data and numerical production parameters.
- Using a sieving apparatus to successfully deposit the calculated, spatially variable volumes onto the analogue sandbox, whilst maintaining desired, homogeneous mechanical properties with the bulk sandpack, required to simulate brittle-frictional behaviours observed in the upper crust.

Future work may seek to increase the lateral scale of the sieving device, so it sufficiently covers extensional topographies developed with typical sandbox rigs (e.g. Adam et al. 2012 - passive margin basins involving gravity-driven deformation).

A computer-controlled loading of sand volumes into cells would also enable both further improved accuracy of deposited sand volumes and reduce time taken from model calculation to deposition; which is particularly important when investigating salt tectonics as the experiment is deforming on short timescales.

When this larger, partly-automated workflow is produced it will permit in-depth investigations into feedback mechanics between tectonic and gravity driven deformation, due to the innovative ability to dynamically deposit realistic, heterogeneous sedimentation onto an analogue stage which will produce genuine tectonic responses to it. Non-tectonic controls such as sea level or climate can also be investigated in more detail, showing how they influence model evolution.

7 Discussion

7.1 Introduction

The aim of the thesis was to integrate the two, previously independent, experimental methods of numerical stratigraphic forward modelling and basin-scale analogue sandbox experiments. This was achieved by the work outlined in chapters 4, 5 and 6, which build upon one another in a structured approach. Successful integration permits calculation and deposition of complex, entirely deterministic, syn-kinematic sedimentary distributions; which when applied to dynamically scaled analogue models, invoke a tectonic response from the model, governing accommodation development for future sedimentation. The developed workflow may be used in future to investigate relationships between sedimentation and tectonics.

This Chapter provides a short summary of the main results, discusses the approaches taken and limitations that are imposed by the modelling procedures. Finally, a number of suggestions are made for future work and improvement.

7.2 Summary of Results

7.2.1 Chapter 4

A sieving device is designed, constructed and tested permitting a new cellular approach for deposition of sand layers with user-defined spatial and temporal thickness variations for use in scaled analogue experiments, enabling the simulation of realistic stratigraphic and syn-tectonic sedimentation patterns. Specification for a prototype device is obtained from testing to achieve comparable mechanical (density and frictional) properties to sandpacks deposited by traditional analogue modelling methods. Sand is flowed through an array of individual tubing lengths, permitting deposition of sand layers with both user-defined thickness variations and homogeneous mechanical properties.

The apparatus is used to construct a variety of sandpacks, demonstrating the capability to produce distinct 3D structures with successive layering. Results are statistically analysed, demonstrating that the apparatus produces sandpacks with both suitable mechanical properties, as well as accurate, repeatable translation of heterogeneous volumes into a given layer.

7.2.2 Chapter 5

Following on from the production and testing of the prototype, SFM software (CarboCAT) is integrated with an analogue sandbox experiment. Imaging of the experiment surface with stereo DIC cameras produces digital topographic data which is input to the SFM and populated with realistic accumulations of carbonate strata. These volumes are then deposited onto the sandbox surface at their relevant positions using the apparatus produced in Chapter 4. This process is repeated several times, with subsequent accumulations of carbonate being governed by previous deposition intervals.

Results demonstrate that the integrated workflow achieves accurate replication of calculated sedimentation patterns onto the analogue surface, with the capacity to develop into complex 3D structures with repeated layering, whilst also depositing a sandpack with the desired mechanical properties.

7.2.3 Chapter 6

Chapter six documents the application of the integrated workflow to a dynamically-scaled sandbox experiment. Subsidence is dynamically derived from the ongoing tectonic deformation of the analogue surface. From this data, subsidence rates are calculated for discrete sedimentation intervals, using the change in elevation observed over that increment. Both topography and subsidence rate data are shown to be derived from the evolving analogue model and used as suitably scaled inputs for the SFM to generate carbonate sedimentary distributions in a realistic fashion.

Dependent upon the extension rate used, accumulated carbonate volumes and subsequently developed syn-kinematic architectures vary considerably. This stage demonstrates fully working integration between the numerical stratigraphic forward modelling software and a dynamically-scaled analogue sandbox experiment.

7.3 Critical evaluation

7.3.1 Granular material properties

All testing within this thesis used Prince Minerals Silica Sand (BL60); a very high purity (99.7% SiO2) quartz sand. Work done has taken place over four consecutive years and as a result multiple batches of the sand have been used. Differences in batches of the material have been noted over the course of the project, including changes in grain sorting and angularity, particularly an increase in the amount of ultra-fine components (Figure 7.1 and 7.2). Changes are hypothesised to arise as a result of the material being quarried, and over time different areas with varying granulometric distributions are being used for production.

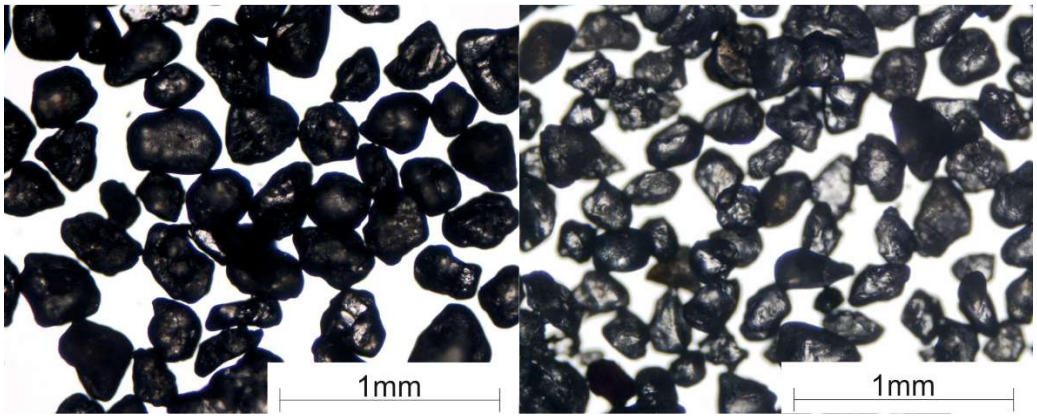

Figure 7.1: Microscope images (transmitted light) of BL60 used at the project onset (left) and from 2018 onwards (washed) (right)

Figure 7.2: Photo demonstrating the high amount of fine material in later batches of sand. This behaviour was not observed in early batches of BL60.

To remove the fine material the sand was washed, seeking to make it as similar as possible to sand used for previous work. In this process the sand is added to a large container with several litres of water and then left for the larger grains to settle, whilst the fines remain in suspension. Excess water is then poured away, and the process repeated. After several repetitions when excess water appears normally clear, the sand is poured into a tray and placed in an oven to be dried.

Following washing, a difference in granular material behaviour was observed in depositional pattern when flowing sand through the sieving device (Figure 7.3). Sand used for early work produced mounds of sand during deposition (peaking in the centre of the cell and becoming shallower towards the edges). In later work the depositional profile of sand was cratered, shallowest in the centre and higher at the edges, the exact opposite behaviour.

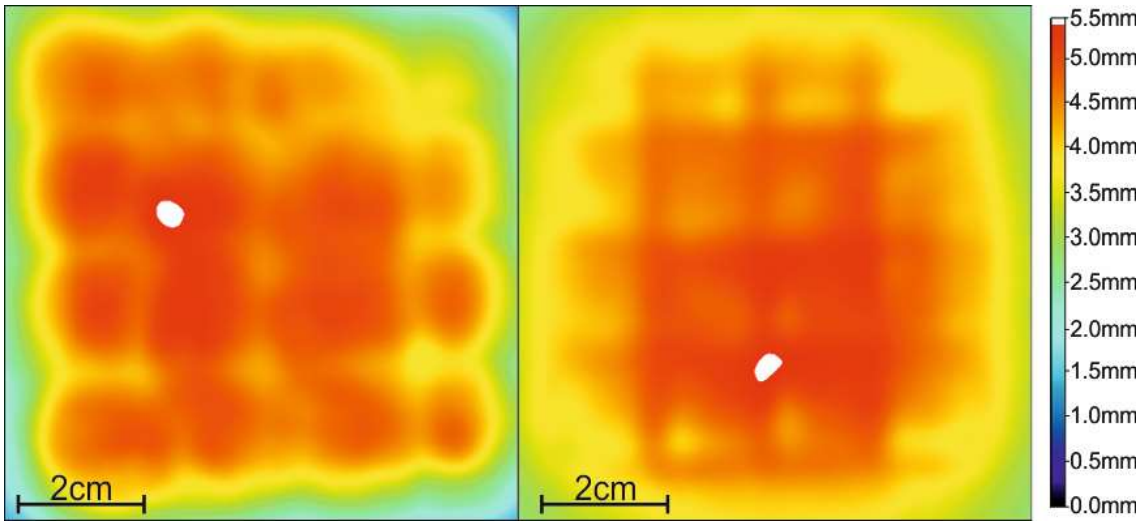

Figure 7.3: Depositional behaviour forming 'mounds', earlier batch (left). Depositional behaviour forming 'ridges', later batch (right).

The effect of the change in depositional pattern was substantial enough to affect model evolution, with the ridges effectively forming pseudo-structural highs which facilitated formation of isolated platforms in the numerical model (Figure 7.4). This behaviour was not observed in earlier testing with mounds, likely because they produce a more consistent surface topography with a lower variance, meaning carbonate accumulations were more homogeneous and not isolated.

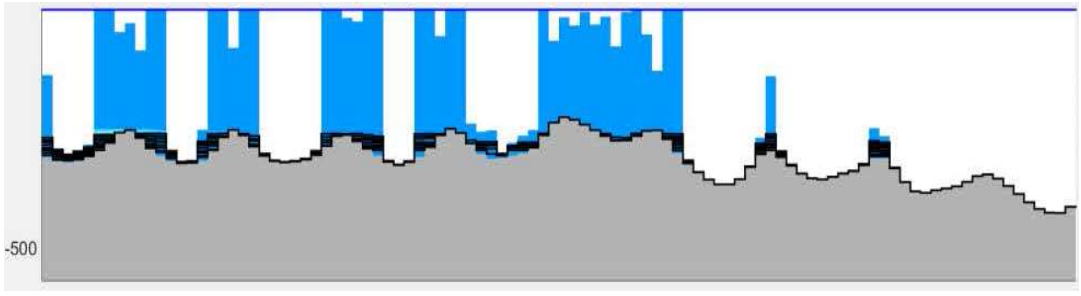

Figure 7.4: CarboCAT cross-section, showing the input sandbox topography from a previously deposited sedimentation interval (ridges) in grey, with calculated carbonate accumulation above in blue.

Substantial testing was conducted in an attempt to verify the reason for the formation of these ridges, including; grounding the whole apparatus, changing total fall height, varying volumes in adjacent cells, changing the metal plate to an acetate sheet, washing new sand with a different water source/apparatus. None of these impacted the subsequent behaviour of the sandpack. Unfortunately, washing of the sand could not be determined as the cause of the behaviour as there was no original sand remaining to run comparison testing with

Due to the formation of these ridges impacting the calculated sedimentation patterns, washed sand could not be used in conjunction with the sieving device to deposit syn-kinematic sandpacks. This behaviour was still observed when deposition was done by hand, ruling out the sieving device as a cause.

Given that the unwashed sand still produced a suitable depositional profile, ring-shear testing was carried out to ensure that frictional behaviour of unwashed sand was appropriate, with a view to continuing its use within the project. Results were compared to that of the original, as well as the washed sand (Figure 7.5 and Table 7.1).

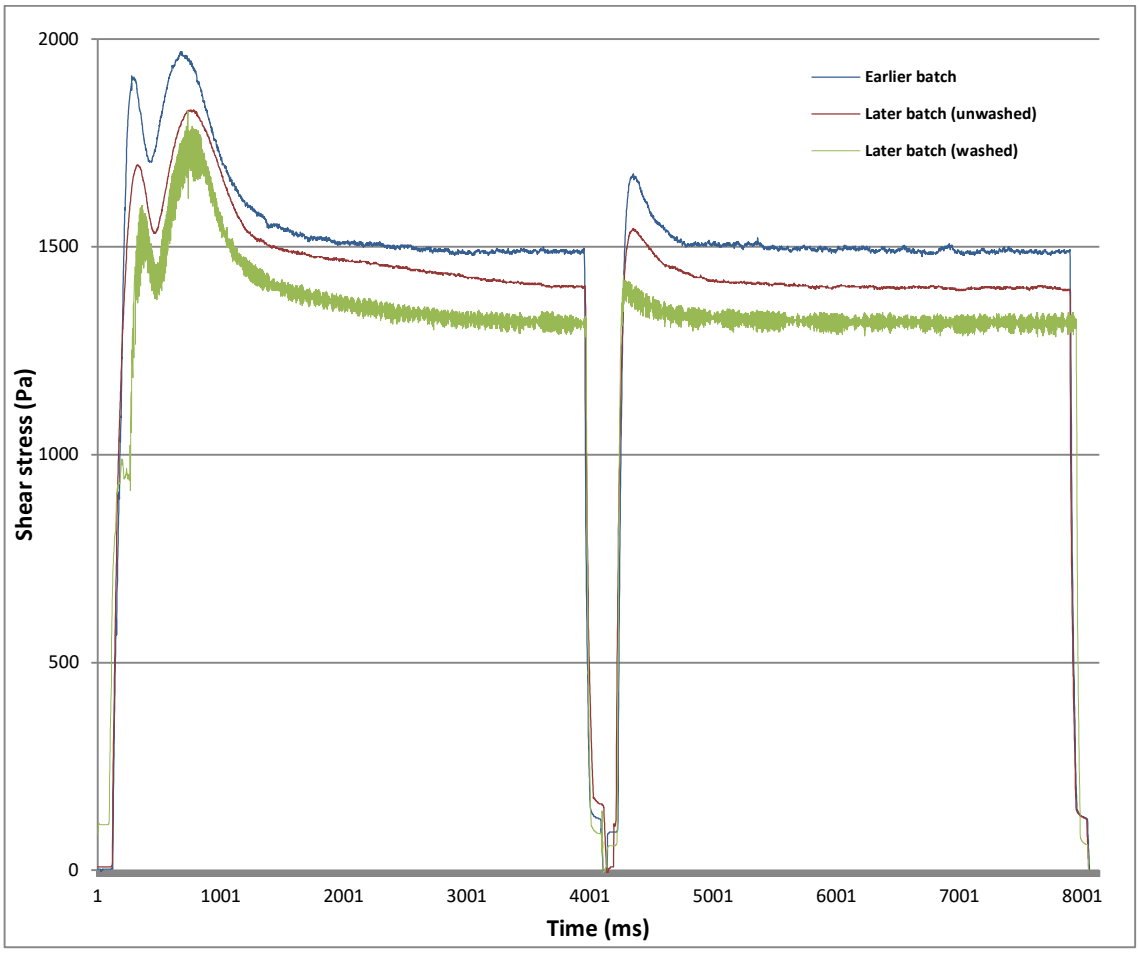

Figure 7.5: Material testing profiles for BL60 sand batches, demonstrating peak, static and dynamic friction.

	Peak friction (Pa)	Static friction (Pa)	Dynamic friction (Pa)
Earlier batch	1950	1650	1470
Later batch (unwashed)	1830	1570	1410
Later batch (washed)	1750	1411	1340

Table 7.1: Peak, static and dynamic friction results for BL60 sand batches.

One striking finding from ring-shear testing is the apparent stick-slip behaviour (confirmed with multiple tests) which arises in the sand when washed, potentially being linked to the change in depositional profile. The significant increase in finer material, which is removed by washing, may be acting as a 'lubricant'; preventing angular grains locking and then unloading, developing the erratic profile in Figure 7.5

Overall the profiles from the three sands are very similar, despite attaining slightly different frictional values. They all display the characteristic 'double-peaking' behaviour of quartz sand (Panien et al. 2006). Results indicate that despite the larger component of fine material within the later batch of unwashed sand it still behaves in a suitable manner to be applied to dynamically scaled analogue models.

For the work contained within this thesis, the effect of changes in granular material behaviour derived from differing sand batches should have had a negligible impact. No strain analysis, palinspastic reconstructions or study of complex faulting within the sandpack (domino rig controlled the only faults) was conducted. Therefore, slight variations in frictional values has not impacted model evolution or produced results. However, given logistical issues associated with the unwashed sand (constant deep cleaning of surfaces/increased risk of inhaling the material) and unsuitability of it after washing, it is recommended that the alternate quartz sands be investigated for future purchase.

7.3.2 Numerical modelling complexity

The most complex CarboCAT models contained within this work had increments run at a 100x100 cell (representing a 20x20cm area of the sandbox) complexity for 2000 iterations. Even when conducted on a workstation, this took in excess of 4 hours. In its current state the workflow cannot be applied to experiments investigating salt tectonic processes with PDMS (Polydimethylsiloxane) (e.g. Adam et al. 2012).

One remedy would potentially be to use a supercomputer; however, typically workloads are queued up and delivered back to the user once completed. For successful integration with salt tectonics experiments, it would need to be instantaneously input to minimise impact to the experiment, given that the silicone polymer will be continually deforming on short timescales (minutes).

For this work at basin-scale the SFM is being used to provide first-order sedimentation patterns to be input to the analogue model. With the resolution that is capable of being deposited onto the analogue stage (0.5mm thickness increments), certain features within CarboCAT (e.g. wave energy) are providing a negligible impact, whilst increasing the time to calculate the 3D lithofacies distributions. If model complexity was suitably reduced, gross sedimentation patterns could likely be preserved, whilst reducing computation times.

7.3.3 Fall height to model surface

The length of aluminium tubing for the 10x10 prototype apparatus was 25cm and permits construction of sandpacks with comparable density and frictional properties to that of sandpacks produced by hand-sieving (i.e. isotropic) (Chapter 4 results). If applying this method to kinematic sandbox experiments which can generate substantial (>5cm) topographic differences across the depositional area, there will be different cumulative fall heights (tubing length + unconfined fall to model surface). A change of 5cm fall height imparts approximately a 0.01g/cm^3 difference to the sandpack density. This may slightly impact peak friction, however, sandpacks produced within analogue modelling can never be truly isotropic due to fluctuations in sand composition. Investigations of perfectly isotropic materials is something only achievable with numerical modelling.

A further complication is the lateral spread of sand when deposited. An increasing unconfined fall distance means the sand has more opportunity to spread laterally, into adjacent cells. Model calculations from the SFM are cellular, thus calculated volumes are cuboid in shape. This can never be perfectly replicated in the analogue model as sand is cohesionless and can only be stacked as steeply as its angle of repose allows. This lateral spread has a cumulative effect over several sedimentation increments. If the volume of sand being deposited is spreading beyond the confines of its 2cm^2 target area, then the height is being diminished. When the next sedimentation interval is run in CarboCAT, that point on the surface starts at a deeper bathymetry than desired, meaning carbonate production is diminished and subsequent accumulation is less. This issue potentially results in areas of the platform prematurely drowning.

7.3.4 Withdrawing metal plate in sieving device

The method of deposition used for this project has been withdrawing a solid metal plate from beneath the pre-loaded cells which overlay their relevant tubing lengths. When using this method there is a roughly constant loss of sand occurring, due to it being withdrawn on top of the plate. This compounds the previous issue of lateral spread, as not only is the height of a given point lower due to sand spreading out laterally, but also due to the fact that there is a lower volume of sand being deposited in the first place. The combination of these two factors means that translation of generated volumes from the numerical model is not perfectly accurate and the surface commonly is at a slightly lower point than it should be. Given the carbonate production profile used (Schlager 2005), this means that even a 1mm difference in analogue topography will be the difference between the main (tropical) carbonate factory producing or being entirely beyond its production window within the SFM. This issue particularly highlights the sensitivity of the model, given that the margin of error is commonly within the median thickness of a single grain of sand (Chapter 5 results).

7.3.5 Manual loading of sand into apparatus

Loading of the sand volumes into the sieving apparatus has been done by hand for the entirety of this project, using measuring spoons to incrementally deposit set weights of sand. An excess of sand is scooped into the spoon, followed by being levelled flat and tipped into the relevant cell to load all the sand volumes for a given layer. The relevant weights deposit desired volumes when flowed through the tubing and deposited with the appropriate density.

When manually loading the spoons or transferring sediment to the apparatus there is potential for human error, either loading too much or too little sand to a given position. Excess sand being delivered to a cell has minimal impact, as ongoing subsidence will eventually return it to its correct position where it can begin

producing again. However, if too little sand is transported to a cell, then there is the potential for premature drowning. Sand loading may also not be evenly spread out, dominantly deposited towards one side of the cell. This has a largely negligible impact, as the 25cm falling distance gives ample time for sand to disperse evenly across the cell prior to reaching the model surface.

Testing was also conducted to verify the consistency of weights across the measuring spoons. Measured weights in the table below were averaged from 5 readings. Actual vertical thicknesses deposited by the spoons were calculated by using the predicted density (1.57g/cm^3) of sand when using the sieving apparatus and the precise target cell size of 2x2cm. Given that the sand has potential to spread laterally and physically cannot form exact columns as would be derived from the numerical model, the precision of the weights being loaded by the spoons is satisfactory.

Spoon size (tsp)	Target vertical thickness	Measured weight of sand	Actual thickness deposited	Percentage versus target thickness
(1/4)	**4mm**	2.4467g	3.90mm	97.5%
(1/8)	**2mm**	1.2770g	2.03mm	101.5%
(1/16)	**1mm**	0.5934g	0.95mm	95%
(1/32)	**0.5mm**	0.2919g	0.47mm	94%

Table 7.2: Comparison of target thicknesses and actual thicknesses deposited when using spoons to manually load the sand into the sieving apparatus.

7.4 Future Work

There is an abundance of improvements which could be made to advance the workflow further. These seek to improve repeatability, accuracy, and seek to permit subsequent investigations which could be conducted using it. Initial work has already begun in several of these areas.

7.4.1 Automated loading of sand volumes

Manual loading of the sand into the sieving device is a highly time-consuming process. An automated approach would enable rapid infilling of the cells; being of particular importance when investigating salt tectonic processes using PDMS (Polydimethylsiloxane), as the model is actively deforming on short timescales (Adam et al. 2012).

A mechanical approach would also remove the potential for human error. When loading sand volumes into the apparatus by hand, there is a greater potential for inaccuracies; whether slight differences in transferring loaded weights or alternatively user-errors in depositing amounts in the wrong locations. The precision of the automated approach should also ensure that deposited volumes are centralised within the cell, preventing bias of volumes being deposited overtly towards one side of that particular cell.

The required code has already been written and successfully tested using the apparatus in Figure 7.6. This pictured system can move to a set of coordinates which will overlie the relevant deposition location for each cell, using a two-axis guide-and-rail system. Once there, it is instructed to dwell and will operate a rotating cylinder system (in development) (Figure 7.7) which will deposit the relevant amount of sand, obtained from the numerical model output.

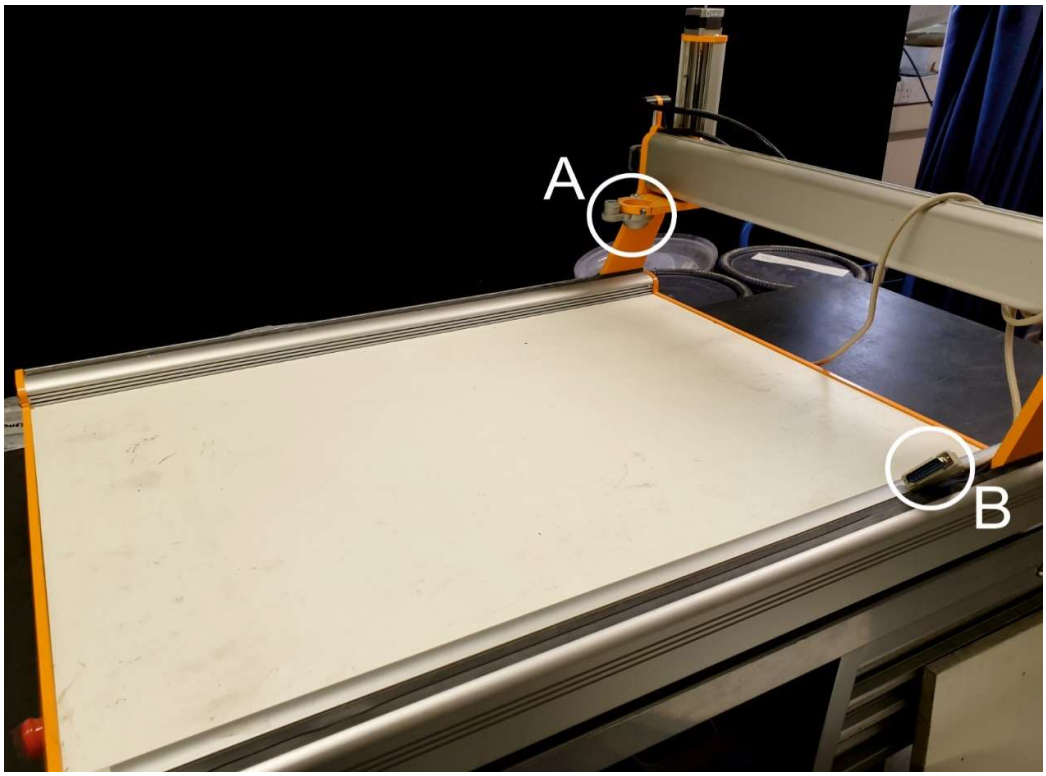

Figure 7.6: CNC (Computer Numerical Control) machine, originally designed as a 3D printer, the system has been modified to hold the sand depositing valve system (in production, not pictured) (A), which will be fed by a funnel filled with the sand to be delivered. Information is transmitted to the apparatus using a computer connection (B), so the apparatus systematically moves to target coordinates and delivers the required amount of sand. The top layer of the apparatus developed in Chapter 4 can be removed and transferred onto this CNC machine to be loaded with sand, before being transferred back on top of the tubing lengths for deposition.

Work is currently being undertaken to finalise apparatus which can deposit the correct volumes at with enough speed and precision (Figure 7.7). The designed apparatus will have a constant loading of sand being delivered from a funnel above, and consists of a central rotating cylinder, with 6 precise notches. Each of these notches represents an identical weight of sand, thus a controlled number of rotations will allow it to incrementally deposit sand up to the desired amount.

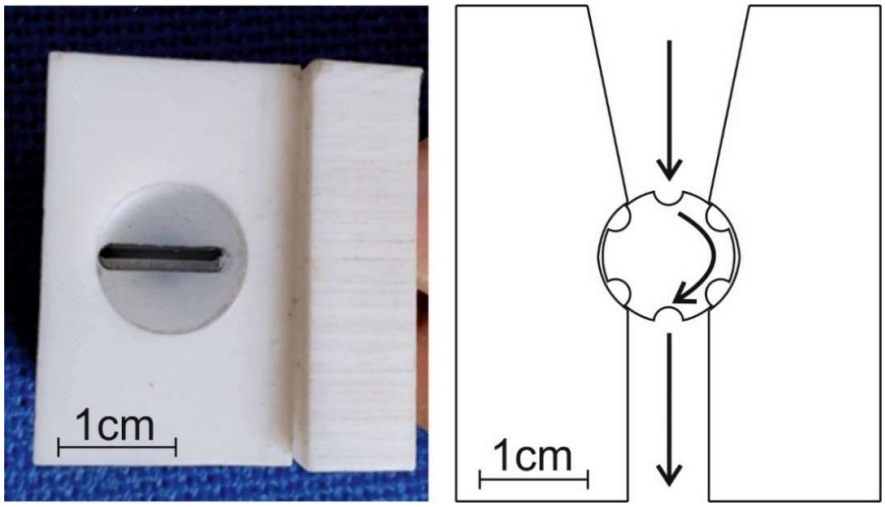

Figure 7.7: Left: Plan photo of the apparatus to deposit sand. Right: Schematic cross-section, arrows indicate the pathway of sand when being transported through the apparatus and rotation of the notched cylinder.

7.4.2 Integrate siliciclastic processes

Lobyte3D (Burgess et al. 2019) is clastic stratigraphic forward modelling software, scripted in MATLAB in a similar style to CarboCAT (Figure 7.8). It calculates deposition in dispersive-flow fan systems, dynamically affected by complex, evolving bathymetry.

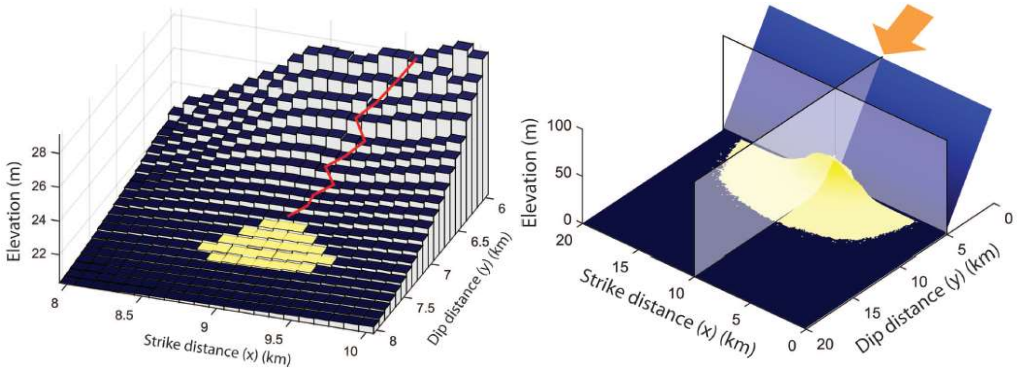

Figure 7.8: Left: Subset of Lobyte3D model grid showing sea-floor topography. Red line represents deepest-descent route a single event package of sediment would follow over the topography formed by previous fan lobes. Yellow squares represent locations of deposited sediment from the flow which becomes dispersive when topographic gradient and hence flow velocity drops below the deposition threshold (Burgess et al. 2019). Right: Total fan thickness deposited by 1000 flows forming a 3D accumulation of clastic material in Lobyte3D. Arrow represents the point of entry onto the grid for all sediment flows (Burgess et al. 2019).

If this were harmonised with the existing CarboCAT SFM, then it would permit calculation of realistic clastic and carbonate sedimentary distributions to be input to the analogue model. Volumes would also potentially be significantly increased and more representative of sedimentation within extensional settings which do not solely comprise of carbonate production, yielding more typical tectonic loading.

Typical rift evolution could also be better represented, with early-stage, primarily terrestrial sedimentation, having little-to-no carbonate accumulation and predominantly clastic fan systems. As marine conditions become more pervasive later into the rifting process there would be an increasing rate of carbonate sedimentation.

7.4.3 Improve subsidence quality in numerical modeller

Currently subsidence is calculated from the difference in elevation/bathymetry between the initial and final surfaces of a given extension interval and then divided by the total number of timesteps to calculate a subsidence rate. Subsidence is not linear, in either sandbox models or nature, so the m-files within CarboCAT could be amended to provide multiple subsidence rates within a given sedimentation increment. If computation/time limitations were not an issue; the DIC setup could capture enough images, 1000-2000 per extension interval, that each calculated timestep in CarboCAT be given its own discrete subsidence amount, increasing the accuracy of the translated subsidence from the analogue surface and near-identically replicating the tectonic history into the numerical modeller.

This methodology however would still mean that sedimentation for a model occurs during several distinct events, rather than the largely constant behaviour of sedimentation in nature, barring instantaneous events such as turbidites. Model sedimentation intervals could be increased in frequency, though work would need to be done on streamlining the process of translating captured data from the model into the numerical modeller to be calculated, as well as completion of the automatic sediment loading system. Sedimentation intervals covering a shorter time interval would be quicker to calculate and applying more of these smaller depositional events would provide a more realistic tectonic loading throughout a models lifespan.

7.4.4 Alternative mechanism of material deposition

An issue, previously discussed, is the method of withdrawing an aluminium plate from beneath loaded cells to permit deposition of sand onto the analogue surface. There is a compromise between having confining layers which 'trap' the aluminium plate, tight enough that sand is not pulled out on top of the plate, whilst being loose enough that the plate can still be withdrawn. There is a roughly consistent loss of sand occurring, effectively filling 'accommodation' on the plate, meaning layers with smaller volumes are more affected, as they lose a greater percentage of the sand to be deposited. This would not easily be remedied by adjusting the input volumes to account for it as the sedimentation patterns being derived are variable in both amount and relative position versus the underlying plate.

To remedy this, a new prototype (Figure 7.9) has been designed involving initially offset holes. The upper layer is loaded with the desired sediment volumes, before being slid a short distance to align holes with the underlying layer and initiating deposition. Testing has shown that this method should reduce the lost sand volumes to almost nil, whilst also permitting truly synchronous deposition of the volumes across the entire model surface.

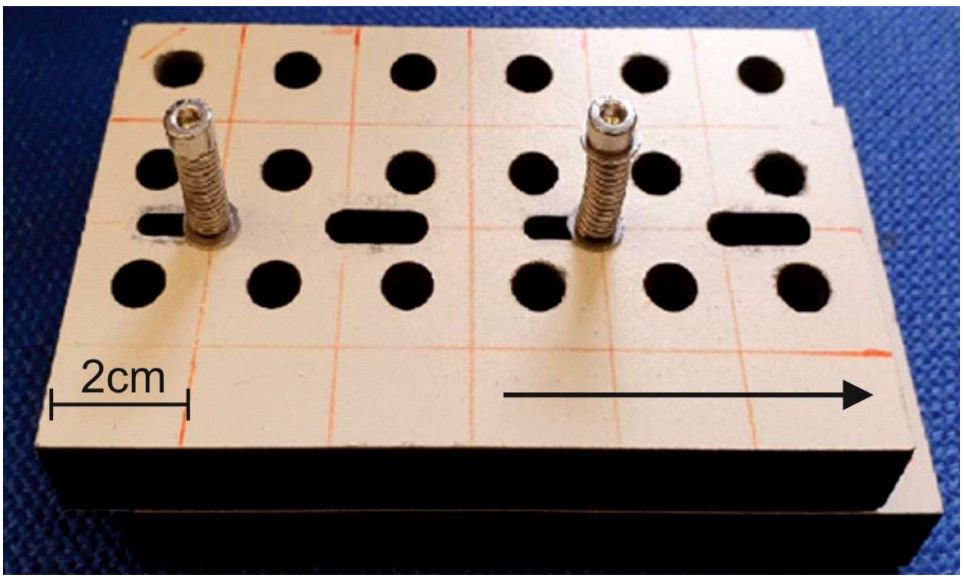

Figure 7.9: New prototype sieving mechanism. Arrow indicates the movement of the upper-layer to align cells and initiate deposition of sand.

7.4.5 Experiments using a different scaling factor

Work is currently being undertaken at Royal Holloway, in a different research project, to produce granular materials for use within analogue sandbox experiments which represent a different geometric scaling factor (10^4 rather than 10^5). Once complete, this material could be tested with the workflow produced in this thesis. A potential issue is that the new material is not cohesionless, which may inhibit its ability to be passed through the sieving device. Furthermore, the material is currently being produced as single blocks, which are currently undergoing testing to deform them, e.g. shearing (Figure 7.10). Aggregates would need to be produced which successfully maintain the correct mechanical properties. If the new material works successfully with the sieving device, then there is potential for modelling of 'outcrop-scale' carbonate successions.

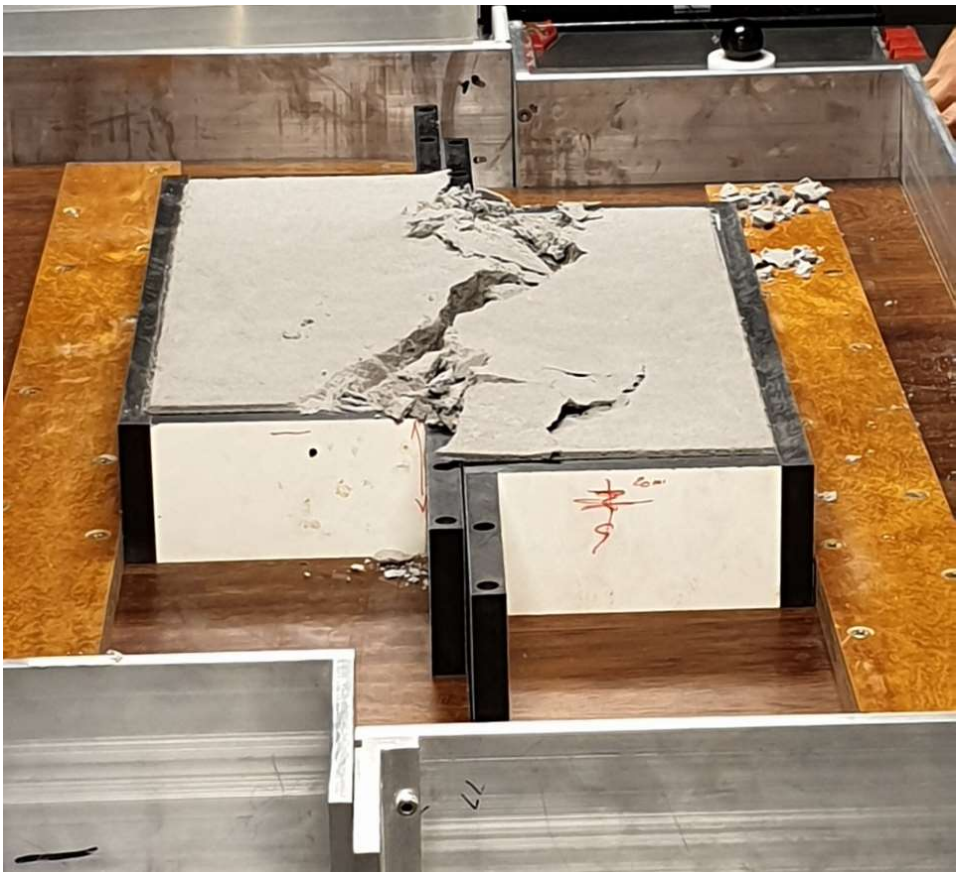

Figure 7.10: Testing of the new granular materials by shearing the 'sandpack'. Of note is the capability to sustain open fractures as the granular material has cohesion.

7.4.6 Application to different experiment setups

The sieving apparatus could be increased in lateral scale, sufficiently covering extensional topographies developed with typical sandbox rigs (e.g. Adam et al. 2012). This would permit in-depth investigations into feedback mechanics between sedimentation and tectonic deformation, due to the innovative ability to dynamically deposit realistic, heterogeneous sedimentation onto an analogue stage which will produce genuine tectonic responses to it. Given that sedimentation has been shown to have a demonstrable effect upon tectonic evolution (Bialas and Buck 2009), insights to feedback mechanisms between the two may be obtained with more representative sedimentation when applied to analogue experiments.

Results produced using the new workflow could be compared and contrasted to traditional, by-hand syn-kinematic sedimentation methods, quantifying the impact of workflow-generated sedimentation on the final architectures, which may turn out to be drastically different. The inclusion of the SFM also now means that climatic impact on rift evolution can by systematically investigated.

Examples of 'rigs' available at Royal Holloway are a 3D-rift (perpendicular / oblique / segmented) and a passive margin involving gravity-driven deformation (as described in Adam et al. 2012). Figure 7.11 shows an example areal extent of border-faulting exhibited in a final-stage syn-rift surface, as well as the predicted coverage required by a sieving device to permit integration with the workflow developed in this thesis.

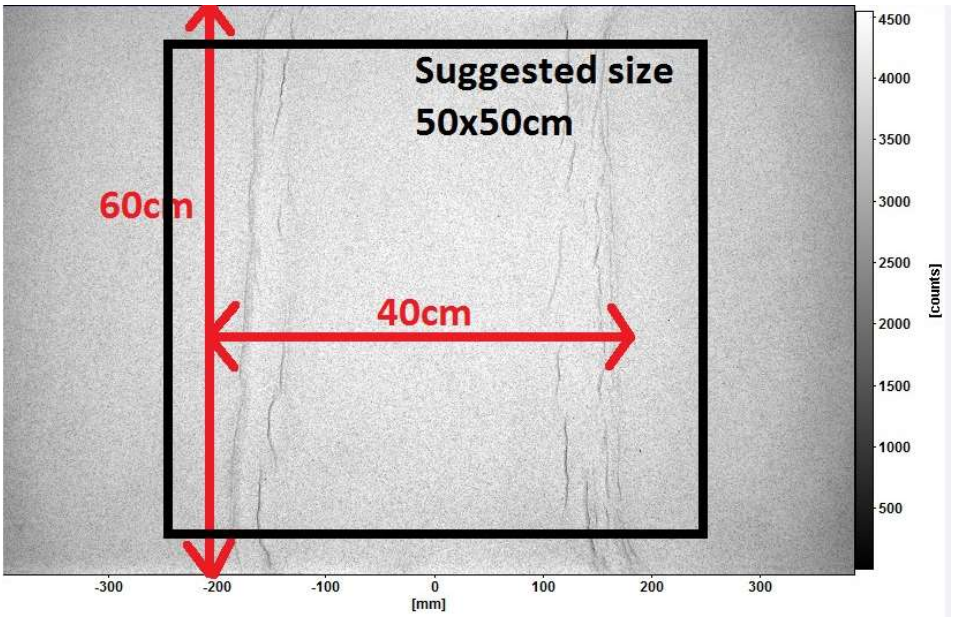

Figure 7.11: Surface image of a 3D rift sandbox experiment. Areal extent of the rift is shown in red, which is overlain by the size of tubing (black box) required to sufficiently cover this experiment.

A new array of tubing lengths has already been produced (Figure 7.12), of identical length to the prototype, 25x25 tubes (50x50cm) in size. This is currently awaiting production of a system to suspend it above larger-scale rigs, as it needs to be in place to deposit sand volumes, but then removed to permit the cameras to continue capturing surface evolution. This will involve the apparatus being on a guide-rail so it can be easily manoeuvred.

Figure 7.12: Newly produced 25x25 cell tubing arrangement (50x50cm).

7.4.7 Geological feasibility

An important consideration of the current workflow is to what extent it simplifies the natural development that it is trying to recreate (syn-extensional sedimentary basins constrained by tectonic, depositional and climatic processes). The two modelling approaches applied each have a simplification compared to natural morphological development, as well as differing from each other:

- Analogue modelling will have an outward splaying of sand upon deposition due to a combination of the energy dissipating upon contact with the surface and the maximum angle of repose (approximately 34°, Al-Hashemi and Al-Amoudi 2018). This results in them being unable to match natural examples such as carbonate atolls which can achieve up to 50° dip angle at their margins (Betzler et al. 2016). Furthermore, as discussed in 7.4.5, an innate issue when using quartz sand is the scaling factor (10^{-5}). Subsequently it is impossible to truly accurately recreate sedimentary distributions at basin scale or smaller, or particularly steep-sided features (>34°) within the sandbox.
- Numerical modelling is composed of discretised cells of given height (I.e. calculated thicknesses) which are the output to be translated onto the analogue model. These all have perfectly vertical sides, which again is in contradiction with nature. However, this could be mitigated by increasing the resolution of the numerical model.

Despite the modelling approaches' differences to natural development, the workflow's primary purpose is to apply deterministically-calculated, scaled sedimentary distributions onto actively deforming sandboxes, which it demonstrably achieves. The discussion is to what extent realistic distributions are being accurately recreated in the sandbox with potential to influence tectono-structural development within the model, recreating natural examples of complex interplay between sedimentation and tectonics (e.g. Erratt et al. 2010), as the processes of sedimentation and erosion (surface processes) have been shown to

have an impact on syn- and post-rift tectonic evolution (Burov and Cloetingh 1997; Burov and Poliakov 2001; Olive et al. 2014).

An example of an extensional setting which could be suitable for modelling using the integrated workflow is the Southern Adda-do rift of Southern Afar (Figure 7.13). The newly produced 25x25 cell tubing arrangement (7.4.6) represents an extent of 50x50km which covers the majority of the Southern Adda-do rift depicted. The large basin-bounding fault system coupled with the comparatively simple sedimentary distribution and drainage system may yield a setting suitable for systematic testing of the workflow to investigate the impact of loading applied by sedimentation and potential feedback mechanisms from the tectonic response and subsequent accommodation development.

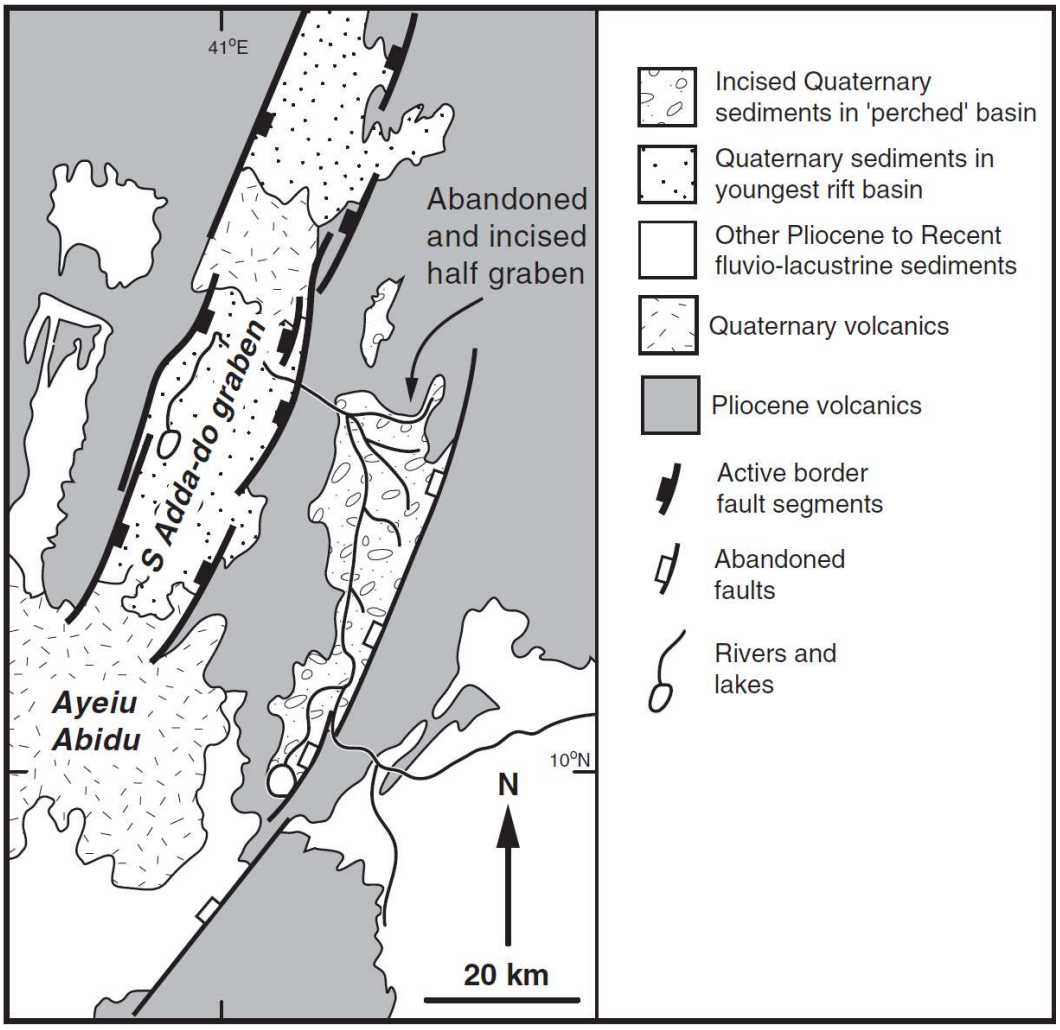

Figure 7.13: Southern Adda-do rift of Southern Afar (Gawthorpe and Leeder 2000).

The workflow could also be used to simulate both continental and marine rift systems, deterministically generating differences in syn-extensional fill and resulting architecture (clastic diagrammatic examples in figures 7.14 & 7.15). The difference in final architecture in these figures develops solely as a result of the initial model setting (continental vs. coastal/marine), which undergoes a similar tectonic history. When the developed workflow has both modelling of carbonate and clastic systems (7.4.2), it should be capable of producing a similar representation of the two models, with observed variation both along strike and down-dip, albeit at a lower resolution. The current apparatus has the capability to model basin-scale depositional systems such as facies belts and fan systems (i.e. depositional sequences and facies observed in the cross-section views of 7.14 & 7.15), however it will not be capable of developing the individual fans, depicted at surface level, within the analogue sandbox (though they would make up the numerical model from which analogue volumes are derived).

When recreating basin evolution, the clastic component of the numerical model will dominate in early stages due to widespread terrestrial conditions, simulating depositional fan systems. Over time, as marine/lacustrine conditions become more pervasive due to subsidence driving basin linkage, the carbonate component will begin accumulating and the dispersive fan systems will become more laterally extensive. Differences between models will arise deterministically as a result of the initial water levels (assuming similar initial tectonic deformation), with coastal/marine settings having a significantly higher accumulation of carbonate and different distributions from the clastic fan systems. Over time, ongoing sedimentation patterns derived from the numerical modelling will apply tectonic loading onto the sandbox and potentially induce a notably different tectonic evolution within models, influencing accommodation development for further sedimentation to infill.

This is the novel improvement yielded from stratigraphic forward modelling software; deterministic application of complex depositional systems dependent upon climatic / environmental factors, something currently unachievable with even in-depth syn-kinematic sedimentation methodologies (e.g. Adam et al. 2012).

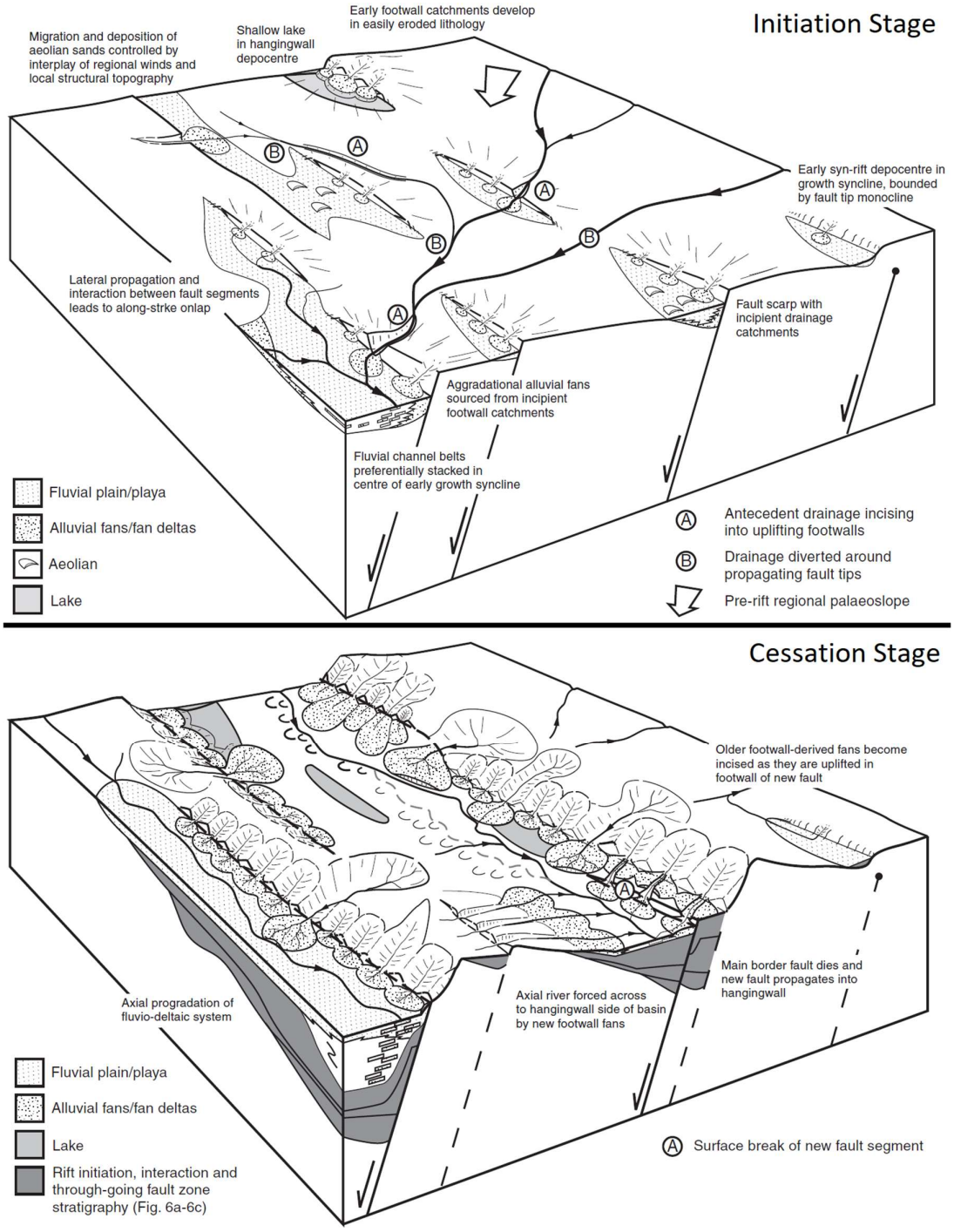

Figure 7.13: Continental environment tectono-sedimentary evolution of a normal fault array at basin-scale, highlighting depositional systems present at onset of extensional faulting activity and the resulting basin architecture at the point of fault death (Gawthorpe and Leeder 2000).

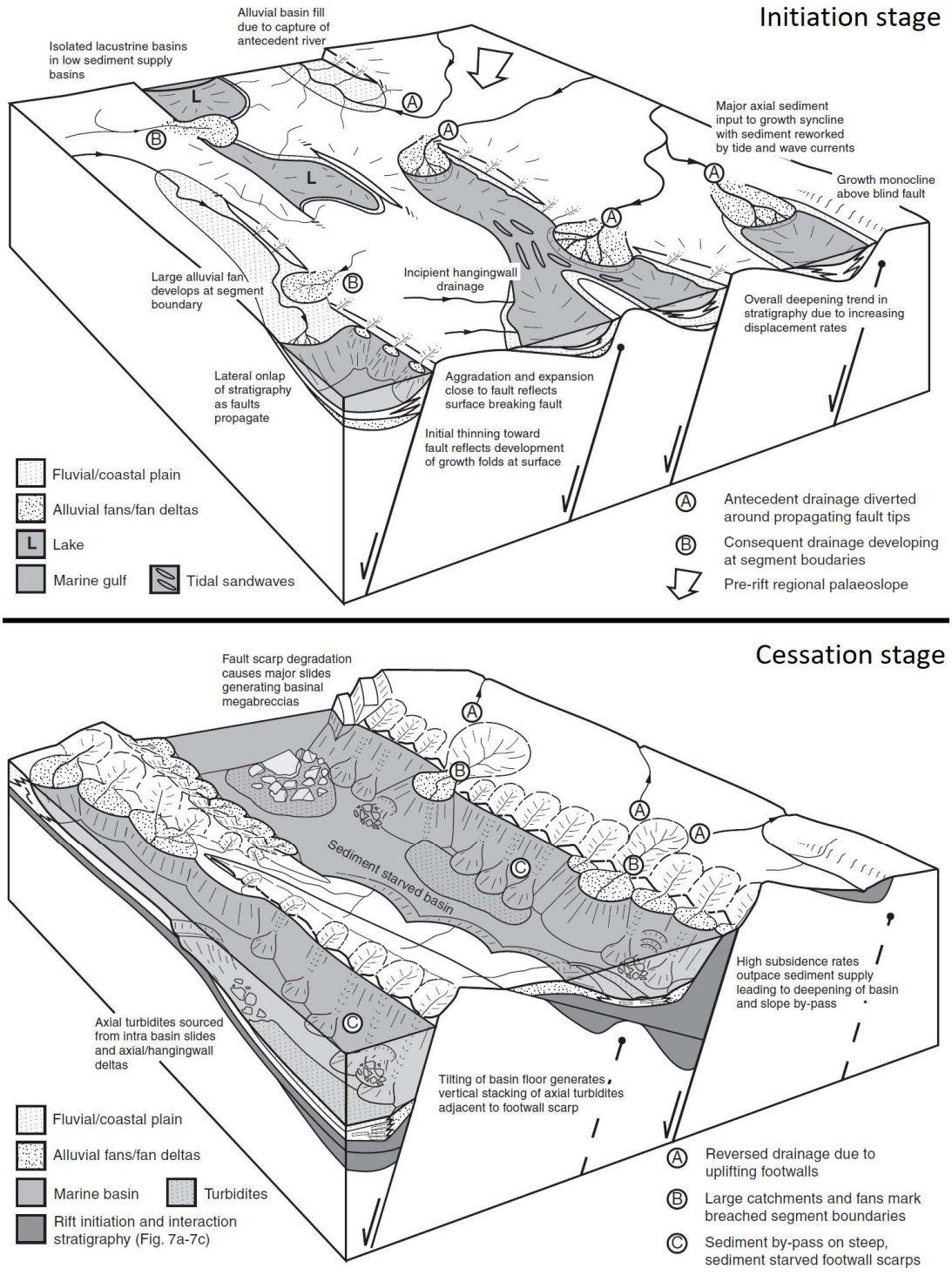

Figure 7.14: Coastal/marine environment tectono-sedimentary evolution of a normal fault array at basin-scale, highlighting depositional systems present at onset of extensional faulting activity and the resulting basin architecture at the point of fault death (Gawthorpe and Leeder 2000).

Gawthorpe and Leeder (2000) state that basin architecture depends upon the interaction of 3D basin linkage through fault propagation (simulated by analogue modelling), evolution of drainage and catchments (simulated by numerical modelling), effects of changing climate and variations in water level (simulated by numerical modelling). Given that the input volumes derived from the numerical modeller have previously been shown to be realistic (Burgess 2013) and this thesis has demonstrated that the volumes are being accurately translated onto the analogue sandbox; the integrated workflow permits development of all these factors for the first time in a single integrated model.

However, as mentioned, and as with any model, there are simplifications compared to nature, so a systematic study quantifying the impact of the accuracy of deposited bodies impacting tectonic development will be required in future. Alongside this, work to either change the scaling or improve modelling resolution (more cells in the numerical model and a denser tubing arrangement for the analogue model) would be significant for improving the model's reproduction of natural deposystems. Alternatively, improvements to the numerical model, for example; addition of modelling features such as aeolian dunes or fluvial systems with overbank deposition would also improve the geological feasibility of the workflow.

8 Conclusions

- A sieving device has been designed, constructed and tested. When depositing granular sandpacks consisting of near-pure quartz sand it has been shown to yield the mechanical properties (density and internal friction profile) required to successfully replicate brittle-frictional behaviours observed in the upper-crust. This permits construction of isotropic sandpacks if employed to deposit syn-kinematic sand layers on top of pre-kinematic layering deposited by hand. A mechanical sieving approach also offers far better repeatability and precision than traditional, by-hand methods.

- The sieving apparatus has the unique capability of being able to deposit a heterogeneous distribution of volumes within individual layers, whilst maintaining a consistent density and internal friction within the sandpack. This permits replication of realistic sedimentation patterns, and the subsequent tectonic loading they apply to dynamically scaled analogue sandbox experiments.

- Numerical stratigraphic forward modelling software has been successfully employed to provide input sedimentation distributions and volumes for the analogue sandbox experiments. This is achieved by adapting topographic data, derived from the analogue surface using stereo DIC techniques, to represent scaled topography and subsidence inputs. This data is then run in CarboCAT (MATLAB) with a series of input parameters to generate a realistic accumulation of carbonate strata in three dimensions. Calculated volumes are converted to the cellular resolution of the sieving device and scaled to weights representing volumes to be deposited; enabling translation of the complex, spatially variable volumes calculated from CarboCAT onto the analogue surface. This process is then repeated, with subsequent layering

being influenced by evolving sandbox surface topography, producing structurally complex 3D syn-kinematic sedimentation patterns.

- This integrated analogue and numerical workflow was systematically tested in a series of scaled static (depositional ramp) and dynamic (asymmetric half-graben) analogue experiments with varying initial parameters for both the analogue and numerical models. Models are purely deterministic, producing diverse final architectures solely as a result of numerical production parameters and sandbox surface evolution.

- This thesis has laid groundwork by developing a novel integrated workflow. If subsequent steps, outlined in the future work section, are completed, thereby adapting the sieving device to suit a different analogue setup (e.g. segmented rift / passive margin basins involving gravity-driven deformation); investigations into feedback mechanisms between sedimentation and tectonics are possible, as well as climatic implications on basin evolution.

9 References

Adam J, Urai JL, Wieneke B, Oncken O, Pfeiffer K, Kukowski N, Schmatz J. 2005. Shear localisation and strain distribution during tectonic faulting—new insights from granular-flow experiments and high-resolution optical image correlation techniques. Journal of Structural Geology. 27(2): 283-301.

Adam J, Ge Z, Sanchez M. 2012. Salt-structural styles and kinematic evolution of the Jequitinhonha deepwater fold belt, central Brazil passive margin. Marine and Petroleum Geology. 37(1): 101-120.

Adam J, Krezsek C. 2012. Basin-scale salt tectonic processes of the Laurentian Basin, Eastern Canada: insights from integrated regional 2D seismic interpretation and 4D physical experiments. Geological Society, London, Special Publications. 363(1): 331-360.

Adam J, Klinkmüller M, Schreurs G, Wieneke B. 2013. Quantitative 3D strain analysis in analogue experiments simulating tectonic deformation: Integration of X-ray computed tomography and digital volume correlation techniques. Journal of Structural Geology. 55: 127-149.

Al-Hashemi BHM, Al-Amoudi BOS. 2018. A review on the angle of repose of granular materials. Powder Technology. 330: 397–417.

Allen J, Beaumont C. 2016. Continental margin syn-rift salt tectonics at intermediate width margins. Basin Research. 28(5): 598-633.

Allken V, Huismans RS, Thieulot C. 2011. Three-dimensional numerical modeling of upper crustal extensional systems. Journal of Geophysical Research. 116(B10): B10409.

Allken V, Huismans RS, Thieulot C. 2012. Factors controlling the mode of rift interaction in brittle-ductile coupled systems: A 3D numerical study. Geochemistry, Geophysics, Geosystems. 13(5): Q05010.

Alsop GI, Marco S. 2011. Soft-sediment deformation within seismogenic slumps of the Dead Sea Basin. Journal of Structural Geology. 33(4): 433-457.

Athmer W, Luthi SM. 2011. The effect of relay ramps on sediment routes and deposition: A review. Sedimentary Geology. 242(1-4): 1-17.

Aurell M, Bosence D, Waltham D. 1995. Carbonate ramp depositional systems from a late Jurassic epeiric platform (Iberian Basin, Spain): a combined computer modelling and outcrop analysis. Sedimentology. 42(1): 75–94.

Balsamo F, Storti F. 2010. Grain size and permeability evolution of soft-sediment extensional sub-seismic and seismic fault zones in high-porosity sediments from the Crotone basin, southern Apennines, Italy. Marine and Petroleum Geology. 27(4): 822-837.

Barrier L, Nalpas T, Gapais D, Proust JN. 2013. Impact of synkinematic sedimentation on the geometry and dynamics of compressive growth structures: Insights from analogue modelling. Tectonophysics. 608: 737-752.

Betzler C, Hübscher C, Lindhorst S, Lüdmann T, Reijmer JJG, Braga JC. 2016. Lowstand wedges in carbonate platform slopes (Quarternary, Maldives, Indian Ocean). The Depositional Record. 2(2): 196-207.

Bialas RW, Buck WR. 2009. How sediment promotes narrow rifting: Application to the Gulf of California. Tectonics. [accessed 2019 December 17]; 28(4): TC4014. https://agupubs.onlinelibrary.wiley.com/doi/10.1029/2008TC002394. doi:10.1029/2008TC002394.

Bohacs K, Carroll A, Neal J, Mankiewicz P. 2000. Lake-Basin Type, Source Potentional, and Hydrocarbon Character: An Integrated Sequence-Stratigraphic-Geochemichal Framework. Lake Basins through Space and Time. AAPG Studies in Geology. 46: 3-33.

Bosence D, Waltham D. 1990. Computer modeling the internal architecture of carbonate platforms. Geology. 18(1): 26-30.

Bosence DWJ, Pomar L, Waltham DA, Lankester THG. 1994. Computer modeling a Miocene carbonate platform, Mallorca, Spain. AAPG Bulletin. 78(2): 247–266.

Bosence DWJ. 1998. Stratigraphic and sedimentological models of rift basins. In: Purser BH, Bosence DWJ, editors. Sedimentation and Tectonics in Rift Basins Red Sea: Gulf of Aden. London: Cambridge University Press. p. 9-25.

Bosscher H, Schlager W. 1992. Computer simulation of reef growth. Sedimentology. 39(3): 503–512.

Bowman SA, Vail PR. 1999. Interpreting the stratigraphy of the Baltimore Canyon Section, Offshore New Jersey with PHil, a stratigraphic simulator. In: John W, Harbaugh W, Lynn W, Eugene CR, Rudy S, Robert HG, Evan KF, editors. SEPM Special Publication #62 Numerical Experiments in Stratigraphy: Recent Advances in Stratigraphic and Sedimentologic Computer Simulations. Broken Arrow (OK): SEPM Publications. p. 117–138; [accessed December 17, 2019]. https://doi.org/10.2110/pec.99.62.0117.

Brun JP, Buck R, McClay K, Kusznir N, Louden K E, McKenzie D. 1999. Narrow Rifts Versus Wide Rifts: Inferences for the Mechanics of Rifting from Laboratory Experiments [and Discussion]. Philosophical Transactions of the Royal Society of London: Mathematical, Physical and Engineering Sciences. 357(1753): 695-712.

Brun JP, Fort X. 2011. Salt tectonics at passive margins: Geology versus models. Marine and Petroleum Geology. 28(6): 1123-1145.

Brune S, Williams SE, Müller RD. 2018. Oblique rifting: the rule, not the exception. Solid Earth. 9: 1187–1206.

Buck WR. 1991. Modes of continental lithospheric extension. Journal of Geophysical Research: Solid Earth. 96(B12): 20161-20178.

Burgess PM, Wright VP, and Emery D. 2001. Numerical forward modelling of peritidal carbonate parasequence development: implications for outcrop interpretation. Basin Research. 13(1): 1-16.

Burgess PM, Emery DJ. 2004. Sensitive dependence, divergence and unpredictable behaviour in a stratigraphic forward model of a carbonate system. Geological Society, London, Special Publications. 239(1): 77–94.

Burgess PM. 2012. A brief review of developments in stratigraphic forward modelling, 2000–2009. In: Roberts G, Bally A, editors. Regional Geology and Tectonics: Principles of Geologic Analysis. Oxford: Elsevier. p. 379–404.

Burgess PM. 2013. CarboCAT: A cellular automata model of heterogeneous carbonate strata. Computers & Geosciences. 53: 129-140.

Burgess PM, Masiero I, Toby SC, Duller RA. 2019. A Big Fan of Signals? Exploring Autogenic and Allogenic Process and Product in a Numerical Stratigraphic Forward Model of Submarine-Fan Development. Journal of Sedimentary Research. 89 (1): 1–12.

Burliga S, Koyi HA, Chemia Z. 2012. Analogue and numerical modelling of salt supply to a diapiric structure rising above an active basement fault. Geological Society, London, Special Publications. 363(1): 395-408.

Burov E, Cloetingh S. 1997. Erosion and rift dynamics: new thermomechanical aspects of post-rift evolution of extensional basins. Earth and Planetary Science Letters. 150(1-2): 7-26.

Burov E, Poliakov A. 2001. Erosion and rheology controls on synrift and postrift evolution: Verifying old and new ideas using a fully coupled numerical model. Journal of Geophysical Research. 106(B8): 16461-16481.

Burton D, Wood LJ. 2010. Seismic geomorphology and tectonostratigraphic fill of half grabens, West Natuna Basin, Indonesia. AAPG Bulletin. 94(11): 1695-1712.

Byerlee J. 1978. Friction of rocks. Pure and applied geophysics. 116(4): 615-626.

Cadell HM. 1889. VII.—Experimental Researches in Mountain Building. Earth and Environmental Science Transactions of The Royal Society of Edinburgh. 35(1): 337-357.

Corti G, Bonini M, Conticelli S, Innocenti F, Manetti P, Sokoutis D. 2003. Analogue modelling of continental extension: a review focused on the relations between the patterns of deformation and the presence of magma. Earth-Science Reviews. 63(3): 169-247.

Corti G, Bonini M, Sokoutis D, Innocenti F, Manetti P, Cloetingh S, Mulugeta G. 2004. Continental rift architecture and patterns of magma migration: A dynamic analysis based on centrifuge models. Tectonics. [accessed 2019 December 17]; 23(2): TC2012. https://agupubs.onlinelibrary.wiley.com/doi/full/10.1029/2003TC001561. doi:10.1029/2003TC001561.

Corti G. 2008. Control of rift obliquity on the evolution and segmentation of the main Ethiopian rift. Nature Geoscience, 1(4): 258-262.

Corti G. 2012. Evolution and characteristics of continental rifting: Analog modeling-inspired view and comparison with examples from the East African Rift System. Tectonophysics. 522: 1-33.

Costa E, Vendeville BC. 2002. Experimental insights on the geometry and kinematics of fold-and-thrust belts above weak, viscous evaporitic décollement. Journal of Structural Geology. 24(11): 1729-1739.

Cross NE, Bosence DWJ. 2008. Tectono-Sedimentary Models for Rift-Basin Carbonate Systems. In: Lukasik J, Simo JA, editors. SEPM Special Broadcast #89 Controls on Carbonate Platform and Reef Development. Broken Arrow (OK): SEPM Publications. p. 83-105; [accessed December 17, 2019]. https://doi.org/10.2110/pec.08.89.0083.

Csato I, Kendall CG. 2002. Modelling of stratigraphic architectural patterns in extensional settings towards a conceptual model. Computers & Geosciences. 28(3): 351-356.

Dalmasso H, Montaggioni L, Bosence D, Floquet M. 2001. Numerical modelling of carbonate platforms and reefs: Approaches and opportunities. Energy Exploration & Exploitation. 19(4): 315-345.

Desrues J, Viggiani G. 2004. Strain localization in sand: an overview of the experimental results obtained in Grenoble using stereophotogrammetry. International Journal for Numerical and Analytical Methods in Geomechanics. 28(4): 279-321.

Dorobek SL. 2008. Tectonic and Depositional Controls on Syn-Rift Carbonate Platform Sedimentation. In: Lukasik J, Simo JA, editors. SEPM Special Broadcast #89 Controls on Carbonate Platform and Reef Development. Broken Arrow (OK): SEPM Publications. p. 57-81; [accessed December 17, 2019]. https://doi.org/10.2110/pec.08.89.0057.

Drummond CN, Dugan PJ. 1999. Self-organizing models of shallow-water carbonate accumulation. Journal of Sedimentary Research. 69(4): 939-946.

Duerto L, Mcclay K. 2009. The role of syntectonic sedimentation in the evolution of doubly vergent thrust wedges and foreland folds. Marine and Petroleum Geology. 26(7): 1051-1069.

Ellis PG, McClay, KR. 1988. Listric extensional fault systems - results of analogue model experiments. Basin Research. 1(1): 55-70.

Erratt D, Thomas GM, Hartley NR, Musum R, Nicholson PH, Spisto Y. 2010. North Sea hydrocarbon systems: some aspects of our evolving insights into a classic hydrocarbon province. Geological Society, London, Petroleum Geology Conference series. 7: 37-56.

Fabbi S, Santantonio M. 2012. Footwall progradation in syn-rift carbonate platform-slope systems (Early Jurassic, Northern Apennines, Italy). Sedimentary Geology. 281: 21-34.

Faerseth RB, Sjøblom TS, Steel RJ, Liljedahl T, Sauar BE, Tjelland T. 1995. Tectonic controls on bathonian-volgian syn-rift successions on the visund fault block, northern North Sea. Norwegian Petroleum Society Special Publications. 5: 325-346.

Furuichi M, Nishiura D, Kuwano O, Hori T, Bauville A, Sakaguchi, H. 2018. Arcuate stress state in accretionary prisms from real-scale numerical sandbox experiments. Scientific Reports. 8: 1-11.

Gawthorpe RL, Leeder, MR. 2000. Tectono-sedimentary evolution of active extensional basins. Basin Research. 12(3-4): 195-218.

Ge H, Jackson MPA, Vendeville BC. 1997. Kinematics and dynamics of salt tectonics driven by progradation. AAPG Bulletin. 81(3): 398-423.

Gemmer L., Beaumont C, Ings SJ. 2005. Dynamic modelling of passive margin salt tectonics: effects of water loading, sediment properties and sedimentation patterns. Basin Research. 17(3): 383-402.

Gibson JR, Walsh JJ, Watterson J. 1989. Modelling of bed contours and cross-sections adjacent to planar normal faults. Journal of Structural Geology. 11(1): 317-328.

Gomes C, Caldeira J, Freitas A. 2010. The influence of different colours on the mechanical behaviour of quartz sand – first results. Paper presented at: Geomod 2010: Modelling in Geosciences; Minas Gerais, Brazil.

Gueydan F, Morency C, Brun JP. 2008. Continental rifting as a function of lithosphere mantle strength. Tectonophysics. 460(1): 83-93.

Hall, J. 1815. On the vertical position and convolution of certain strata and their relation with granite. Earth and Environmental Science Transactions of The Royal Society of Edinburgh. 7(1): 79-108.

Hall SA, Desrues J, Viggiani G, Bésuelle P, Andò E. 2012. Experimental characterisation of (localised) Deformation Phenomena in Granular Geomaterials from Sample Down to Inter-and Intra-grain Scales. Procedia IUTAM. 4: 54-65.

Hemelsdaël R, Ford M. 2014. Relay zone evolution: a history of repeated fault propagation and linkage, central Corinth rift, Greece. Basin Research. 28(1): 34-56.

Hinsken S, Ustaszewski K, Wetzel A. 2007. Graben width controlling syn-rift sedimentation: the Palaeogene southern Upper Rhine Graben as an example. International Journal of Earth Sciences. 96(6): 979-1002.

Hubbert, MK. 1937. Theory of scale models as applied to the study of geologic structures. Geological Society of America Bulletin. 48(10): 1459-1520.

Jackson CAL, Chua ST, Bell RE, Magee C. 2013. Structural style and early stage growth of inversion structures: 3D seismic insights from the Egersund Basin, offshore Norway. Journal of Structural Geology. 46(1): 167-185.

Jackson CAL, Gawthorpe RL, Leppard CW, Sharp IR. 2006. Rift-initiation development of normal fault blocks: insights from the Hammam Faraun fault block, Suez Rift, Egypt. Journal of the Geological Society. 163(1): 165-183.

Jackson JA, White NJ. 1989. Normal faulting in the upper continental crust: Observations from regions of active extension. Journal of Structural Geology. 11(1): 15-36.

Jagger LJ, McClay KR. 2018. Analogue modelling of inverted domino-style basement fault systems. Basin Research. 30(1): 363-381.

Jarvis GT, McKenzie DP. 1980. Sedimentary basin formation with finite extension rates. Earth and Planetary Science Letters. 48(1): 42-52.

Jervey MT. 1988. Quantitative Geological Modeling of Siliciclastic Rock Sequences and Their Seismic Expression In: Cheryl K, Bruce S, Hastings HP, Van Wagoner J, Ross C, Kendall C, editors. SEPM Special Broadcast #42 Sea Level Changes: An Integrated Approach. Broken Arrow (OK): SEPM Publications. p. 47-69; [accessed December 17, 2019]. https://doi.org/10.2110/pec.88.01.0047.

Korme T, Chorowicz J, Collet B, Bonavia F. 1997. Volcanic vents rooted on extension fractures and their geodynamic implications in the Ethiopian Rift Journal of Volcanology and Geothermal Research. 79(3-4): 205-222.

Korneva I, Tondi E, Jablonska D, Di Celma C, Alsop I, Agosta F. 2016. Distinguishing tectonically-and gravity-driven synsedimentary deformation structures along the Apulian platform margin (Gargano Promontory, southern Italy). Marine and Petroleum Geology. 73: 479-491.

Koša E, Hunt DW. 2005. Growth of syndepositional faults in carbonate strata: Upper Permian Capitan platform, New Mexico, USA. Journal of Structural Geology. 27(6): 1069-1094.

Koyi H. 1997. Analogue Modelling: From a qualitative to a quantitative technique – A historical outline. Journal of Petroleum Geology. 20(2): 223-238.

Kozlowski EN. 2017. Multi-scale forward modelling of microbial lacustrine carbonates [PhD Theses]. [Egham (UK)]: Royal Holloway University and Bedford New College.

Krantz RW. 1991. Measurements of friction coefficients and cohesion for faulting and fault reactivation in laboratory models using sand and sand mixtures. Tectonophysics. 188(1): 203-207.

Kusznir NJ, Marsden G, Egan SS. 1991. A flexural-cantilever simple-shear/pure-shear model of continental lithosphere extension: applications to the Jeanne d'Arc Basin, Grand Banks and Viking Graben, North Sea. Geological Society, London, Special Publications. 56(1): 41-60.

Lallemand SE, Schnuerle P, Malavieille J. 1994. Coulomb theory applied to accretionary and nonaccretionary wedges; possible causes for tectonic erosion and/or frontal accretion. Journal of Geophysical Research: Solid Earth. 99(B6): 12033-12055.

Lanteaume C, Fournier F, Pellerin M, Borgomano J. 2018. Testing geologic assumptions and scenarios in carbonate exploration: Insights from integrated stratigraphic, diagenetic, and seismic forward modelling. The Leading Edge. 37(9): 672-680.

Leeder MR, Gawthorpe RL. 1987. Sedimentary models for extensional tilt-block/half-graben basins. Geological Society, London, Special Publications. 28(1): 139–152.

Leeder M, Jackson J. 1993. The interaction between normal faulting and drainage in active extensional basins, with examples from the western United States and central Greece. Basin Research. 5(2): 79-102.

Lister GS, Etheridge MA, Symonds PA. 1991. Detachment models for the formation of passive continental margins. Tectonics. 10(5): 1038-1064.

Lohrmann J, Kukowski N, Adam J, Oncken O. 2003. The impact of analogue material properties on the geometry, kinematics, and dynamics of convergent sand wedges. Journal of Structural Geology. 25(10): 1691-1711.

Maillot, B. 2013. A sedimentation device to produce uniform sand packs. Tectonophysics. 593: 85-94.

Marone C. 1998. The effect of loading rate on static friction and the rate of fault healing during the earthquake cycle. Nature. 391(6662): 69-72.

Mastrogiacomo G, Moretti M, Owen G, Spalluto L. 2012. Tectonic triggering of slump sheets in the Upper Cretaceous carbonate succession of the Porto Selvaggio area (Salento peninsula, southern Italy): Synsedimentary tectonics in the Apulian Carbonate Platform. Sedimentary Geology. 269: 15-27.

McClay KR, Ellis PG. 1987. Analogue models of extensional fault geometries. Geological Society, London, Special Publications. 28(1): 109-125.

McClay KR. 1990. Deformation mechanics in analogue models of extensional fault systems. Geological Society, London, Special Publications. 54(1): 445-453.

McClay KR, White MJ. 1995. Analogue modelling of orthogonal and oblique rifting. Marine and Petroleum Geology. 12(2): 137-151.

McClay KR, Dooley T, Whitehouse P, Fullarton L, Chantraprasert S. 2004. 3D Analogue Models of Rift Systems: Templates for 3D Seismic Interpretation. Geological Society, London, Memoirs. 29(1): 101-115.

McKenzie D. 1978. Some remarks on the development of sedimentary basins. Earth and Planetary Science Letters. 40(1): 25-32.

Michon L, Merle O. 2003. Mode of lithospheric extension: Conceptual models from analogue modeling. Tectonics. [accessed 2019 December 17]; 22(4): 1028. https://agupubs.onlinelibrary.wiley.com/doi/full/10.1029/2002TC001435. doi:10.1029/2002TC001435, 4.

Moragas M, Vergés J, Nalpas T, Saura E, Martín-Martín JD, Messager G, Hunt DW. 2017. The impact of syn- and post-extension prograding sedimentation on the development of salt-related rift basins and their inversion: Clues from analogue modelling. Marine and Petroleum Geology. 88: 985-1003.

Morley CK. 1999. Patterns of displacement along large normal faults: implications for basin evolution and fault propagation, based on examples from East Africa. AAPG Bulletin. 83: 613–634.

Morley CK, Nelson RA, Patton TL, Munn SG. 1990. Transfer zones in the East African Rift System and their relevance to hydrocarbon exploration in rifts. AAPG Bulletin. 74(8): 1234-1253.

Olive J-A, Behn MD, Malatesta LC. 2014. Modes of extensional faulting controlled by surface processes. Geophysical Research Letters. 41: 6725-6733.

Panien M, Schreurs G, Pfiffner A. 2006. Mechanical behaviour of granular materials used in analogue modelling: insights from grain characterisation, ring-shear tests and analogue experiments. Journal of Structural Geology. 28(9): 1710-1724.
Paola C. 2000. Quantitative models of sedimentary basin filling. Sedimentology. 47: 121–178.

Parcell WC. 2003. Evaluating the Development of Upper Jurassic Reefs in the Smackover Formation, Eastern Gulf Coast, U.S.A. through Fuzzy Logic Computer Modeling. Journal of Sedimentary Research. 73(4): 498-515.

Paul D, Mitra S. 2013. Experimental models of transfer zones in rift systems. AAPG Bulletin. 97: 759–780.

Pomar L, Hallock P. 2008. Carbonate factories: A conundrum in sedimentary geology. Earth-Science Reviews. 87(3 - 4): 134-169.

Ramberg H. 1967. Model Experimentation of the Effect of Gravity on Tectonic Processes. Geophysical Journal International. 14(1-4): 307–329.

Ravnås R, Steel R. 1998. Architecture of Marine Rift-Basin Sassions. American Association of Petroleum Geologists Bulletin. 82. 110-146.

Ravnås R, Nøttvedt A, Steel RJ, Windelstad J. 2000. Syn-rift sedimentary architectures in the Northern North Sea. Geological Society, London, Special Publications. 167(1): 133-177.

Ring U. 1994. The influence of preexisting structure on the evolution of the Cenozoic Malawi rift (East African rift system). Tectonics. 13(2): 313-326.

Rosendahl BR. 1987. Architecture of Continental Rifts with Special Reference to East Africa. Annual Review of Earth and Planetary Sciences. 15(1): 445-503.

Rossi D, Storti F. 2003. New artificial granular materials for analogue laboratory experiments: aluminium and siliceous microspheres. Journal of Structural Geology. 25(11): 1893-1899.

Schellart WP. 2000. Shear test results for cohesion and friction coefficients for different granular materials: scaling implications for their usage in analogue modelling. Tectonophysics. 324(1): 1-16.

Schlager, W. 2000. Sedimentation rates and growth potential of tropical, cool-water and mud-mound carbonate systems. Geological Society, London, Special Publications. 178(1): 217-227.

Schlager W. 2005. SEPM Concepts in Sedimentology and Paleontology #8 : Carbonate Sedimentology and Sequence Stratigraphy. Broken Arrow (OK): SEPM Publications.

Schlische RW. 1991. Half-graben basin filling models: new constraints on continental extensional basin development. Basin Research. 3(3): 123-141.

Schreurs G, Buiter SJH, Boutelier D, Corti G, Costa E, Cruden AR, Nilforoushan, F. 2006. Analogue benchmarks of shortening and extension experiments. Geological Society, London, Special Publications. 253(1): 1-27.

Shafie KRK, Madon M. 2008. A review of stratigraphic simulation techniques and their applications in sequence stratigraphy and basin analysis. Bulletin of the Geological Society of Malaysia. 54: 81-89.

Sugan M, Wu JEL, McClay K. 2014. 3D analogue modelling of transtensional pull-apart basins: comparison with the Cinarcik basin, Sea of Marmara, Turkey. Bollettino di Geofisica Teorica ed Applicata. 55(4): 699-716.

Warrlich GMD, Waltham DA, Bosence DWJ. 2002. Quantifying the sequence stratigraphy and drowning mechanisms of atolls using a new 3-D forward stratigraphic modelling program (CARBONATE3D). Basin Research. 14(3): 379-400.

Wernicke B. 1981. Low-angle normal faults in the Basin and Range Province: nappe tectonics in an extending orogen. Nature. 291(5817): 645-648.

Wernicke B, Burchfiel BC. 1982. Modes of extensional tectonics. Journal of Structural Geology. 4(2): 105-115.

Williams HD, Burgess PM, Wright VP, Della Porta G, Granjeon D. 2011. Investigating Carbonate Platform Types: Multiple Controls and a Continuum of Geometries. Journal of Sedimentary Research. 81(1): 18-37.

Wilson MEJ, Bosence DWJ, Limbong A. 2000. Tertiary syntectonic carbonate platform development in Indonesia. Sedimentology. 47(2): 395-419.

Withjack MO, Jamison WR. 1986. Deformation produced by oblique rifting. Tectonophysics. 126(2): 99-124.

Withjack M, Schlische R, Olsen P. 2002. Rift-basin structure and its influence on sedimentary systems. SEPM Special publication. 73: 57-81.

Vasquez L, Nalpas T, Ballard JF, Veslud C, Simon B. 2018. 3D geometries of normal faults in a brittle-ductile sedimentary cover: Analogue modelling. Journal of Structural Geology. 112: 29-38.

Versfelt J, Rosendahl BR. 1989. Relationships between pre-rift structure and rift architecture in Lakes Tanganyika and Malawi, East Africa. Nature. 337: 354-357.

Zwaan F, Schreurs G, Naliboff J, Buiter SJH. 2016. Insights into the effects of oblique extension on continental rift interaction from 3D analogue and numerical models. Tectonophysics. 693: 239-260.

Zwaan F, Schreurs G. 2017. How oblique extension and structural inheritance influence rift segment interaction: Insights from 4D analog models. Interpretation. 5(1): 119-138.

Zwaan F, Schreurs G, Adam J. 2018. Effects of sedimentation on rift segment evolution and rift interaction in orthogonal and oblique extensional settings: Insights from analogue models analysed with 4D X-ray computed tomography and digital volume correlation techniques. Global and Planetary Change. 171: 110-133.

Zwaan F, Schreurs G, Buiter S. 2019. A systematic comparison of experimental set-ups for modelling extensional tectonics. Solid Earth Discussions. 10:1063–1097.

Zwaan F, Schreurs G, Rosenau M. 2020. Rift propagation in rotational versus orthogonal extension: Insights from 4D analogue models. Journal of Structural Geology. 135: 103946.